

FLUORESCENT PROBES: SYNTHESIS AND INVESTIGATION OF THEIR USE IN RECOGNITION OF ANIONS, CATIONS AND BIOMOLECULES

THESIS SUBMITTED TO
COCHIN UNIVERSITY OF SCIENCE AND TECHNOLOGY
IN PARTIAL FULFILLMENT OF THE REQUIREMENTS FOR THE DEGREE OF
DOCTOR OF PHILOSOPHY IN CHEMISTRY
UNDER THE FACULTY OF SCIENCE

By

HARI SHANKAR B.

Under the Supervision of

Dr. D. Ramaiah




**Photosciences and Photonics
Chemical Sciences and Technology Division
CSIR–National Institute for Interdisciplinary
Science and Technology (CSIR–NIIST)
Thiruvananthapuram-695 019, Kerala**

AUGUST 2015

DECLARATION

I hereby declare that the Ph. D. thesis entitled: **“FLUORESCENT PROBES: SYNTHESIS AND INVESTIGATION OF THEIR USE IN RECOGNITION OF ANIONS, CATIONS AND BIOMOLECULES”** is an independent work carried out by me at the Photosciences and Photonics Section, Chemical Sciences and Technology Division of the CSIR-National Institute for Interdisciplinary Science and Technology (CSIR-NIIST), Trivandrum, under the supervision of Dr. D. Ramaiah and the same has not been submitted elsewhere for a degree, diploma or title.

In keeping with the general practice of reporting scientific observations, due acknowledgement has been made wherever the work described is based on the findings of other investigators.


(HARI SHANKAR B.)



डा. डी रामैया, एफ ए एससी
निदेशक
Dr. D. Ramaiah, F.A.Sc
DIRECTOR

सीएसआईआर-उत्तर पूर्व विज्ञान तथा प्रौद्योगिकी संस्थान
वैज्ञानिक तथा औद्योगिक अनुसंधान परिषद्
जोरहाट-785006, आसाम, भारत


CSIR-NORTH EAST INSTITUTE OF SCIENCE & TECHNOLOGY
COUNCIL OF SCIENTIFIC & INDUSTRIAL RESEARCH (CSIR)
JORHAT-785006, ASSAM, INDIA



August 01, 2015

CERTIFICATE

This is to certify that the work embodied in the thesis entitled: **"FLUORESCENT PROBES: SYNTHESIS AND INVESTIGATION OF THEIR USE IN RECOGNITION OF ANIONS, CATIONS AND BIOMOLECULES"** has been carried out by Mr. Hari Shankar B. under my supervision and guidance at the Photosciences and Photonics, Chemical Sciences and Technology Division of the CSIR-National Institute for Interdisciplinary Science and Technology (CSIR-NIIST), Trivandrum and the same has not been submitted elsewhere for a degree. All the relevant corrections, modifications and recommendations suggested by the audience and the doctoral committee members during the pre-synopsis seminar of Mr. Hari Shankar B. have also been incorporated in the thesis.


(D. Ramaiah) 01/08/2015

Thesis Supervisor
(Formerly, Head, Chemical
Sciences and Technology Division
CSIR-NIIST, Trivandrum)

ACKNOWLEDGEMENTS

I have great pleasure in placing on record my deep sense of gratitude to Dr. D. Ramaiah, my thesis supervisor, for suggesting the research problem and for his guidance, support and encouragement, leading to the successful completion of this work.

I would like to express my sincere thanks to Professor M. V. George for his constant support during the tenure of this work.

I wish to thank Dr. A. Ajayaghosh, Dr. Suresh Das, and Dr. Gangan Prathap, present and former Directors of the CSIR-NIIST, Thiruvananthapuram for providing me the necessary facilities for carrying out the work.

I sincerely thank Dr. K. R. Gopidas, Dr. K. George Thomas, Dr. Joshy Joseph, Dr. N. Unni, Dr. B. P. Deb, Dr. V. Karunakaran, Dr. K. Yoosaf, and Dr. C. Vijayakumar, present and former Scientists of the Photosciences and Photonics, for all the help and support extended to me.

I thank all the members of the Photosciences and Photonics and in particular, Dr. Jisha, Dr. Rekha, Dr. Akhil, Dr. Suneesh, Dr. Sanju, Dr. Nandajan, Mr. Adarsh, Dr. Dhanya, Dr. Betsy, Mr. Albish, Mr. Shanmugasundaram, Ms. Viji, Mr. Shameel, Dr. Nidhi, Dr. Lavanya, Ms. Sreelakshmi, Ms. Rahi and Mr. Aswin for their help and cooperation. I would like to thank Mr. Robert Philip and Mr. Kiran S. for their help and support. I also thank Mr. Adarsh, Ms. Saumini, Mr. Saran, Ms. Viji, Ms. Athira, Mr. Kiran M., and Mrs. Lucy for NMR, Mass, TEM and SEM analysis.

Words are inadequate to express my gratitude to my parents, sister, and other family members for their endless love, support and understanding. I am also indebted and deeply grateful to Mr. Dayalan, Ms. Selvi and Ms. Nandhini, who constantly stood as a source of encouragement and confidence. I take this opportunity to pay respect to all my teachers who guided me.

I sincerely thank Council of Scientific and Industrial Research (CSIR), and DST Government of India for financial assistance.

Hari Shankar B.

CONTENTS

	Page
Statement	i
Certificate	ii
Acknowledgements	iii
Contents	iv
Preface	vii
Chapter 1	ORGANIC FLUORESCENT PROBES: AN OVERVIEW
1.1	Introduction 1
1.2	Basic Aspects of Fluorescence Detection 3
1.3	Mechanism of Fluorescence Detection 5
1.3.1	Photoinduced Electron Transfer 6
1.3.2	Energy Transfer Mechanism 8
1.3.3	Aggregation Induced Emission (AIE) 11
1.4	Types of Targets and Detection 14
1.4.1	Recognition of the Anions 15
1.4.2	Detection of the Cations 20
1.4.3	Recognition of the Biomolecules 25
1.5	Objectives of the Present Investigation 28
1.6	References 30
Chapter 2	DESIGN OF ARYL-INDOLIUM CONJUGATES: STUDY OF THEIR ANION DETECTION ASPECTS
2.1	Abstract 36
2.2	Introduction 38
2.3	Results 40
2.3.1	Synthesis of the Indolium Conjugates 40
2.3.2	Photophysical Properties of the Indolium Conjugates 41

2.3.3	Anion Recognition Properties	45
2.3.4	Mechanism of Cyanide Detection	48
2.3.5	Design of a Prototype Device	54
2.3.6	Quantification of Endogenous Cyanide	58
2.4	Discussion	59
2.5	Conclusions	62
2.6	Experimental Section	63
2.7	References	68
Chapter 3	DANSYL-NAPHTHALIMIDE DYADS: STUDY OF THEIR METAL ION RECOGNITION PROPERTIES	
3.1	Abstract	73
3.2	Introduction	75
3.3	Results	77
3.3.1	Synthesis of the Dansyl-Naphthalimide Dyads	77
3.3.2	Absorption and Fluorescence Properties	79
3.3.3	Recognition of the Metal Ions	82
3.3.4	Selectivity and Reversibility of the Recognition	86
3.3.5	Nature of the Metal Ion Complexation	89
3.3.6	Laser Flash Photolysis Studies	95
3.4	Discussion	96
3.5	Conclusions	100
3.6	Experimental Section	101
3.7	References	106
Chapter 4	NOVEL NAPHTHALENE IMIDE SYSTEMS: STUDY OF THEIR SELF-ASSEMBLY AND DNA BINDING ASPECTS	
4.1	Abstract	111
4.2	Introduction	113
4.3	Results	115

4.3.1	Synthesis of the Amphiphilic Conjugates	115
4.3.2	Photophysical and Self-Assembly Aspects	116
4.3.3	Interactions with Biomolecules	124
4.3.4	Nature of DNA Binding Interactions	131
4.3.5	DNA Mediated Disassembly	135
4.4	Discussion	138
4.5	Conclusions	140
4.6	Experimental Section	141
4.7	References	148
	List of Publications	153

PREFACE

Development of molecular probes for the selective and sensitive detection of analytes has been an active area of research because such effective molecules can have biological and medicinal applications. Of the various probes reported, the fluorescence based systems have attracted much attention owing to their high sensitivity, fast response time, non-invasiveness and technical simplicity. However, the quantification of a target analyte using the fluorescent probe that acts through a single emission response (either increase or decrease in the fluorescence intensity) can have disadvantages, when compared to the systems that show either dual emission or ratiometric changes. In the case of the systems that exhibit ratiometric changes, the ratio of the fluorescence intensity of the two different wavelengths can be utilized for the quantification of the analyte of interest. Such an observation will have an effective internal referencing that greatly increases the sensitivity of the detection. In this context, it was our objective to develop functional organic systems and to explore their potential as sensitive fluorescent probes for the recognition of anions, cations and biomolecules. The present thesis has been divided into four chapters and of which the first chapter gives an overview on the organic fluorescent probes, with a particular emphasis on their mechanism of molecular recognition. In addition, the specific objectives of the present thesis were also briefly described at the end of this chapter.

The design, synthesis and development of the aryl-indolium conjugates as molecular probes for the detection of anions form the subject matter of the second chapter of the thesis. In this context, we have synthesised two indolium conjugates **1** and

2, based on anthracene and pyrene moieties, and have investigated their photophysical properties under different conditions. These conjugates were characterised with the aromatic part as the electron donor and the indolium moiety as the electron acceptor unit. These systems showed prominent absorption bands in the region 330–390 nm and 500–515 nm, wherein the first band can be attributed to the characteristic absorption of the aromatic chromophore, while the latter to the intramolecular charge transfer (ICT) interactions. Expectedly, these conjugates showed significant solvatochromism as well as exhibited significant hypsochromic shift (negative solvatochromism) with the increasing in polarity of the solvent.

The interactions of these conjugates with various biologically important anions such as CN^- , SCN^- , F^- , Br^- , PO_4^{3-} etc. have been investigated through photophysical and biophysical techniques. Of the various anions tested, these systems showed selective interactions with CN^- ions and the limit of detection was found to be 32 and 10 ppb, respectively, for both the conjugates. Of these systems, the pyrene based conjugate **2** showed dual colorimetric and fluorescent responses with ratiometric fluorescence changes in the presence of the CN^- ions. Upon addition of the CN^- ions, the emission spectra featured quenching of the ICT induced emission at 637 nm, with the concomitant increase in the emission at 395 nm, corresponding to the pyrene monomer. Such changes have led to a visual change in the fluorescence intensity from red to blue, in the presence of the CN^- ions.

The nature of the interactions with the CN^- ions have been evaluated through various techniques such as ^1H and ^{13}C NMR, IR, HRMS and isothermal titration

calorimetric (ITC) experiments. The results of these studies have confirmed the formation of a 1,2-adduct through the nucleophilic addition of the CN^- ions to the iminium group of the indolium moiety of the probe. The reversibility of the CN^- ions recognition by the probe was investigated through the reaction with trifluoroacetic acid. We observed the revival of the fluorescence properties as that of the starting materials, thereby demonstrating that the probe **2** acts as a reversible chemodosimeter. Uniquely, this probe can also be coated on a glass surface to fabricate a simple solid-state device called dip-stick. Such a dip-stick device could be used for the visual detection of the cyanide ions in presence of other competing anions in solution. This probe can be furthermore coated on polymeric film as well as on filter paper strip. Both these prototypes could also be successfully used for the detection of the cyanide ions in solution and also for the quantification of the endogenous cyanide content in the natural sources such as Indian almonds.

The third chapter of the thesis deals with the synthesis and investigation of photophysical and cation recognition properties of a few dansyl-naphthalimide dyads **1-5**, linked through varying methylene spacer group. The characteristic property of these dyads is that they exhibited a dual fluorescence with maxima at 378 and 525 nm, corresponding to the naphthalimide chromophore and the dansyl moiety, respectively. These dyads exhibited both singlet-singlet energy transfer (SSET) and photoinduced electron transfer (PET) processes, which decreased with the increase in the spacer length. The interaction of these dyads with various metal ions such as Cu^{2+} , Zn^{2+} , Na^+ , K^+ etc. have been investigated through UV-Vis, fluorescence, NMR, isothermal titration

calorimetric (ITC) and laser flash photolysis techniques. Interestingly, all these dyads exhibited selective interactions with the Cu^{2+} and Zn^{2+} ions, when compared to other competent metal ions. The changes in the emission spectra of the dyads, upon addition of the Cu^{2+} ions, were found to be ratiometric with the increase in the naphthalimide chromophore emission at 378 nm, with the concomitant decrease in the dansyl emission intensity at 525 nm. On the other hand, only the fluorescence intensity of the naphthalimide chromophore of the lower homologues (**1–3**) was altered by the Zn^{2+} ions, with negligible changes in the dansyl emission. Jobs plot analysis showed that these dyads form 2:3 and 1:1 complexes with the Cu^{2+} and Zn^{2+} ions, respectively. The association constants for the Zn^{2+} and Cu^{2+} ions were calculated through Benesi-Hildebrand analysis and were found to be in the order 10^3 – 10^5 M^{-1} . Furthermore, irrespective of the length of the spacer group, these dyads interestingly act as fluorescence ratiometric molecular probes for the Cu^{2+} ions by altering the emission intensity of both the dansyl and naphthalimide chromophores.

The nature of the complexation was analysed through NMR, and isothermal calorimetric techniques. These measurements indicated the fact that both the sulphonamide and dimethylamine groups of the dansyl moiety were involved in the complexation with the Cu^{2+} ions, while only the latter group was involved with Zn^{2+} ions. Furthermore, we have carried out the laser flash photolysis of the dyads, which showed formation of a transient absorption, which can be attributed to the radical anion of the naphthalimide chromophore, whereas, only the triplet excited state of the dyads was observed in the presence of the Cu^{2+} ions. However, in the presence of the Zn^{2+} ions, we

observed the radical anion transient absorption, albeit with lower intensity, indicating the existence of PET process under these conditions. The complexation of the dyads with the Cu^{2+} ions affected both PET and SSET processes, whereas only the PET process was partially inhibited by the Zn^{2+} ions in the case of the lower homologues (**1–3**). Our results demonstrated that the spacer length dependent variation of the photophysical properties of these dyads enable not only the selective detection of the Cu^{2+} and Zn^{2+} ions, but also aid in discriminating these two biologically important metal ions, under similar conditions.

Investigation of photophysical, self-assembly and DNA binding properties of a few naphthalene imide amphiphilic conjugates **1** and **2**, is the subject matter of the fourth chapter of the thesis. Both these conjugates exhibited good solubility in the aqueous medium and showed characteristic absorption and fluorescence bands of the naphthalene di- and monoimide chromophores at 382 and 390 nm; 344 and 378 nm, respectively. Interestingly, these conjugates exhibited self-assembly in the aqueous medium as confirmed through photophysical as well as microscopic techniques, including TEM, SEM and DLS measurements. Of these systems, the bolamphiphile **1** formed the vesicular assemblies of diameter *ca.* 220 nm having a wall thickness of 5 nm in the aqueous medium at and above critical aggregation concentration (CAC) of 0.4 mM. The naphthalimide conjugate **2**, on the other hand, showed the formation of the lamellar flake like structures, at and above the CAC of 0.25 mM. Interestingly, the vesicular structures thus formed in the aqueous medium were found to encapsulate the

hydrophobic guest molecules such as Nile red as confirmed through absorption, fluorescence and fluorescence microscopic measurements.

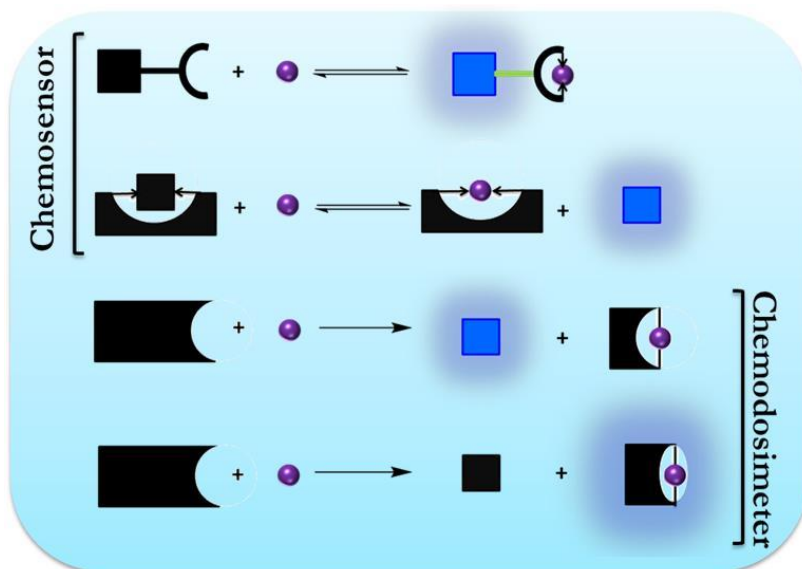
To evaluate the potential of the biomolecules as stimuli, we have studied the interactions of these conjugates with proteins, (for example, BSA), ct-DNA and synthetic polynucleotides under different concentrations. These systems showed negligible interactions with BSA but exhibited affinity for DNA. Interestingly, with the addition of DNA, the conjugate **1** exhibited significant hypochromicity (*ca.* 42%) in its absorption spectrum. We observed a regular decrement in the fluorescence intensity at 390 nm with a concomitant enhancement at 510 nm. Similar observations have also been made with the amphiphilic conjugate **2**. The mode of interaction of these conjugates with DNA was evaluated through photophysical and biophysical techniques such as ethidium bromide displacement assay, circular dichroism (CD), viscosity and thermal denaturation techniques. Results, thus obtained, have revealed that these conjugates interact with DNA through intercalation and exhibited binding constants in the range $K_{\text{DNA}} \sim 5\text{--}8 \times 10^4 \text{ M}^{-1}$. These investigations have also confirmed that the driving force for the formation of the excimer in the presence of DNA could be attributed to the synergistic effects of both hydrophobic and electrostatic interactions. Furthermore, when the vesicular structures of the conjugate **1** were allowed to interact with DNA, we observed their disassembly, with the release of the encapsulated dye molecules.

In summary, we report the synthesis of novel functional organic systems and investigations of their photophysical properties and molecular recognition properties. These systems showed good solubility in both organic and aqueous media and exhibited

favourable absorption and fluorescence properties. Of these systems, the aryl-indolium conjugates can serve as selective and sensitive probes for the on-site analysis and quantification of the cyanide ions. The dansyl-naphthalimide dyads, on the other hand, showed selectivity for the biologically important cations, such as Cu^{2+} and Zn^{2+} ions through ratiometric fluorescence changes. Lastly, the naphthalene imide based amphiphilic systems, which exhibited self-assembly leading to the formation vesicular structures, can be utilized for the encapsulation and release of the hydrophobic molecules, employing DNA as the stimuli. Overall, our results demonstrate that, the organic systems reported in the thesis can have interesting and potential applications as optical probes and the results presented are useful in developing sensitive molecular probes for various biological applications.

***Note:** The numbers of various compounds given here correspond to those given under the respective Chapters.*

ORGANIC FLUORESCENT PROBES: AN OVERVIEW



1.1. INTRODUCTION

Molecular recognition is a fundamental and vital process in biology, which mostly involves specific interactions, be covalent or non-covalent, between a receptor (host) and an analyte (guest).¹ These interactions, generally, are accompanied by the formation of chemical ensembles, which successively cause changes in the physical and chemical properties of either the receptor/analyte or both the units.² The progress in the field led to the development of new areas such as host-guest chemistry and supramolecular chemistry. In the host-guest chemistry the term “sensor” is more closely related to a molecular event, which upon

stimulation by any form of energy results in change of its own state or properties.³ These changes can be successfully utilized for the qualitative as well as quantitative analysis of the stimulant. Depending on the type of signals produced with respect to the binding event, sensors may be classified into two categories; electronic sensors or optical sensors.⁴ The former produces signals in the form of changes in the electrochemical properties, which can be further categorised into five types such as ion-selective electrodes (ISEs), field-effect transistors (FETs), electroactive sensors, biosensors and microelectrodes. The optical sensors, on the other hand, act as a result of changes in the optical properties of the receptor molecules. The optical and photo-physical changes that occur in a receptor molecule are found to be more valuable owing to their technical simplicity and non-invasiveness.⁵

The optical molecular probes can be further classified into two categories such as (i) chromogenic (or colorimetric) and (ii) fluorogenic (or fluorescent) molecules. In the former case, the interactions with guest entities result in the changes in the absorption (colour) properties of the receptor molecule, whereas, in the latter cases involve the alteration of the fluorescence properties. Even though the colorimetric probes can offer qualitative and quantitative information through visual changes, but the ultrasensitive sub-micromolar estimation of guest species can be achieved through the fluorescence technique. Moreover, this technique requires low concentrations of the analyte and probe (*ca.* 10^{-6} M) for the detection. This chapter gives an overview on organic fluorescent probes with a particular emphasis on their recognition properties. The objectives of the present thesis are also included at the end of this chapter.

1.2. BASIC ASPECTS OF FLUORESCENCE DETECTION

The fluorescent probes, in general, consist of two main components: a signalling moiety (the fluorophore) and a recognition moiety or binding site (the receptor) separated by a spacer unit. The signalling moiety acts as a signal transducer, converting the information (recognition event) into a fluorescence response, whereas, the recognition moiety is responsible for binding to the analyte in an efficient and selective manner. This depends on the nature of the ligands, characteristics of the target analytes, solvent properties like pH, ionic strength, and polarity, which can have a significant effect on the ability of the receptor to recognize and interact with the analyte. The design of fluorescent probes can be broadly classified under three approaches, which include; (i) binding site-signalling subunit approach (chemosensors), (ii) displacement approach and (iii) chemodosimeter approach.^{2a,6} These three approaches differ in the manner in which the arrangement of the binding site or reactive site, and the signalling subunit and also mode of interactions with the analyte. In the “binding site-signalling subunit” approach^{6b} (Figure 1.1A), these two parts are linked by a covalent bond. The interactions of the target analyte with the binding site induce changes in the excited state properties of the signalling subunit resulting in its detection. The molecules used for this purpose are generally termed as “chemosensors”, which work in an operating principle based on coordination events with the target analyte, and therefore the accompanying fluorescence changes are predominantly reversible.

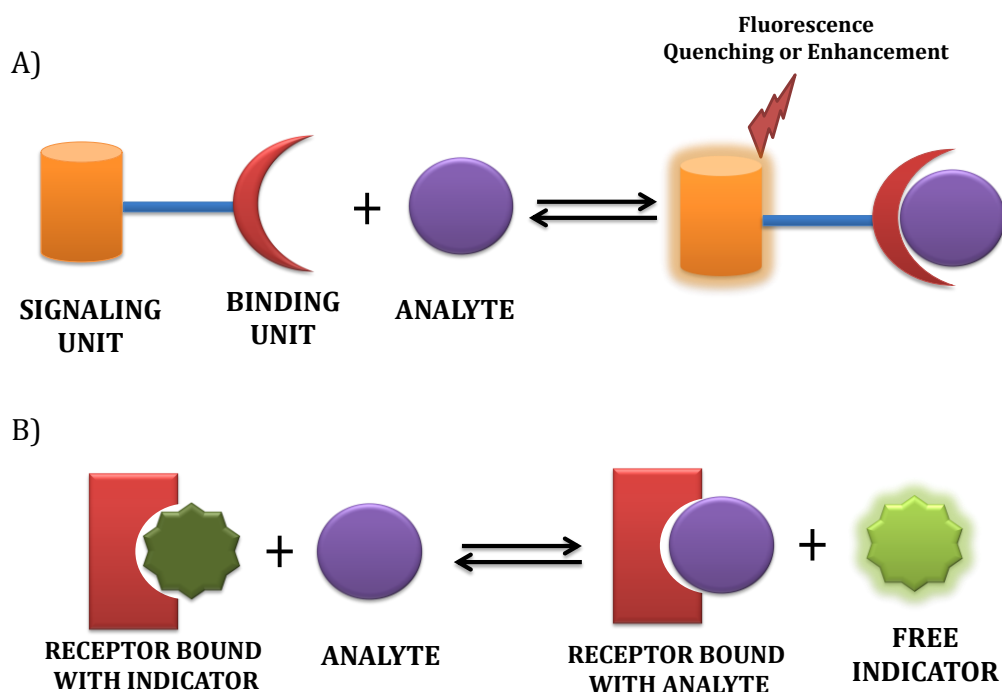


Figure 1.1. Schematic representation of the A) binding site-signalling and B) displacement approaches employed in the development of the fluorescent probes.

The displacement approach^{6c} (Figure 1.1B), on the other hand, is based on the formation of binding site-signalling subunit “molecular ensembles” through non-covalent interactions. The introduction of the analyte leads to regeneration of spectroscopic behaviour of the non-coordinated indicator. In other words, the indicator is displaced from the binding site upon the addition of analyte, resulting in a change from a coordinated to non-coordinated state. An appropriate choice of an indicator can be achieved based on its favourable photophysical properties and also higher affinity constant towards the signalling unit, when compared to that of the analyte of interest. A third approach called “chemodosimetric approach” (Figure 1.2), which relies on the occurrence of specific, most often irreversible chemical

reactions,^{6d} that occur upon interactions with the analyte. Such reactions lead to the formation of a product with an observable signal output (fluorescence), that can be directly related to the analyte concentration.

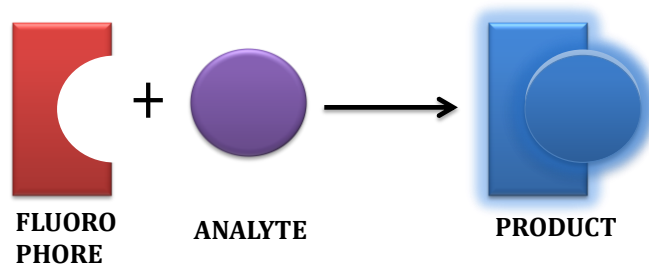


Figure 1.2. Schematic representation of the chemodosimeter approach employed in the development of the fluorescent probes.

1.3. MECHANISM OF FLUORESCENCE DETECTION

A number of signalling mechanisms have been developed and are currently widely used for the detection of various analytes through fluorescence technique. These include; photoinduced electron transfer (PET),⁷ charge transfer (CT),⁸ fluorescence resonance energy transfer (FRET),⁹ through-bond energy transfer (TBET),¹⁰ and excimer formation.¹¹ In fact, to-date, the fluorescent probes have been effectively used for the quantitative determination of several target analytes as well as the fluorescence imaging of toxic substances associated with various human diseases. Recently, besides the conventional methods, a number of new emerging design principles have also been utilized in the fluorescence detection. For example, the conformational restriction of small organic molecules causes significant changes in photophysical properties, especially, fluorescence intensity or lifetimes and due

to which this strategy has received considerable attention in recent times. The emerging sensing mechanisms based on the conformational restriction of the molecules comprise aggregation induced emission (AIE),¹² excited state intramolecular proton transfer (ESIPT)¹³, C=N isomerisation¹⁴ etc. have been the subjects of intensive investigations. The following sections mainly focus on the sensing mechanisms primarily based on the photoinduced electron transfer, energy transfer and aggregation induced emission, because these strategies have been efficiently utilized for recognition of a variety of important targets/analytes.

1.3.1. Photoinduced Electron Transfer

Among the various mechanisms, the photoinduced electron transfer (PET), has been the most widely applied strategy for the development of the fluorescent probes. Upon excitation of the fluorophore, an electron of the highest occupied molecular orbital (HOMO) is promoted to the lowest unoccupied molecular orbital (LUMO), which enables PET from HOMO of the donor (analyte-free receptor) to that of the fluorophore, causing fluorescence quenching of the latter. However, the interaction with the analyte, the redox potential of the donor becomes altered so that the relevant HOMO becomes lower in energy than that of the fluorophore; thus, disrupting the PET with the concomitant enhancement in fluorescence intensity (Figure 1.3).^{7c} The chemosensors have the advantage of PET mechanism in such a way that the presence of analyte induces the alteration of energy levels between HOMO and LUMO, which results in quenching or enhancement of emission intensity.

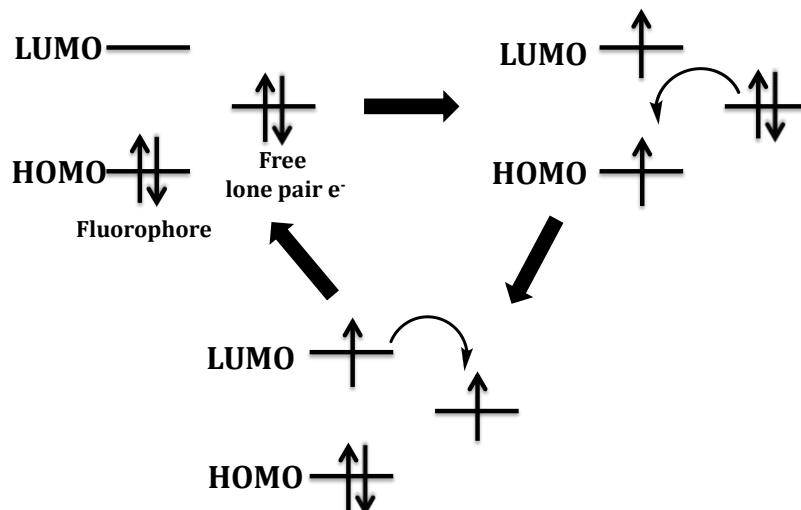


Figure 1.3. Photoinduced electron transfer (PET) process with participation of HOMO and LUMO of the fluorophore as well as an external molecular orbital of the analyte.

The anthracene based probe **1**,^{15a} for example, showed a remarkable enhancement in the emission intensity, in the presence of the phosphate ions at pH 6. At this pH, both the polyamine and the phosphate groups were partially protonated. The fluorescence enhancement observed could be attributed to a favourable intra-complex proton transfer that led to the protonation of the benzylic amine group (Figure 1.4). The alternative explanation could be due to the formation of the hydrogen bonding between the lone pair of the benzylic nitrogen with the hydroxy group of the phosphate anions, thereby resulting in the inhibition of PET process. On the other hand, the probe **2** illustrates the tuning of the selectivity towards anions by controlling the topology of the binding site, without changing the signalling unit. Thus, the probe **2** was able to bind preferentially to the

pyrophosphate over the other phosphate ions.^{15b} The two polyammonium arms of the probe were geometrically inclined for the six external oxygen atoms of the pyrophosphate anion. However, the recognition mechanism was found to be similar to that of the probe **1**. In the case of metal ion recognition, this effect was referred to as chelation-enhanced fluorescence (CHEF) that has been quite well exploited for the detection of various ions in the literature.^{15c}

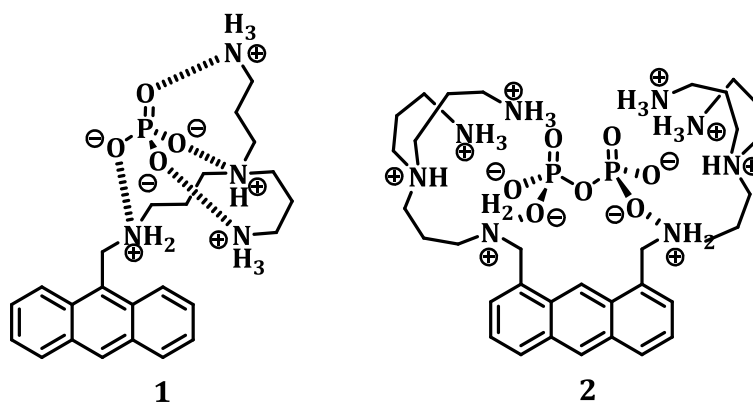


Figure 1.4. Binding pattern of the photoinduced electron transfer based probes **1** and **2** with phosphate and pyrophosphate anions, by means of the hydrogen bonding interactions, respectively.

1.3.2. Energy Transfer Mechanism

The energy transfer based probes have attracted much attention due to their immense applications in biology. This strategy comprises of mechanisms such as fluorescence resonance energy transfer (FRET) and through-bond energy transfer (TBET), which involve energy transfer between a pair of fluorophores that act as energy donors and acceptors, respectively.⁹ As adapted in the sensing

applications, the emission of the donor at a relatively short wavelengths activates the emission of the acceptor at the longer wavelengths with the ratio of these two emissions modulated by the target analyte. In these cases, substantial spectral overlap between the donor emission and the acceptor absorption bands is essential to observe a high FRET efficiency.^{9a} As a consequence; FRET-based dyads were typically linked by a non-conjugated spacer to involve the energy transfer reaction occurring through the space (Figure 1.5A). However, in the case of TBET-based systems, the donor and acceptor were linked through an electronically conjugated bond, which prevents the donor and acceptor units from becoming planar. In these cases, the energy transfer can occur through covalent bonds without having substantial spectral overlap between the donor and acceptor chromophores (Figure 1.5B).^{9b}

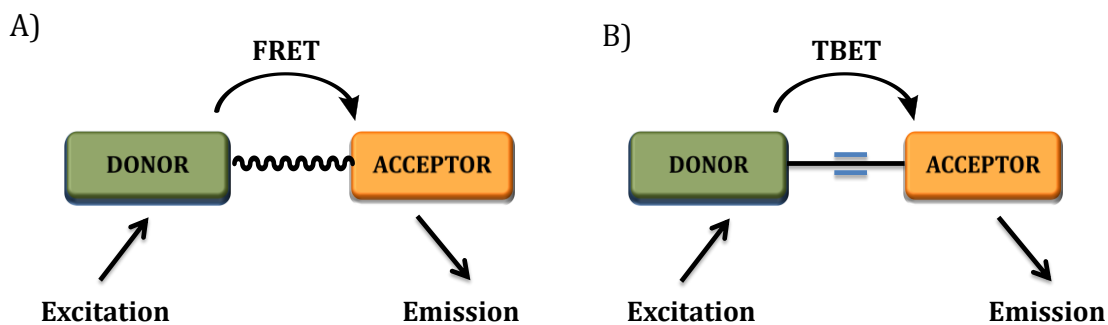


Figure 1.5. Schematic representations showing A) fluorescence resonance energy transfer (FRET) (or through space) and B) through-bond energy transfer (TBET) processes.

Subsequent to these pioneering efforts, several efficient FRET/TBET-based fluorescent probes have been designed for the detection of various analytes. For

example, Han and co-workers¹⁶ have designed a ratiometric probe **3** for the detection of the Zn²⁺ ions in which fluorescein and rhodamine chromophores act as fluorescence donor and acceptor, respectively. In the absence of the Zn²⁺ ions, rhodamine exists in the form of spirolactam with negligible absorption in the visible region and thus unable to act as an acceptor. When excited at 485 nm, the probe **3** (Chart 1.1), exhibited only green emission at 518 nm, corresponding to that of the fluorescein chromophore. However, upon complexation with the Zn²⁺ ions induced the opening of the spirolactam and generation of a new absorption band at 560 nm. Such a transformation has resulted in changes of the fluorescence intensity ratio at 590/518 nm. Thus the ratiometric fluorescence signal changes of the probe observed was based on an intramolecular fluorescence resonance energy transfer (FRET) mechanism, which was modulated by a specific metal ion induced ring-opening of the rhodamine spirolactam.

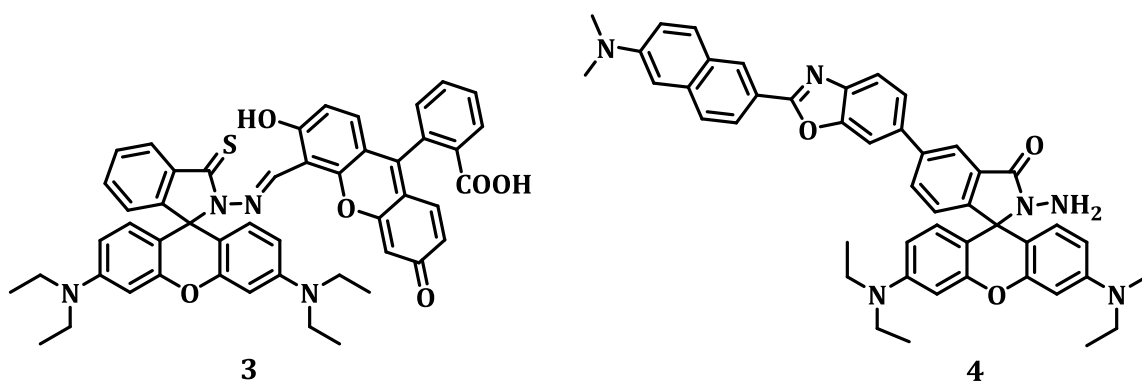


Chart 1.1. The reported rhodamine based ratiometric probes **3** and **4** for cations.

When used in a TBET system, the rhodamine ring-opening process activates a through-bond energy transfer mechanism. This has been successfully demonstrated by Tan and co-workers,¹⁷ who have developed a two-photon

fluorophore probe **4** (Chart 1.1). This probe comprises D- π -A-structured naphthalene derivative and a rhodamine B fluorophore, connected directly through a conjugated bond to form a TBET system. The probe **4** exhibited selectivity for the Cu²⁺ ions, which was modulated ratiometric two-photon fluorescence response having significant efficient energy transfer of *ca.* 94% and two well-resolved emission peaks separated by 100 nm. The selectivity experiments have indicated that only the Cu²⁺ ions trigger the probe's ring opening, while other competitive ions showed no perceptible effect, thereby demonstrating the high selectivity of the probe. Due to its excitation wavelength in the near infra-red region (NIR), the probe **4** was also utilized for the two-photon imaging of living cells and tissues and showed high ratiometric imaging resolution for the detection for the Cu²⁺ ions.

1.3.3. Aggregation Induced Emission (AIE)

Many organic fluorophores, in their aggregated form, show quenched fluorescence emission and this effect is denoted as aggregation-caused quenching (ACQ) mechanism.¹⁸ Due to this, the applications of many organic fluorophores as sensing materials (chemosensors, biosensors) and as organic light-emitting diodes (OLEDs) have been excessively limited.^{12a} To subdue the ACQ effect, bulky cyclic species, branched chains, and dendritic wedges have been covalently attached to the fluorophores to suppress the formation of the aggregates.¹⁹ Interestingly, Tang and co-workers,²⁰ in 2001, have reported an unusual fluorescence enhancement from a solution of the compound 1-methyl-1,2,3,4,5-pentaphenylsilole (**5**) (Chart 1.2), which was then termed as aggregation induced emission (AIE). The fluorescence

quantum yield (Φ_F) of the probe **5** in pure ethanol was 0.063 ± 10^{-3} , but substantially increased to 0.21 when the water fraction was increased to *ca.* 90%. After a series of experiments, the authors have identified that the restriction of intramolecular rotation (RIR) in the aggregates was the main reason for the observed AIE phenomenon. Similarly, tetraphenylethylene **6** (Chart 1.2), due to its propeller-like molecular conformation induced free intramolecular rotation, and thus making it as an AIE active molecule. Upon aggregation, the probe **6** showed effective RIR and thereby significant enhancement in the emission intensity was observed.^{12a}

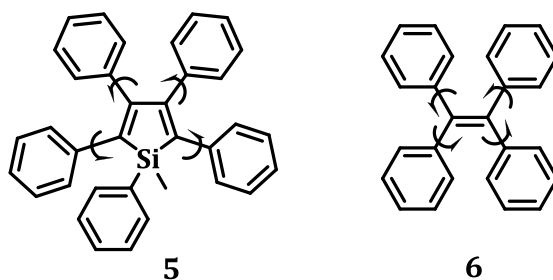


Chart 1.2. First examples of aggregation induced emission (AIE) active pentaphenyl silole **5** and tetraphenylethylene **6** (TPE) molecules reported in literature.

The AIE phenomenon has been successfully utilized to design sensitive and selective bio/chemosensors owing to such unusual fluorescence enhancement. The aggregation of the AIE molecules can be controlled by guest molecules through electrostatic, coordination and hydrophobic interactions, steric hindrance as well as the influence of polarity and viscosity of the medium. For example, the amphiphilic silole derivative **7** bearing a positive ammonium moiety was developed, which showed AIE effect. Interestingly, this probe was combined with hydrophobic heptylanilide **8** to produce a fluorescence “turn-on” sensor for the cyanide ions in

the aqueous solution.²¹ As shown in Figure 1.6, the sensing mechanism was based on an intermolecular assembly process, where the probe **8** was essentially hydrophobic because of the presence of alkyl chains. The nucleophilic addition of the cyanide ions to the trifluoroacetyl group of the probe yielded a water soluble amphiphilic species. Such a reaction induced the aggregation of the amphiphilic species **7** involving hydrophobic and electrostatic interactions. Consequently, upon addition of the cyanide ions to a mixed solution of the systems **7** and **8**, led to the significant enhancement in the fluorescent intensity of the

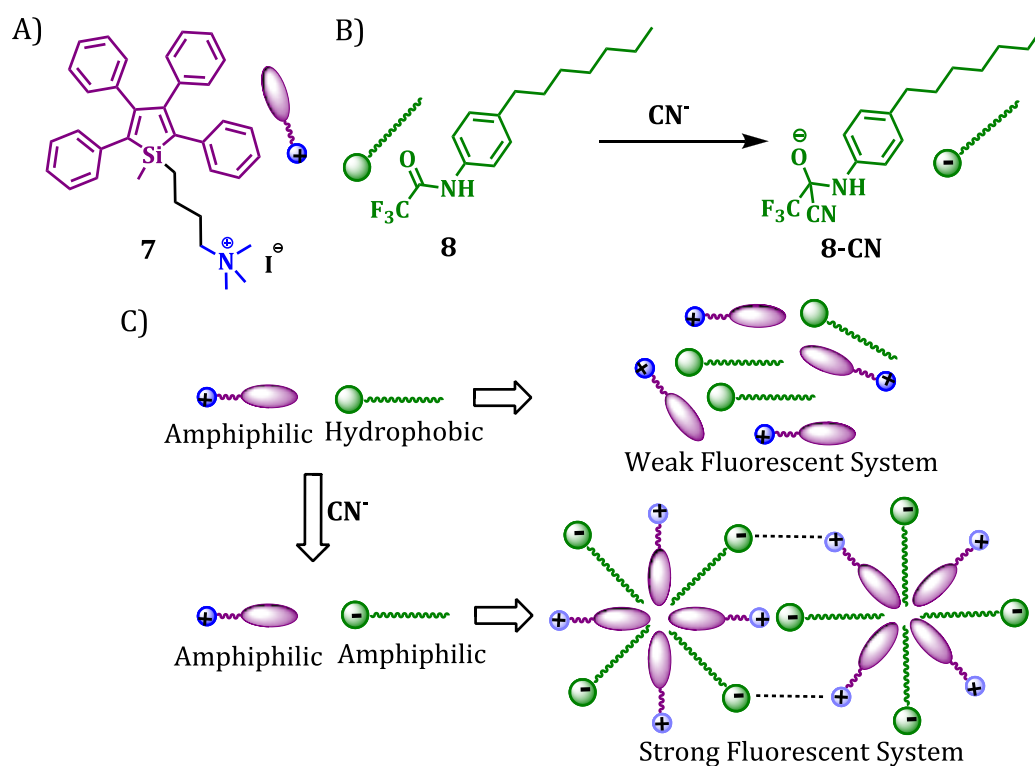


Figure 1.6. A) Chemical structure of a silole derivative **7** having an ammonium group. B) Chemical structure of the heptylanilide **8** and its reaction with cyanide. C) Illustration of the design rationale for the fluorescence "turn-on" detection of the cyanide ions by AIE mechanism.

ensemble system. Moreover, this ensemble also showed good selectivity towards the cyanide ions over other competent inorganic anions.

1.4. TYPES OF TARGETS AND DETECTION

The design of probes for the selective detection of various suitable guests such as anions, metal cations, neutral molecules and biomolecules has been quite challenging and fundamentally an interesting area of research.^{22a,b} This is due to the fact that the recognition of the neutral molecules and ions is important since many of them are involved in various biological and chemical processes. For example, cations such as Na^+ , K^+ , Ca^{2+} , and Zn^{2+} and anions such as carboxylates, halides, cyanide and phosphates are involved in various biological processes such as nerve impulses, muscle contraction, cell activity regulation, and so on.^{22c} These ions are also important for critical care analyses and as markers for various diseases. However, such analysis is not limited to small ions, as the monitoring of small and medium-sized molecules, or even larger biomolecules, has become of vital importance, particularly in medical diagnoses as well as in monitoring various types of illness.^{22d} Moreover, developing accurate and appropriate methods for the monitoring of the environmental samples has become an important area of research, as changing lifestyles have led to drastic increase in the environmental pollution, besides discharge of such ions and other pollutants from industry.²³ Consequently, the need for developing sensitive techniques and effective fluorescent probes for selective recognition and quantification through either a single measurement or continuous monitoring of these analytes is of great current interest.

1.4.1. Recognition of the Anions

A large number of anions play a pivotal role in a variety of biologically important processes such as the transport of hormones, proteins biosynthesis, DNA regulation, and also associated with several diseases. Therefore the development of probes for the detection ions under biological conditions has been an active area of research. Of the various probes reported, the design of fluorescent probes for the anions with high sensitivity and selectivity is quite challenging due to their strong hydration effects of the anions under aqueous conditions. In this regard, various probes have been developed which involved different interactions such as electrostatic interactions, hydrophobic, π -stacking and coordinative interactions.

Of the various strategies adopted, the design of probes that involve electrostatic interactions between the anions and positively charged receptors were generally found to be reversible. In this context, derivatives of the polyamines and substituted imidazolium systems have been used to construct the fluorescent probes (binding-site signalling approach) for the recognition. For example, Kumar and co-workers²⁴ have reported a imidazolium based probe **9** (Chart 1.3) as a highly selective fluorescent probe for the perchlorate ions. This probe exhibited fluorescence quenching in presence of the ClO_4^- ions among a number of other anions tested, and it can be used for the detection of the same in drinking water.

The complexation with metal ions (displacement approach) is another important approach that has been used for designing the probes for various anions.

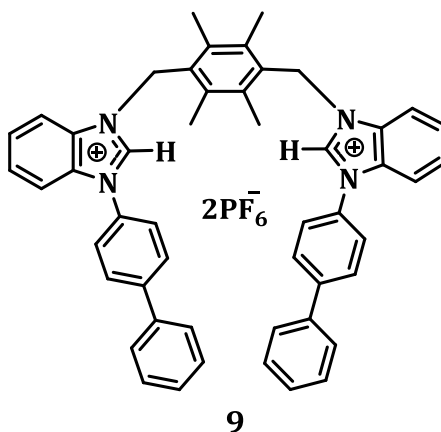


Chart 1.3. The chemosensor **9** used for the recognition of perchlorate anions (ClO_4^-).

in which, a metal ion complex is utilized as a receptor. The strong binding affinity of the metal ion for the negatively charged anions led to the formation of a complex through the competitive displacement, and concomitantly resulting in significant spectroscopic signal changes.²⁵ This strategy has been found to overcome the competing and challenging hydration effect and thereby allowed the anion detection even in the aqueous conditions.²⁶ In the strategy of competitive displacement assay using the complex, a receptor–reporter ensemble is used as a probe, and the receptor binds to an analyte more strongly than the reporter, thus, causing the release of the reporter and hence an irreversible changes were observed.

Anslyn and co-workers²⁷ have proposed for the first time a fluorescent probe for the detection of the citrate ions in the aqueous medium. This probe was synthesised by assembling the reporter (5-carboxyfluorescein) (**10**) and receptor containing three guanidinium groups (**11**), as depicted in Figure 1.7. The strong

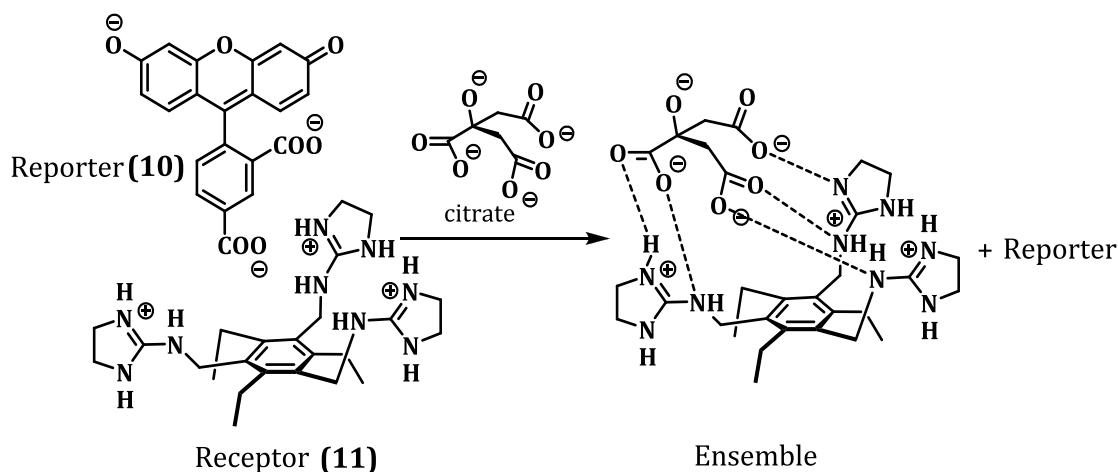


Figure 1.7. The chemosensing ensemble formed between the conjugates **10** and **11**, which has been utilized for the detection of citrate ions in the aqueous medium.

interactions between the receptor and reporter, lowered the pK_a of the phenol moiety of the reporter, causing its deprotonation under these conditions. Upon reaction of the probe with the citrate ions, the reporter was released as a phenol-protonated species *via* competitive displacement complexation. This resulted in decrease in the reporter's fluorescence intensity, which allowed the quantitative analysis of the citrate ions. The probe was found to be selective for the citrate ions when compared to the dicarboxylic and monocarboxylic acids in water and has also been used to determine the citrate concentration in commercial beverages. Similarly, the authors have developed several chemosensing ensembles for the detection of various organic or inorganic ionic systems, such as tartrate,^{28a} phosphate,^{28b} amino acids,^{28c,d} and carboxylates.^{28e}

In 2008, Tang and co-workers,²⁹ have reported few polyacetylene bearing imidazole moieties as a part of the side chain as a sensory polymer **12** for the

selective recognition of the Cu^{2+} ions based on the “turn-off” fluorescence mechanism with a detection limit of 1.48 ppm (Figure 1.8). Interestingly, the quenched fluorescence of the probe **12** by the Cu^{2+} ions could be “turned on” after the addition of the CN^- ions, at concentrations *ca.* 7.0×10^{-5} M. Thus, by employing the “turn-off” and “turn-on” cycle, the probe **12** was effectively utilized as a selective and sensitive chemosensor for the Cu^{2+} and CN^- ions. Interestingly, the detection of the CN^- ions by the probe **12** in the solid state was also achieved, by dipping the film into the aqueous copper nitrate solution to yield the “turn-off” state, then into aqueous CN^- solution to recover the fluorescence intensity.

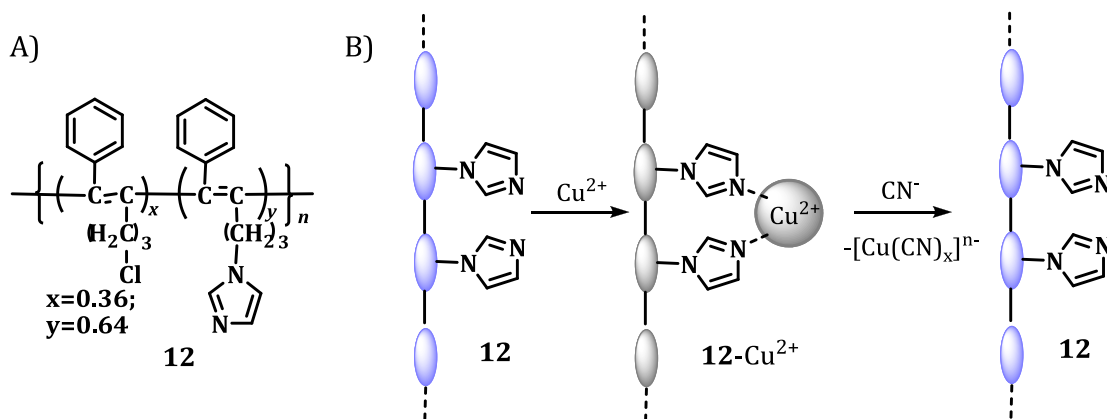


Figure 1.8. A) Structure of a polyacetylene polymer probe **12**. B) Schematic representation of detection of the Cu^{2+} and CN^- ions by the probe based on the fluorescence “turn-off” and “turn-on” mechanism.

To improve the selectivity of detection of the various anions, the chemodosimetric approach involving the cleavage or formation of the covalent bonds has received much attention in recent years.³⁰ The nucleophilic reaction of some of the anions (e.g., F^- and SO_3^{2-}) can lead to the cleavage of the covalent bond

between a removable group (usually electron-deficient group) and a fluorophore, and the observed spectroscopic signals can be utilised for the recognition. By employing the high affinity of silicon towards the fluoride ions, Hong and co-workers³¹ have reported a chemodosimetric probe **13** for detection of the F⁻ ions, whose response mechanism was based on the F⁻ ions mediated cleavage of the Si-O bond (Figure 1.9). The dosimeter **13**, has showed drastic dual changes in absorption and emission properties, selectively with the F⁻ ions over other competitive anions.

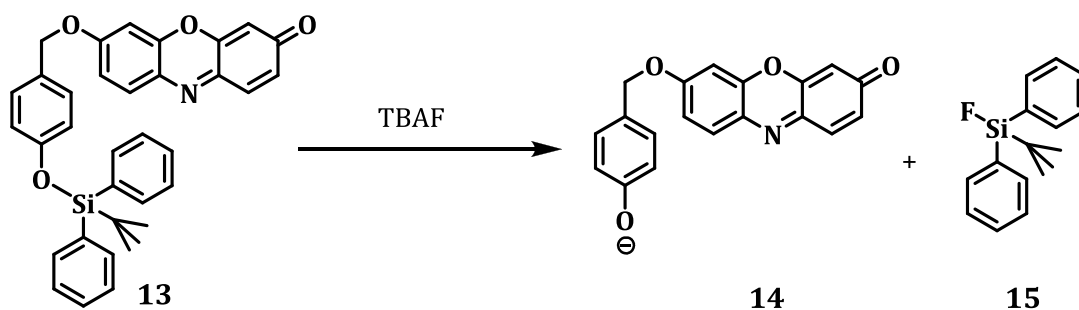


Figure 1.9. Probable mechanism proposed for the spectroscopic changes observed with the probe **13** in the presence of the F⁻ ions.

The formation of covalent bonds has also been used to develop probes for the selective detection of various anions. The chemical reactions such as nucleophilic addition, Michael addition and rearrangements have been used extensively for the sensitive and selective recognition of the anions. For example, Zhao and co-workers^{32a} have demonstrated the utilization of the probe **16** (Chart 1.4) as a substrate for the Michael addition of the bisulfide (HS⁻) ions. Such a reaction was extended to measure the concentration of the analyte in mice blood plasma and also in brain tissues. Similarly, on the basis of the addition of the cyanide

(CN⁻) ions to trifluoromethyl carbonyl group, Li and co-workers^{32b} have reported a coumarin based system **17** (Chart 1.4) for the detection of the CN⁻ ions. The probe **17** exhibited a fast reaction with the CN⁻ ions in acetonitrile/water mixture, with a significant enhancement in fluorescence intensity due to the increased intramolecular charge transfer process.

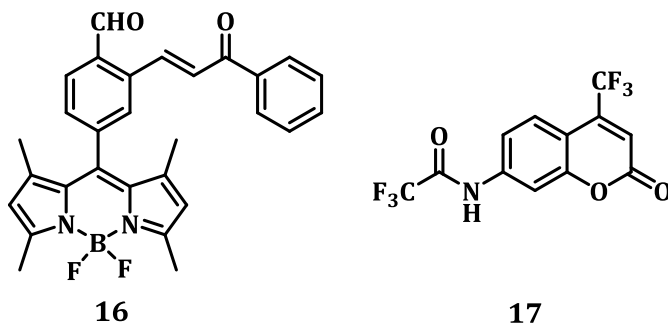


Chart 1.4. The chemodosimeters **16** and **17** reported for the detection of bisulfide and CN⁻ ions.

1.4.2. Detection of the Cations

As in the case of the anions, the recognition of the cations has attracted much attention due to their importance in chemistry, biology and environmental sciences. The monitoring of the metal ions such as Na⁺, K⁺, Mg²⁺ etc., in blood and urine is important for the diagnosis of various diseases. With regard to the toxicity of the metal ions, it is well known that above optimal concentrations, the heavy metal ions such as mercury, lead, cadmium are potential threats to living organisms. Henceforth, the selective and sensitive detection of the metal ions is highly desirable. The general approaches reported for the detection of the metal ions are

mostly based on: (a) appropriate ring/cavity sizes for alkali and alkaline earth metal ions; (b) suitable ligands for convenient formation of five- and six-membered ring complexes with metal ions; and (c) soft-hard acid-base principle, such as the soft sulfur-containing receptors with high affinity for soft metal ions. Moreover, while designing such probes, the photophysical processes like PET, ICT or FRET have been appropriately integrated to translate analyte binding into a signal transduction.

A successful demonstration, in this regard, was shown by He and co-workers³³ using a PET based probe **18** (Chart 1.5) with triazacryptand as a recognition chromophore for the K⁺ ions. The complexation of the probe **18** with the K⁺ ions resulted in increase in the fluorescence intensity at 540 nm, and this response was highly selective for the K⁺ ions over Na⁺ ions. The probe responded rapidly as well as reversibly and can be used to monitor the change of extracellular concentration of the K⁺ ions (e.g. in serum and blood samples), with no interference

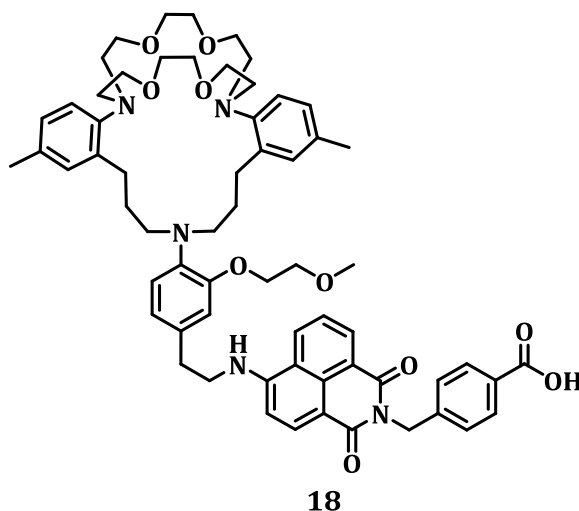


Chart 1.5. Naphthalimide-triazacryptand conjugate **18** reported as a chemosensor for the detection of the K⁺ ions.

from the cellular $\text{Ca}^{2+}/\text{Na}^{+}$ ions or pH was observed. Interestingly, the probe thus developed for the K^{+} ions as a chemosensor is being marketed by M/s Roche OPTI CCA as a commercially available whole blood analyser.

It may be noted that the concentrations of the transition metal ions, including the important Cu^{2+} , Fe^{3+} , and Zn^{2+} ions are extremely low (usually $<10^{-7}$ M) under biological conditions. Thus, the designed probes for these ions should have high sensitivity for their practical applications. Recently, a new ratiometric fluorescent probe **19** (Chart 1.6) was reported for the detection of the Cu^{2+} ions, *via* integrating a 1,8-naphthalimide moiety with the 8-aminoquinoline chromophore.^{34a} This probe exhibited a highly selective ratiometric response to the Cu^{2+} ions over other transition metal ions in the aqueous media by formation of a 1:1 complex having a dissociation constant (K_d) value of *ca.* 34.5 μM . The potential of the probe was also demonstrated for the intracellular imaging the Cu^{2+} ions in MCF-7 cells.

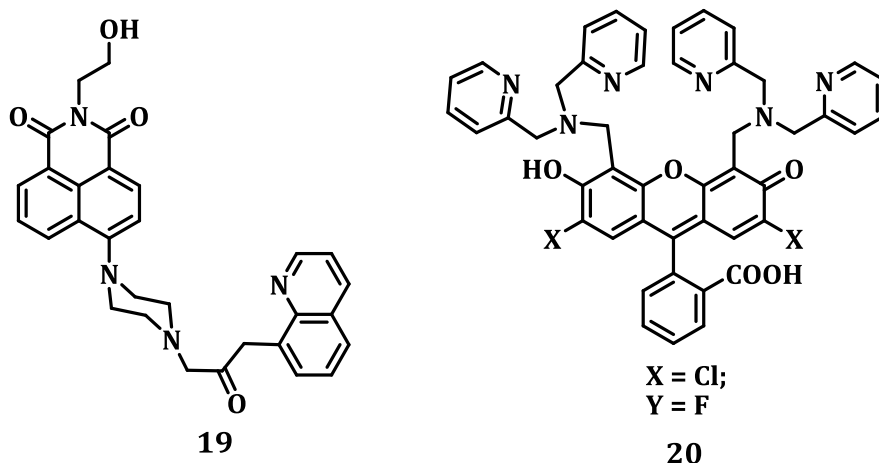


Chart 1.6. The ratiometric chemosensors **19** and **20** developed for the recognition of the transition metal ions.

The complexation unit such as di-2-picolylamine (DPA) is considered to be the most popular receptor which has been exploited for the detection of the Zn^{2+} ions. The secondary amine nitrogen atom of DPA serves as a good reaction site for linking of various fluorophores. Furthermore, this unit can help in effective signal transduction process to respond to the binding events through PET or ICT mechanisms. For example, Lippard and co-workers^{34b} have reported the probe **20** (Chart 1.6) having fluorescein moiety as the emitter, which showed selective interactions with the Zn^{2+} ions over the Ca^{2+}/Mg^{2+} ions. These authors have also reported a fluorescein-based probe **21** (Chart 1.7) by appending a thioether-rich receptor to the xanthenone moiety and it exhibited the selective interactions with the Hg^{2+} ions.^{35a} This probe was non-fluorescent due to the efficient PET process from the aniline moiety to the fluorescein unit. However, upon coordination of **21** with the Hg^{2+} ions, resulted in the enhancement in the fluorescence intensity with a sensitivity of 2 ppb in the buffered aqueous solution. Further, the same authors have developed several ratiometric fluorescent probes based on seminaphthofluoresceins

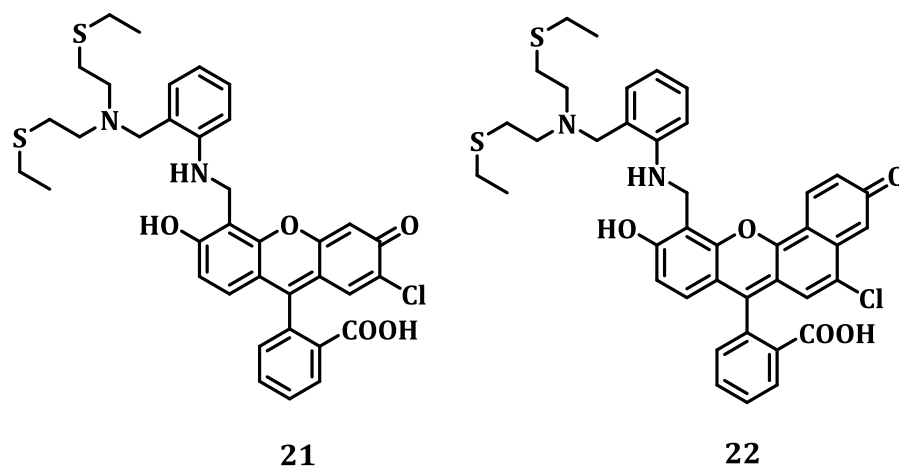


Chart 1.7. Fluorescein based probes **21** and **22** reported for the Hg^{2+} ions.

for example **22** (Chart 1.7), whose selectivity for the Hg^{2+} ions was similar to that of the probe **21**.^{35b,c} Analyses of natural water samples spiked with mercuric salts indicated that the probe **22** rapidly complexes with the Hg^{2+} ions, thereby demonstrating its potential applications. In addition to the direct complexation (i.e. binding site-signalling approach), the chemodosimeters based on S/Se have also been developed for the Hg^{2+} ions. Ma^{36a} and Xu and co-workers^{36b} have reported a rhodamine B thiolactone **23** which exhibited a dual colour change and fluorescence “off-on” in the presence of the Hg^{2+} ions. This probe exhibited ring-opening reaction triggered by the complexation with the Hg^{2+} ions. Interestingly, by introducing KI into the system,

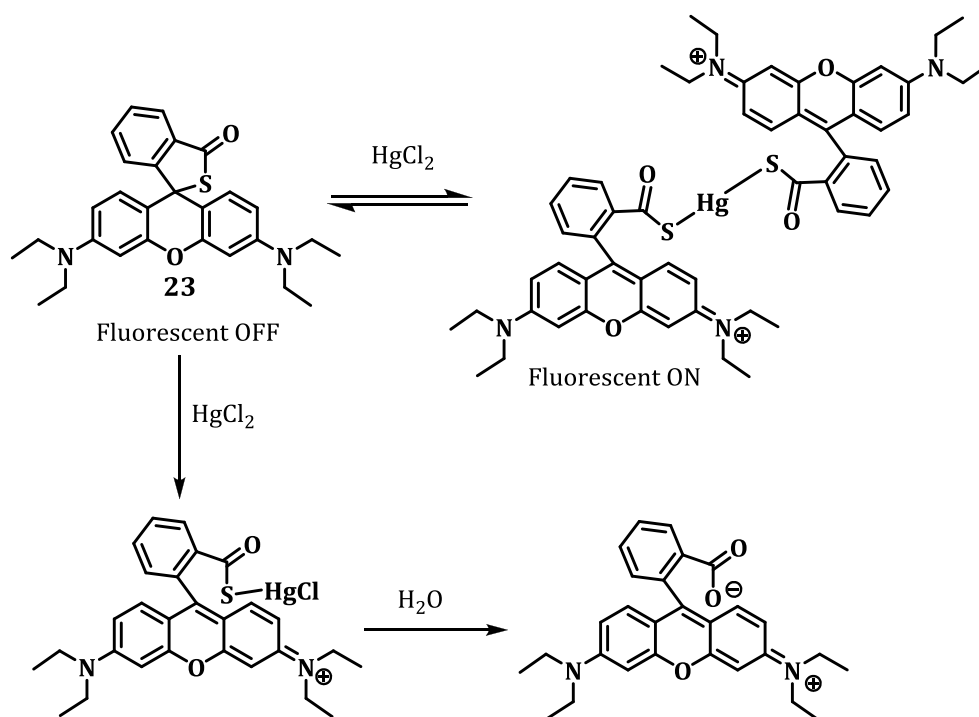


Figure 1.10. Proposed reaction mechanism of the chemodosimeter **23** in the presence of the Hg^{2+} ions.

the authors could reverse the reaction with only ≤ 0.5 equivalents of the Hg^{2+} ions, but restored when treated with higher equivalents. By employing the ESI-MS analytical data, the authors have deduced the mechanism as shown in Figure 1.10. This probe was highly selective for the Hg^{2+} ions over other commonly available ions with a detection limit of 20 nM and can also be utilized to image the Hg^{2+} ions in *Arabidopsis thaliana* (Mouse ear cress).^{36c}

1.4.3. Recognition of the Biomolecules

The understanding of structural features of the biomolecules of interest is essential for designing of molecular receptors or probes. These structural features would determine the type of non-covalent interactions it can undergo and to attain high degree of selectivity.³⁷ Despite the fact that, non-covalent interactions are not as stronger as covalent bonds, the cooperative effect of these interactions would aid and ultimately strengthen the selective recognition process.^{37b} Thus, the multifaceted receptors having different binding motifs, capable of utilizing one or more types of the non-covalent interactions are expected to act as selective and efficient molecular probes. The design of receptors for the selective recognition of the biomolecules and study of the different types of the non-covalent interactions in such a recognition event has attracted a great deal of attention in recent years.³⁸

In this context, a series of novel functionalised cyclophane derivatives based on the anthracene/pyrene chromophores linked through different bridging units have been reported as potential receptors for different nucleosides and nucleotides.³⁹ Among the various cyclophanes developed, the viologen bridged

cyclophane **24** (Chart 1.8) exhibited selective interactions with nucleotides such as ATP and GTP involving synergistic effects of electrostatic, π - π stacking and hydrophobic interactions inside the cavity. Furthermore, the versatility of this probe was successfully demonstrated for the analysis of ATP and GTP in buffer and blood serum by employing a fluorescence indicator (8-hydroxy-1,3,6-pyrene sulfonate, HPTS). These results have indicated that the non-fluorescent complex formed by the cyclophane **24** with HPTS acts a sensitive fluorescence “turn-on” probe for GTP and ATP, through an indicator displacement mechanism.^{39b} The cyclophane **25** having the imidazolium bridging units, on the other hand, exhibited an unusual dual emission in the aqueous medium arising from the locally excited singlet state of the anthracene chromophore (monomer) and an intramolecular excimer emission.⁴⁰ When DNA was added to this solution, it exhibited a significant enhancement in the red shifted excimer emission intensity. These observations were furthermore exploited for the detection of DNA through the visual changes in the fluorescence intensity of **25** in buffer and under gel electrophoresis conditions.

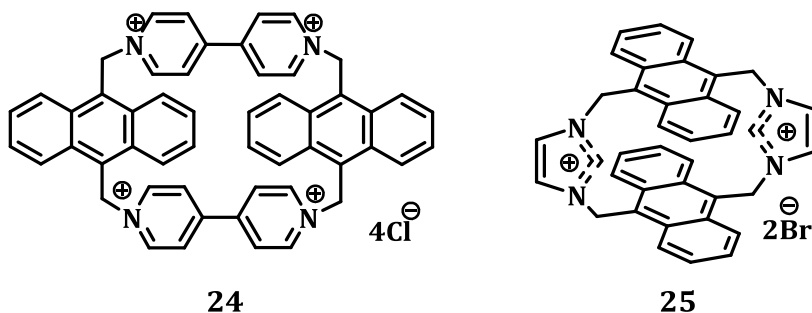


Chart 1.8. The cyclophane based probes reported **24** and **25** for the recognition of ATP, GTP and ds-DNA.

In addition, the pyrene-functionalised oligonucleotides, locked nucleic acids, and molecular beacons (MBs) have also been developed for the ratiometric sensing of the nucleic acids. For example, Schmuck and co-workers⁴¹ have developed a functionalised oligopeptide **26** (Chart 1.9), which showed effective interactions with double-stranded DNA, thereby its potential as a molecular peptide beacon. In this case, the folded form of the pyrene-based peptide beacon **26** showed a typical pyrene excimer emission, whereas in presence of the double stranded DNA, it exhibited a conformational change from a folded form to an extended form. Such a transformation resulted in change of emission from the excimer at 490 nm to the monomer at 406 nm. Thus, monitoring the relative intensities of the two emissions (F_{406}/F_{490}), allowed the detection of the targeted nucleic acids ratiometrically. Moreover, the probe **26** exhibited the selective binding with AT rich polynucleotides over GC counterparts and it was also utilized for the nuclear DNA staining in cells.

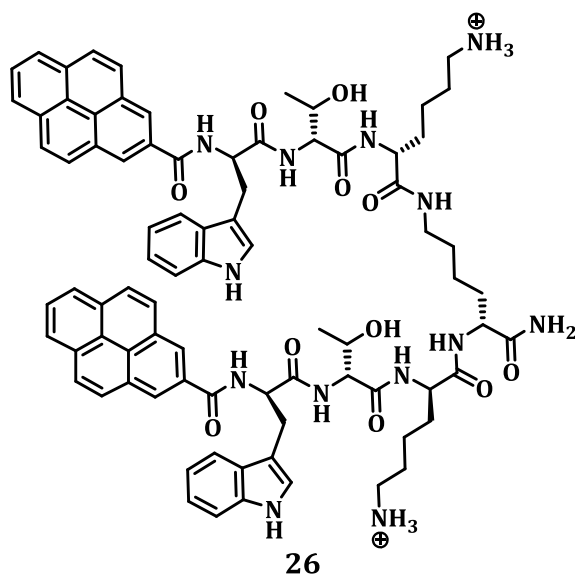


Chart 1.9. The pyrene-peptide beacon **26** developed for the recognition of DNA.

As described above under various sections, the fluorescent probes thus have received considerable attention over the years due to their ultra-high sensitivity, cost-effectiveness, easy handling and also fast response. By exploiting the mechanistic modalities in conjunction with the appropriate fluorophores, analyte-specific receptor interactions, or reactive sites, it has been possible to develop the fluorescent probes that can have practical use in sensing and imaging of toxic substances and essential cellular components, including small chemical species correlated with various human diseases. However, the real-time and on-site analysis of the various analytes under biological conditions is still a challenging task and hence intensive investigations are needed for their recognition.

1.5. OBJECTIVES OF THE PRESENT INVESTIGATION

Development of the functionalised organic systems having favourable photophysical properties and exhibit selective interactions with various analytes has immense significance in diagnostic, medicinal and environmental applications. In this context, our main aim has been to design novel functionalised organic conjugates that can undergo selective interactions with biologically relevant anions, cations and neutral molecules with high sensitivity, so that they can have potential applications as molecular probes. One of the objectives has been to design novel conjugates based on aryl-indolium chromophore, and investigation of their potential as molecular probes for the selective recognition of the anions. Another objective has been to develop novel donor-acceptor based dyads comprising of dansyl and naphthalimide moieties, and systematic investigation of their potential as selective

probes for the biologically relevant metal ions. Yet another objective has been to design the amphiphilic conjugates based on naphthalene imide chromophore and investigation of their self-assembly and interactions with various biomolecules.

Our results indicate that the aryl-indolium systems exhibited favourable photophysical properties and exhibited selective and sensitive interactions with cyanide ions, involving nucleophilic addition reaction, when compared to other biologically relevant anions. We have also extended the potential of these probes for the on-site analysis by coating on various substrates such as alumina, filter paper and polymer matrix. Furthermore, we have also performed the detection of the endogenous cyanide ions present in natural sources such as Indian almonds. With regard to the dansyl-naphthalimide dyads, interestingly, these systems acted as ratiometric fluorescence molecular probes for the recognition of Cu^{2+} and Zn^{2+} ions. Our results indicated that the lower homologues (methylene spacer group of $n=1-3$) of the dyad series showed interactions with both Cu^{2+} and Zn^{2+} ions, while the dyads with longer spacer groups (methylene spacer group of $n=4-5$) exhibited interactions only with Cu^{2+} ions and thereby demonstrating their potential use as ratiometric fluorescence probes.

The amphiphilic conjugates thus investigated based on naphthalene imide chromophore exhibited favourable self-assembly properties, including good affinity for DNA as confirmed through photophysical, biophysical and microscopic techniques. Of these conjugates, the bolamphiphilic naphthalene diimide (NDI) conjugate formed the vesicular structures in the aqueous medium at and above

critical aggregate concentration and which in turn showed selective encapsulation of the hydrophobic dye molecules. Interestingly, in the presence of DNA, we observed the disassembly of these vesicular structures and such a transformation could be utilized for the selective encapsulation and release of hydrophobic molecules using DNA as stimuli. Overall, the functionalised organic conjugates investigated showed interesting properties depending on the nature of the chromophores and spacer groups present and thereby exhibited their potential use as molecular probes for the recognition of cyanide, Cu^{2+} and Zn^{2+} ions and carriers of hydrophobic molecules.

1.6. REFERENCES

1. a) A. P. de Silva, H. Q. N. Gunaratne, T. Gunnlaugsson, A. J. M. Huxley, C. P. McCoy, J. T. Rademacher and T. E. Rice, *Chem. Rev.*, **1997**, *97*, 1515; b) J.-M. Lehn, *Angew. Chem., Int. Ed.*, **1988**, *27*, 89; c) A. W. Czarnik, *Acc. Chem. Res.*, **1994**, *27*, 302.
2. a) R. Martínez-Mañez and F. Sancenón, *Chem. Rev.*, **2003**, *103*, 4419; b) R. Martinez-Manez and F. Sancenon, *Coord. Chem. Rev.*, **2006**, *250*, 3081; c) H. Kobayashi, M. Ogawa, R. Alford, P. L. Choyke and Y. Urano, *Chem. Rev.*, **2010**, *110*, 2620.
3. L. Prodi, *New J. Chem.*, **2005**, *29*, 20.
4. a) L. Prodi, F. Bollta, M. Montalti and N. Zaccheroni, *Coord. Chem. Rev.*, **2000**, *205*, 59; b) O. S. Wolfbeis in *Fibre Optic Chemical Sensors and Biosensors*; CRC Press: Boca Raton, **1991**, Vols. 1 and 2; c) G. Orellana and M. C. Moreno-Bondi

- in *Frontiers in Chemical Sensors: Novel Principles and Techniques*, Springer: New York, **2005**.
5. a) J. Janata, *Chem. Rev.*, **2008**, *108*, 327.
 6. a) E. M. Maria, R. Martinez-Manez and F. Sancenon, *Chem. Soc. Rev.*, **2011**, *40*, 2593; b) R. Bissell, A. P. de Silva, P. H. Q.N. Gunaratne, P. L. M. Lynch, G. E. M. Maguire and K. R. A. S. Sandanayake, *Chem. Soc. Rev.*, **1992**, *187*; c) S. L. Wiskur, H. Aït-Haddou, J. J. Lavigne and E. V. Anslyn, *Acc. Chem. Res.*, **2001**, *34*, 963; d) R. Martínez-Máñez and F. Sancenón, *Coord. Chem. Rev.*, **2006**, *250*, 3081.
 7. a) T. Gunnlaugsson, H. D. P. Ali, M. Glynn, P. E. Kruger, G. M. Hussey, F. M. Pfeffer, C. M. D. Santos and J. Tierney, *J. Fluoresc.*, **2005**, *15*, 287; b) Z. C. Xu, J. Yoon and D. R. Spring, *Chem. Soc. Rev.*, **2010**, *39*, 1996; c) J. S. Kim and D. T. Quang, *Chem. Rev.*, **2007**, *107*, 3780.
 8. a) Q. Zhao, F. Y. Li and C. H. Huang, *Chem. Soc. Rev.*, **2010**, *39*, 3007; b) W. Rettig and R. Lapouyade, Fluorescence probes based on twisted intramolecular charge transfer (TICT) states and other adiabatic photoreactions, in *Topics in Fluorescence Spectroscopy, Probe Design and Chemical Sensing*, ed. J. R. Lakowicz, Plenum Press, New York, **1994**, vol. 4, p. 109.
 9. a) K. E. Sapsford, L. Berti and I. L. Medintz, *Angew. Chem., Int. Ed.*, **2006**, *45*, 4562; b) H. J. Carlson and R. E. Campbell, *Curr. Opin. Biotechnol.*, **2009**, *20*, 19; c) Y. Feng, J. Cheng, L. Zhou, X. Zhou and H. Xiang, *Analyst*, **2012**, *137*, 4885;
 10. J. Fan, M. Hu, P. Zhan and X. Peng, *Chem. Soc. Rev.*, **2013**, *42*, 29.

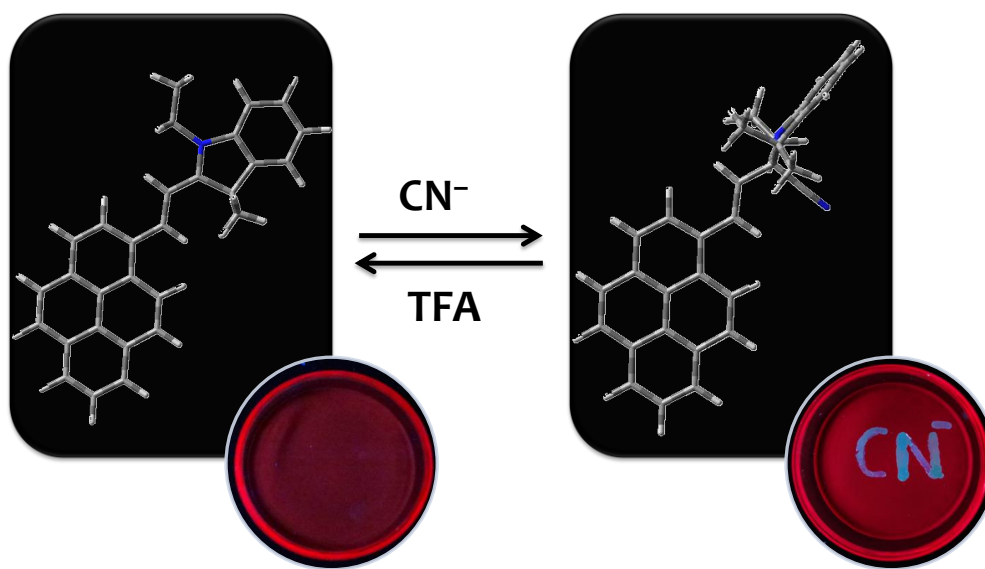
11. C. Lodeiro and F. Pina, *Coord. Chem. Rev.*, **2009**, *253*, 1353.
12. a) Y. N. Hong, J. W. Y. Lam and B. Z. Tang, *Chem. Commun.*, **2009**, 4332; b) M. Wang, G. X. Zhang, D. Q. Zhang, D. B. Zhu and B. Z. Tang, *J. Mater. Chem.*, **2010**, *20*, 1858.
13. a) J. Wu, W. Liu, J. Ge, H. Zhang and P. Wang, *Chem. Soc. Rev.*, **2011**, *40*, 3483.
b) A. P. Demchenko, K.-C. Tang and P.-T. Chou, *Chem. Soc. Rev.*, **2013**, *42*, 1379.
14. J. S. Wu, W. M. Liu, X. Q. Zhuang, F. Wang, P. F. Wang, S. L. Tao, X. H. Zhang, S. K. Wu and S. T. Lee, *Org. Lett.*, **2007**, *9*, 33.
15. a) M. E. Huston, E. U. Akkaya and A. W. Czarnik, *J. Am. Chem. Soc.*, **1989**, *111*, 8735; b) D. H. Vance and A. W. Czarnik, *J. Am. Chem. Soc.*, **1994**, *116*, 9397; c) E. U. Akkaya, M. E. Huston and A. W. Czarnik, *J. Am. Chem. Soc.*, **1990**, *112*, 3590.
16. Z.-X. Han, X.-B. Zhang, Z. Li, Y.-J. Gong, X.-Y. Wu, Z. Jin, C.-M. He, L.-X. Jian, J. Zhang, G.-L. Shen and R.-Q. Yu, *Anal. Chem.*, **2010**, *82*, 3108.
17. L. Zhou, X. Zhang, Q. Wang, Y. Lv, G. Mao, A. Luo, Y. Wu, Y. Wu, J. Zhang and W. Tan, *J. Am. Chem. Soc.*, **2014**, *136*, 9838.
18. S. W. Thomas III, G. D. Joly and T. M. Swager, *Chem. Rev.*, **2007**, *107*, 1339.
19. a) A. Kraft, A. C. Grimsdale and A. B. Holmes, *Angew. Chem., Int. Ed.*, **1998**, *37*, 402; b) S. Hecht and J. M. J. Frechet, *Angew. Chem., Int. Ed.*, **2001**, *40*, 74; c) C. Fan, S. Wang, J. W. Hong, G. C. Bazan, K. W. Plaxco and A. J. Heeger, *Proc. Natl. Acad. Sci. U. S. A.*, **2003**, *100*, 6297.
20. J. D. Luo, Z. L. Xie, J. W. Y. Lam, L. Cheng, H. Y. Chen, C. F. Qiu, H. S. Kwok, X. W.

- Zhan, Y. Q. Liu, D. B. Zhu and B. Z. Tang, *Chem. Commun.*, **2001**, 1740.
21. L. H. Peng, M. Wang, G. X. Zhang, D. Q. Zhang and D. B. Zhu, *Org. Lett.*, **2009**, *11*, 1943.
22. a) E. V. Anslyn, *J. Org. Chem.*, **2007**, *72*, 687; b) B. T. Nguyen and E. V. Anslyn, *Coord. Chem. Rev.*, **2006**, *250*, 3118; c) Chemical sensors and biosensors for medical and biological applications. U. S. Spichiger-Keller, Wiley-VCH, **1998**; d) Special issue on Fluorescent sensors, *J. Mater. Chem.*, **2005**, 2617.
23. a) C. M. G. dos Santos, A. J. Harte, S. Quinn and T. Gunnlaugsson T. *Coord Chem Rev.*, **2008**, *252*, 2512; b) J. P. Leonard, C. B. Nolan, F. Stomeo and T. Gunnlaugsson, *Top. Curr. Chem.*, **2007**, *281*, 1; c) T. Gunnlaugsson, M. Glynn, G. M. Tocci, P. E. Kruger and F. M. Pfeffer, *Coord. Chem. Rev.*, **2006**, *250*, 3094; d) C. Caltagirone and P. A. Gale, *Chem. Soc. Rev.*, **2009**, *38*, 520; e) P. A. Gale, S. E. Garcia-Garrido and J. Garric, *Chem. Soc. Rev.*, **2008**, *37*, 151.
24. R. Kumar, S. Kumar, P. Singh, G. Hundal, M. S. Hundal and S. Kumar, *Analyst*, **2012**, *137*, 4913.
25. P. Das, P. Mahato, A. Ghosh, A. K. Mandal, T. Banerjee, S. Saha and A. J. Das, *Chem. Sci.*, **2011**, *123*, 175.
26. a) T. Routasalo, J. Helaja, J. Kavakka and A. M. P. Koskinen, *Eur. J. Org. Chem.*, **2008**, *2008*, 3190; b) G. Ambrosi, M. Formica, V. Fusi, L. Giorgi, A. Guerri, E. Macedi, M. Micheloni, P. Paoli, R. Pontellini and P. Rossi, *Inorg. Chem.*, **2009**, *48*, 5901.
27. A. Metzger and E. V. Anslyn, *Angew. Chem., Int. Ed.*, **1998**, *37*, 649.
28. a) J. J. Lavigne and E. V. Anslyn, *Angew. Chem., Int. Ed.* **1999**, *38*, 3666; b) S. L.

- Tobey, B. D. Jones and E. V. Anslyn, *J. Am. Chem. Soc.*, **2003**, *125*, 4026; c) D. Leung, J. F. Folmer-Andersen, V. M. Lynch and E. V. Anslyn, *J. Am. Chem. Soc.*, **2008**, *130*, 12318; d) D. Leung and E. V. Anslyn, *J. Am. Chem. Soc.*, **2008**, *130*, 12328; e) L. Zhu, Z. L. Zhong and E. V. Anslyn, *J. Am. Chem. Soc.*, **2005**, *127*, 4260.
29. Q. Zeng, P. Cai, Z. Li, J. Qina and B. Z. Tang, *Chem. Commun.*, **2008**, 1094.
30. a) E. L. Que, D. W. Domaille and C. J. Chang, *Chem. Rev.*, **2008**, *108*, 1517; b) K. Kikuchi, *Chem. Soc. Rev.*, **2010**, *39*, 2048; c) X. Qian, Y. Xiao, Y. Xu, X. Guo, J. Qian and W. Zhu, *Chem. Commun.*, **2010**, 46, 6418.
31. S. Y. Kim and J.-I. Hong, *Org. Lett.*, **2007**, *9*, 3109.
32. a) Y. Qian, L. Zhang, S. Ding, X. Deng, C. He, X. E. Zheng, H.-L. Zhu and J. Zhao, *Chem. Sci.*, **2012**, *3*, 2920; b) H. D. Li, B. Li, L. Y. Jin, Y. H. Kan and B. Z. Yin, *Tetrahedron*, **2011**, *67*, 7348.
33. H. He, M. A. Mortellaro, M. J. P. Leiner, R. J. Fraatz and J. K. Tusa, *J. Am. Chem. Soc.*, **2003**, *125*, 1468.
34. a) Z. P. Liu, C. L. Zhang, X. Q. Wang, W. J. He and Z. J. Guo, *Org. Lett.*, **2012**, *14*, 4378; b) S. C. Burdette, G. K. Walkup, B. Spingler, R. Y. Tsien and S. J. Lippard, *J. Am. Chem. Soc.*, **2001**, *123*, 7831.
35. a) E. M. Nolan, M. E. Racine and S. J. Lippard, *Inorg. Chem.*, **2006**, *45*, 2742; b) E. M. Nolan and S. J. Lippard, *J. Mater. Chem.*, **2005**, *15*, 2778; c) E. M. Nolan and S. J. Lippard, *J. Am. Chem. Soc.*, **2007**, *129*, 5910.
36. a) W. Shi and H. M. Ma, *Chem. Commun.*, **2008**, 1856; b) X.-Q. Zhan, Z.-H. Qian, H. Zheng, B.-Y. Su, Z. Lan and J.-G. Xu, *Chem. Commun.*, **2008**, 1859; c) Y. Y.

- Zhang, W. Shi, D. Feng, H. M. Ma, Y. Liang and J. R. Zuo, *Sens. Actuators, B* **2011**, *153*, 261.
37. a) A. Ojida, I. Takashima, T. Kohira, H. Nonaka and I. Hamachi, *J. Am. Chem. Soc.*, **2008**, *130*, 12095; b) M. D. Pluth and K. N. Raymond, *Chem. Soc. Rev.*, **2007**, *36*, 161; c) D. Ramaiah, P. P. Neelakandan, A. K. Nair and R. R. Avirah, *Chem. Soc. Rev.*, **2010**, *39*, 4158; d) V. S. Jisha, K. T. Arun, M. Hariharan and D. Ramaiah, *J. Phys. Chem. B*, **2010**, *114*, 5912.
38. a) H.-J. Schneider and A. K. Yatsimirsky, *Chem. Soc. Rev.*, **2008**, *37*, 263; b) H.-J. Schneider, *Angew. Chem., Int. Ed.*, **2009**, *48*, 3924; c) B. Linton and A. D. Hamilton, *Chem. Rev.*, **1997**, *97*, 1669.
39. a) P. P. Neelakandan, M. Hariharan and D. Ramaiah, *Org. Lett.*, **2005**, *7*, 5765; b) P. P. Neelakandan, M. Hariharan and D. Ramaiah, *J. Am. Chem. Soc.*, **2006**, *128*, 11334.
40. a) P. P. Neelakandan and D. Ramaiah, *Angew. Chem., Int. Ed.*, **2008**, *47*, 8407; b) P. P. Neelakandan, K. S. Sanju and D. Ramaiah, *Photochem. Photobiol.*, **2010**, *86*, 282.
41. J. Wu, Y. Zou, C. Li, W. Sicking, I. Piantanida, T. Yi and C. Schmuck, *J. Am. Chem. Soc.*, **2012**, *134*, 1958.

DESIGN OF ARYL-INDOLIUM CONJUGATES: STUDY OF THEIR ANION DETECTION ASPECTS



2.1. ABSTRACT

With an objective of developing molecular probes, we synthesised two aryl indolium based conjugates **1** and **2** and have investigated their photophysical and anion recognition properties. Both these conjugates showed good solubility in common organic solvents and exhibited intramolecular charge transfer (ICT) process from the aromatic chromophore to the indolium moiety. As a result of this, we have observed strong ICT absorption band at 510 and 507 nm, respectively, for the conjugates **1** and **2**. When studied the interactions with various anions, these

systems showed prominent changes in their absorption and emission spectra with the addition of the cyanide (CN⁻) ions. Moreover, these systems showed selectivity for the CN⁻ ions, when compared to other biologically relevant anions and the sensitivity of the detection was determined to be 32 and 10 ppb, respectively. Among these two probes, the pyrene conjugate **2** showed an interesting feature of dual colorimetric and fluorescence response with ratiometric changes in the presence of the CN⁻ ions. The nature of interactions has been investigated through ¹H & ¹³C NMR, IR, HRMS, and isothermal calorimetric (ITC) measurements, which confirmed that the probe **2** forms a thermodynamically favourable 1,2-adduct with the CN⁻ ions. The kinetic studies employing the probe **2** showed the completion of the reaction with the CN⁻ ions within 15 s and exhibited a rate constant of $k' = 0.522 \pm 0.063 \text{ s}^{-1}$. Moreover, we have also confirmed the reversibility of this reaction in the presence of trifluoroacetic acid (TFA), owing to the dynamic nature of the covalent bond formed between the indole moiety and the cyano group. Our results demonstrated that the probe **2** acts as a reversible chemodosimeter for the selective and sensitive detection of the CN⁻ ions. Uniquely, this probe can be coated on the solid state dip-stick, polymer matrix and filter paper for the on-site analysis and quantification of the CN⁻ ions. Furthermore, we have also employed this probe for the quantification of the endogenous cyanide ions present in natural sources like Indian almonds, which gave a value of *ca.* $100 \pm 12 \text{ ppm}$, which is in agreement with the values reported in the literature.

2.2. INTRODUCTION

The development of colorimetric and fluorescent sensors for various anions has been an active area of research in recent years, due to their pivotal role in various biological processes.^{1,2} Amongst the various anion targets, cyanide is considered as one of the most active and highly poisonous to living beings. Upon chronic exposure to cyanide, a chemical warfare agent, can lead to inhibition of the enzyme cytochrome oxidase by interfering the electron transport chain that ultimately results in hypoxia.^{3a} In addition, serious adverse effects on central nervous (CNS), respiratory and cardiovascular systems have also been evidenced.³ The United States Environmental Protection Agency (US-EPA) has set a maximum contaminant levels of cyanide ions in drinking water at 0.2 mg/L, which is equivalent to 200 parts per billion (ppb).⁴ Moreover, cyanide is also being used extensively in the preparation of a wide variety of products such as plastics, fibres, gold, pharmaceuticals, dyes etc.⁵ Due to this widespread usage, the cyanide pollution has become a major concern because of its high toxicity and activity to inhibit several biologically important metallo/non-metallo enzymes.⁶

A variety of colorimetric⁷ and fluorescent⁸⁻¹³ probes have been reported for the easy and rapid detection of the cyanide ions. Of which, the fluorescent probes are known for their promising characteristics such as ultra-high sensitivity, cost-effectiveness, easy handling and also fast response.¹⁴ Recently, an immense attention has also been given towards the development of reaction-based small-molecule

fluorescent probes for the detection of various analytes owing to their high selectivity and sensitivity.¹⁵ The fluorescent reactive probes for cyanide are mainly based on the reactions such as nucleophilic addition,¹⁶ the benzil rearrangement reaction,¹⁷ and cyanide complexation/addition.¹⁸ On the basis of nucleophilic addition, various substrates such as dicyanovinyl, salicyladimines and indolium salts have also been reported.¹⁹ However, most of the known systems have a demanding necessity to address drawbacks such as sensitivity, selectivity, and also the ability of the recognition processes in the solid state.

Many plant species, especially of the clade *Rosids*, are known to be potential sources of CN⁻ poisoning due to the presence of endogenous cyanides. In particular, these plants constitute cyanogenic glycosides such as in linamarin (cassava), amygdalin (almond seeds) as CN⁻ source, which upon regular consumption leads to neurological disorders. It is quite challenging to develop a highly efficient, simple and selective probe for the detection of the cyanide ions in the natural sources. However, the probes so far developed for the detection of cyanogenic glycosides in biological samples have been limited.²⁰ More recently, Torroba and co-workers have evaluated the indene based derivatives for the detection and reliable quantification of endogenous cyanide in bitter almonds.^{20c}

In this context, we have designed and synthesised two indolium conjugates based on anthracene/pyrene chromophores **1** and **2** (Chart 2.1) and have investigated their interactions with various anions. Of these conjugates, the probe **2** showed a sensitivity of *ca.* 10 ppb for the CN⁻ ions and signalled the event through

dual changes in colour and reversible ratiometric fluorescence enhancement, when compared to other anions. In addition, this probe can be coated on a dip-stick for the on-site analysis and detection of the cyanide ions in the natural sources such as Indian almonds.

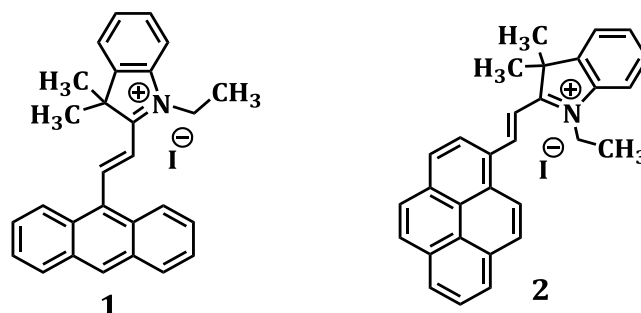
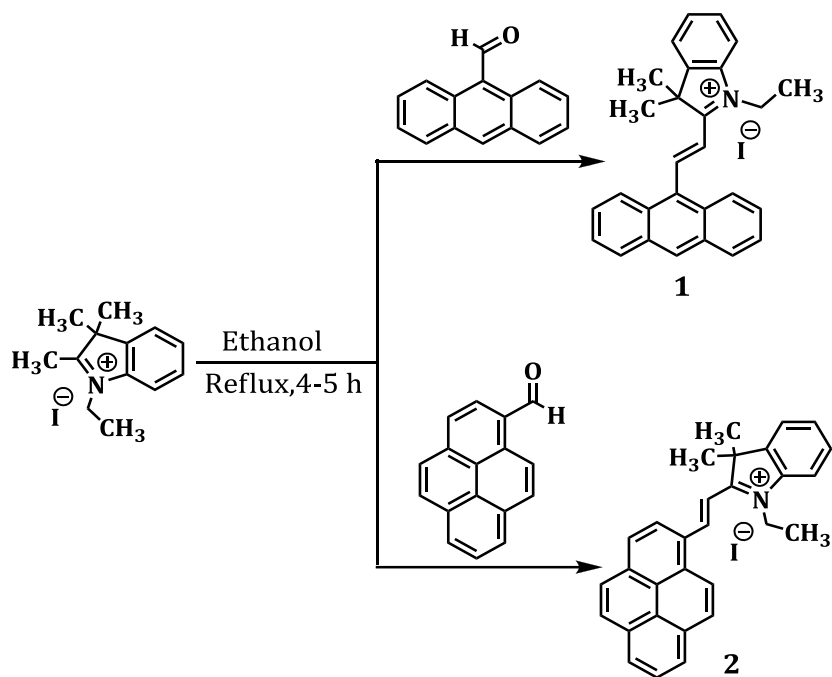


Chart 2.1. Structures of the conjugates **1** and **2**.

2.3. RESULTS

2.3.1. Synthesis of the Indolium Conjugates

We have designed two aryl-indolium conjugates **1** and **2** as molecular probes, because the systems based on such chromophore have attracted much attention as sensors¹⁹ and photochromic materials.²¹ The synthesis of the probes **1** and **2** is achieved as outlined in Scheme 2.1. The condensation reaction of the 9-anthraldehyde or 1-pyrenecarboxaldehyde, respectively, with 2,3,3-trimethyl-1-ethyl-3H-indolium iodide in ethanol solution yielded *ca.* 72% and 86%, of the conjugates **1** and **2**, respectively. These conjugates were purified through column chromatography and were unambiguously characterised by spectroscopic and analytical evidence such as IR, UV-Vis, ¹H and ¹³C NMR, HRMS, and CHN analysis.



Scheme 2.1. Synthesis of the anthracene or pyrene-indolium conjugates **1** and **2**.

2.3.2. Photophysical Properties of the Indolium Conjugates

The photophysical studies of these conjugates were carried out in different organic solvents. Figure 2.1 shows their absorption and emission spectra in acetonitrile. The conjugate **1** showed an absorption spectrum having maximum at 386 nm and a broad band centred at 510 nm with molar extinction coefficient values of 2.26×10^4 and $1.24 \times 10^4 \text{ M}^{-1} \text{ cm}^{-1}$, respectively. Similar observations were made with the pyrene conjugate **2**, wherein it showed the absorption with two maxima at 331 and 507 nm, respectively, with extinction coefficient values of 2.45×10^4 and $2.72 \times 10^4 \text{ M}^{-1} \text{ cm}^{-1}$. The absorption peaks of **1** and **2** at 386 and 331 nm, respectively, can be attributed to the characteristic absorption of the chromophores, anthracene and pyrene, respectively. The long wavelength and broad absorptions at

510 and 507 nm, can be assigned due to the intramolecular charge transfer (ICT) process from the aromatic chromophore to the electron deficient indolium moiety. Further, we have recorded the fluorescence spectra of both **1** and **2** in acetonitrile and which showed characteristic ICT induced emission at 560 and 637 nm ($\phi_F = 0.01$ and 0.007), respectively.

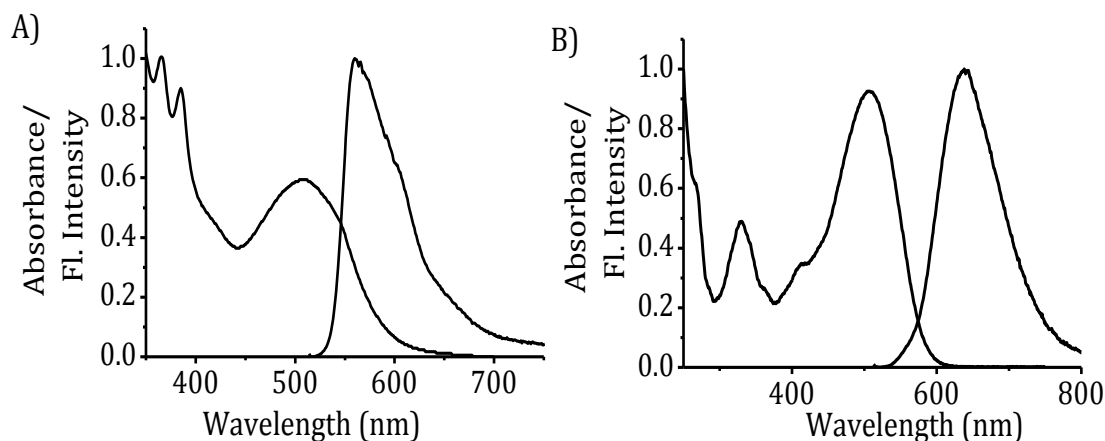


Figure 2.1. Normalized absorption and fluorescence spectra of the conjugate A) **1** (8 μM) and B) **2** (8 μM) in acetonitrile. Excitation wavelengths, 510 nm and 508 nm, respectively.

The solvatochromic effects on the absorption features of the indolium conjugates, **1** and **2**, were studied in different organic solvents of varying polarity like toluene, dichloromethane, tetrahydrofuran, acetonitrile and methanol. The long wavelength absorption band at *ca.* 510 nm observed for the derivative **1** showed a hypsochromic shift (negative solvatochromism) as the solvent polarity increased. For example, by increasing the polarity from toluene to acetonitrile, we observed a hypsochromic shift of *ca.* 37 nm in the absorption maximum. The UV-Vis absorption

spectra of **1** recorded in different solvents are shown in Figure 2.2A. Similar observations were made in the case of the derivative **2**, wherein we observed a hypsochromic shift of *ca.* 35 nm (Figure 2.2B).

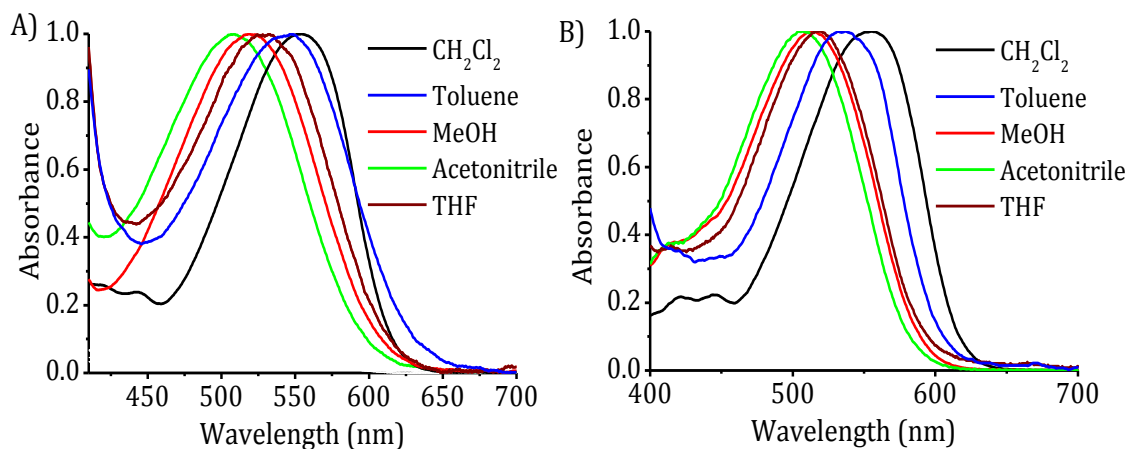


Figure 2.2. Normalized absorption spectra of the probes A) **1** (8 μ M) and B) **2** (8 μ M) in solvents having different polarity.

Furthermore, we have recorded the fluorescence spectra of the derivatives **1** and **2**, in different solvents with varying polarity. The conjugate **1** showed the emission maximum (λ_{em}) at *ca.* 549 nm in the nonpolar solvent like toluene, while in methanol, it showed a bathochromically shifted emission at 564 nm. Similar observations were made in the case of **2**. In this case and upon increasing the polarity from toluene to methanol, we observed a bathochromically shifted emission maximum from 618 to 643 nm (Figure 2.3A). To understand the polarity effect of various solvents, the solvent dependent spectral shifts were investigated. As shown in Figure 2.3B, we studied the dependence of the polarity index $E_T(30)$ on the fluorescence maxima of the probe **2**, for which we observed a linear relation, thus depicting the presence of intramolecular charge transfer in the excited state.²²

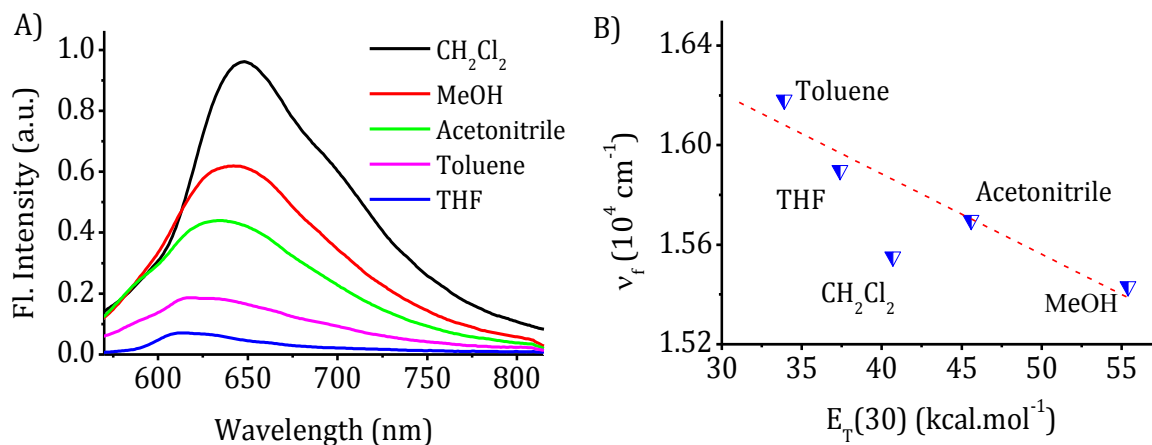


Figure 2.3. A) Emission spectra of the probe **2** (8 μM) in solvents having different solvent polarity. B) The corresponding plot in different solvents showing the variation of emission maximum of **2** as a function of solvent polarity parameter.

Table 2.1. Changes in the absorption and fluorescence properties of the conjugates **1** and **2** in different solvents.*

Solvent	$E_T(30)$ (kcal.mol^{-1})	λ_{abs} (nm)		λ_{em} (nm)		Φ_F ($\times 10^{-2}$)	
		1	2	1	2	1	2
Toluene	0.02	545	534	549	618	0.3	0.2
THF	0.21	527	518	545	629	0.4	0.4
DCM	40.7	551	553	571	648	2.8	2.1
Acetonitrile	45.6	508	507	560	637	1.1	0.7
Methanol	55.4	521	515	564	643	1.8	1.8

*Average of more than two independent experiments. λ_{abs} : absorption maximum, λ_{em} : emission maximum Φ_F : quantum yield of fluorescence determined employing Nile red in dioxane as the standard.

2.3.3. Anion Recognition Properties

To investigate the potential of the conjugates **1** and **2** as molecular probes, we have studied their interactions with various anions. Notably, with the addition of 8 μM of CN^- , the probe **1** showed a *ca.* 94% hypochromicity at 510 nm with a concomitant increase (*ca.* 20%) in the absorption band at 386 nm and exhibited an isosbestic point at 398 nm (Figure 2.4A). Similarly, in the emission spectra of the probe **1**, we observed a gradual decrease in the ICT emission centred at 560 nm with a *ca.* 97% quenching in intensity (Figure 2.4B). The observed changes can be attributed to the decreased ICT absorption with the addition of CN^- ions. However, upon choosing the isosbestic point at 398 nm as the excitation wavelength, we observed only the emission corresponding to the anthracene monomer, albeit with low intensity. Similarly, with the addition of the cyanide ions to the probe **2**, we observed *ca.* 98% hypochromicity corresponding to the ICT absorption, along with

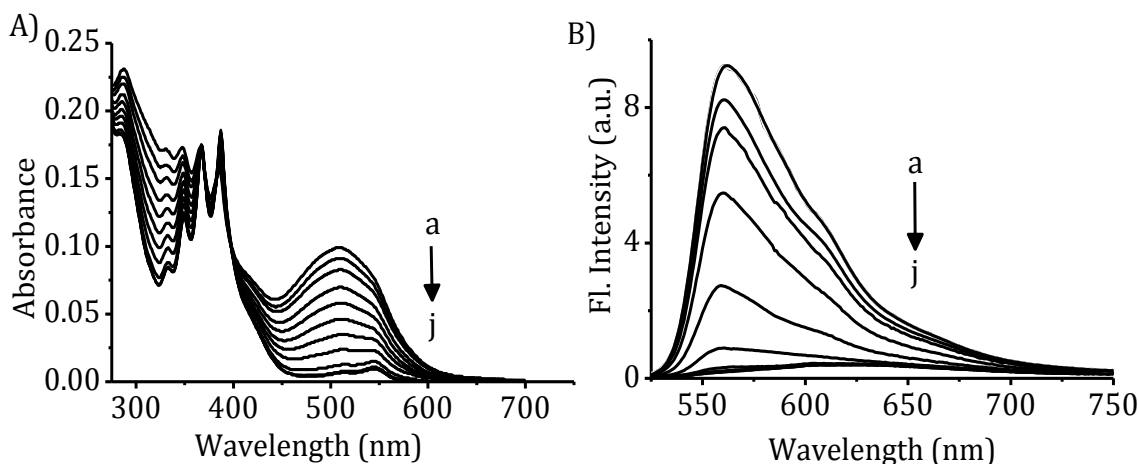


Figure 2.4. Changes in the A) absorption and B) emission spectra of the probe **1** (8 μM) with the addition of CN^- ions in acetonitrile, a) 0 and j) 8 μM in acetonitrile solution. Excitation wavelength, 510 nm.

the concomitant increase in the pyrene monomer absorption at 331 nm (Figure 2.5A). Interestingly, when we used the isosbestic point at 370 nm as the excitation wavelength in this case, we observed an emission spectrum having two well-spaced maxima at 395 nm and 637 nm. By the incremental addition of CN^- ions, we observed a regular decrease in the ICT emission at 637 nm, followed by a concomitant increase in the pyrene monomer emission at 395 nm with a well-defined isoemissive point at 548 nm (Figure 2.5B). These observations clearly indicated that the pyrene conjugate **2** serves as a superior and selective ratiometric fluorescent probe for the cyanide ions when compared to the anthracene based probe **1**. Moreover, as shown in Figure 2.6 A, the emission spectral changes observed with the probe **2** in the presence of CN^- were analysed by means of Jobs

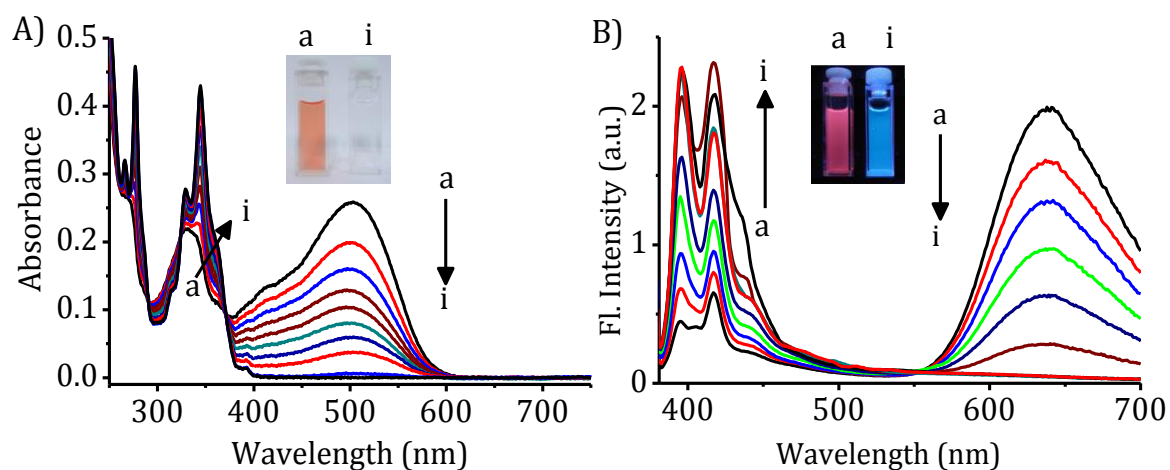


Figure 2.5. Changes in the A) absorption and B) emission spectra of the probe **2** (8 μM) with the addition of the CN^- ions in acetonitrile, a) 0 and i) 8 μM . Insets of A and B show the corresponding changes in absorption and emission spectra. Excitation wavelength, 370 nm.

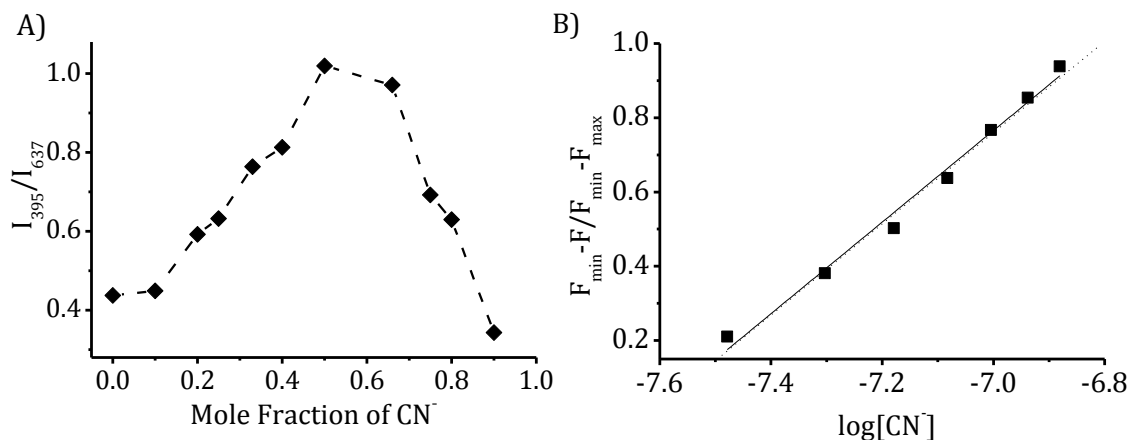


Figure 2.6. A) Job plot of titration of the probe **2** (15 μM) with CN^- ions (15 μM) in acetonitrile, plotted as a function of fluorescence intensity at 395 nm against mole fraction of CN^- ions. Excitation wavelength, 370 nm. B) Fluorescence intensity of the probe **2** (8 μM) at each concentration of CN^- added, normalized between the minimum fluorescence intensity, found at zero equivalents of CN^- , and the maximum fluorescence intensity, observed at $[\text{CN}^-] = 10$ ppb.

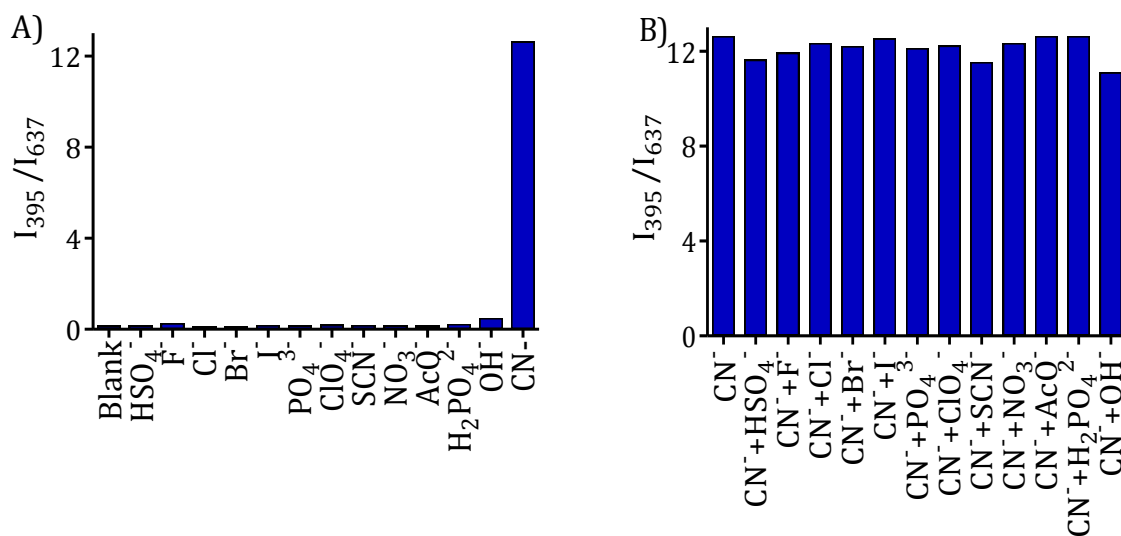


Figure 2.7. A) Selectivity plot showing the increase in the fluorescence ratio (I_{395}/I_{637}) of the probe **2** (8 μM) with various anions (40 μM) in acetonitrile. B) Fluorescence changes of the probe **2** (8 μM) in the presence of different anions (40 μM) along with the cyanide ions (8 μM). Excitation wavelength, 370 nm.

plot²³, which gave a 1:1 stoichiometry, indicating the presence of only one interacting site for the target. The lowest level of recognition of CN⁻ by the probe **2** was calculated and it was found to be quite sensitive with a detection limit of *ca.* 10 ppb (Figure 2.6 B).

With a view to investigate the selectivity of the probe **2** towards CN⁻, we have studied its interactions with various biologically relevant anions such as HSO₄⁻, F⁻, Cl⁻, Br⁻, I⁻, PO₄³⁻, ClO₄⁻, SCN⁻, NO₃⁻, AcO⁻, H₂PO₄⁻ and OH⁻ ions. These studies were carried out in the presence as well as the absence of CN⁻. The addition of all these anions showed negligible changes in both the absorption and emission spectra of both the conjugates. These observations clearly indicate that the pyrene conjugate **2** serves as a superior probe **2**, and which exhibits the ratiometric (I_{395}/I_{637}) emission changes (Figure 2.7) only in presence of the CN⁻ ions.

2.3.4. Mechanism of Cyanide Recognition

2.3.4.1. ¹H-NMR Titration Studies

To gain better insights of the mechanism, the reaction was further monitored through NMR titration. As shown in Figure 2.8, with the addition of the CN⁻ ions in CD₃CN at 25 °C, we observed the prominent changes in the ¹H NMR spectrum of the probe **2**. Especially, the peaks corresponding to the vinylic protons H_a and H_b showed up-field shift from 9.4 and 7.77 ppm ($J=15$ Hz), respectively, to 8.13 and 6.37 ppm in the presence of CN⁻ ions (Figure 2.8). The negligible changes observed in the coupling constants of the protons H_a and H_b ($J=15$ Hz) in the

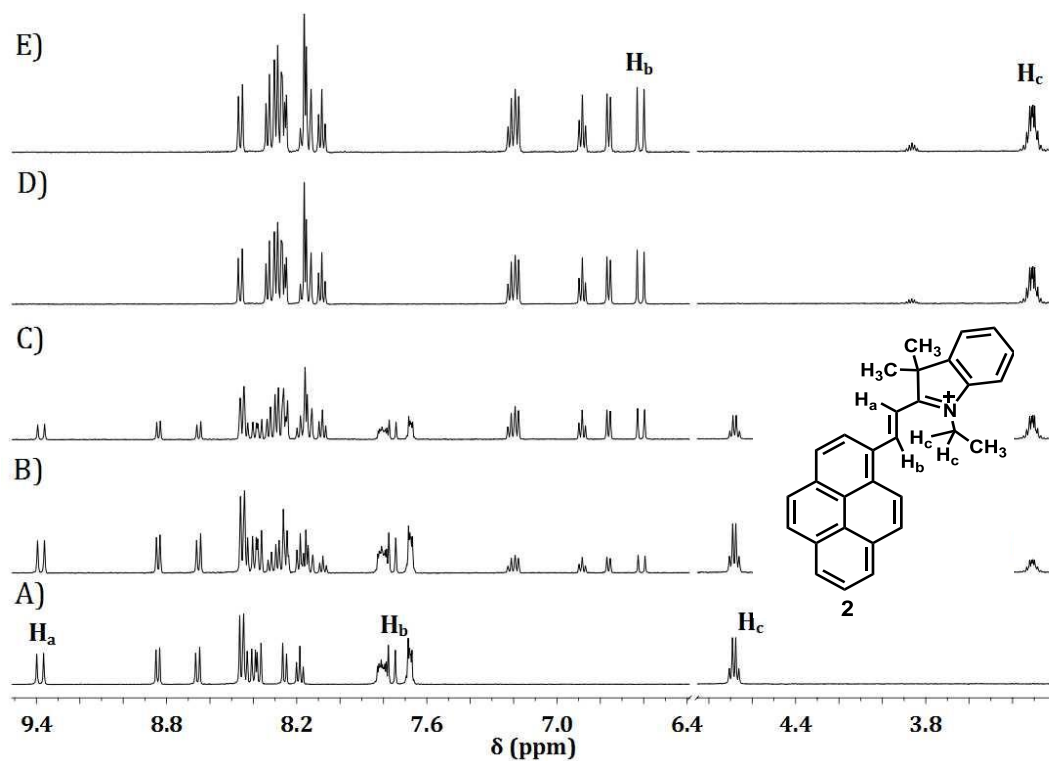


Figure 2.8. Changes in the ^1H NMR spectra of the probe **2** (1 mM) alone and with the addition of the CN^- ions in CD_3CN . $[\text{CN}^-]$ (A) 0, and (E) 1.5 mM.

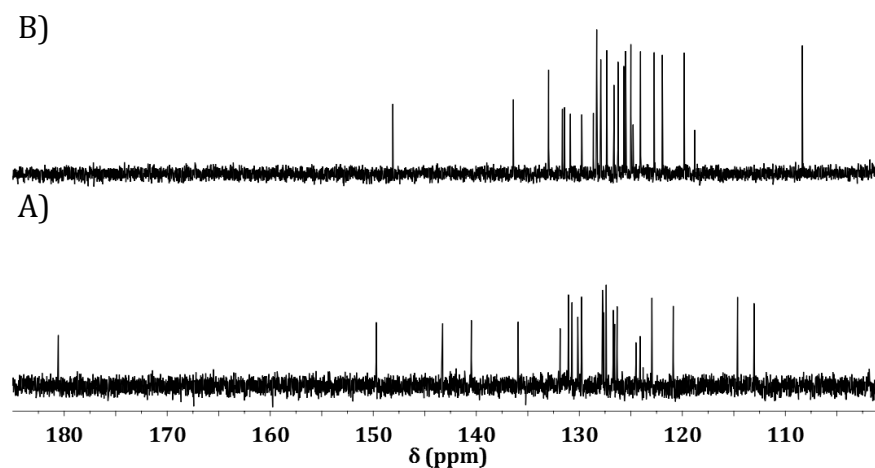


Figure 2.9. ^{13}C NMR spectra of the A) probe **2** (5 mM), B) probe **2**- CN adduct (5 mM) in CD_3CN .

presence and absence of CN^- ions indicate the fact that the nucleophilic addition product formed is as a result of 1,2-addition instead of 1,4-addition. Besides this, the signals corresponding to $-\text{N}^+-\text{CH}_2-$ i.e. H_c protons exhibited an up-field shift from 4.69 to 3.31 ppm, indicating the fact that the nitrogen of the indolium group in the product is no longer present in the quaternised state. Furthermore, we have isolated the product, 1,2-adduct and which was unambiguously characterised through ^1H , ^{13}C NMR and HRMS analysis. It can be noted from the ^{13}C spectra, of the probe **2** and the 2-CN adduct that the peak corresponding to the $-\text{C}=\text{N}^+-$, which was found at 180.6 ppm in the former was found to be disappeared in the product corroborating the fact that the reaction involves the imidium group of the indolium moiety (Figure 2.9).

2.3.4.2. Kinetic Studies

As the detection strategy requires a fast response to the practical applications, it was of our interest to investigate the kinetics of the reaction between the probe, **2** and the CN^- ions. We observed the completion of the reaction within 15 s and that the reaction requires only one equivalent of the analyte (Figure 2.10A) as analysed through fluorescence spectroscopy. The rate constant for the reaction of the probe **2** with the CN^- ions was determined using a pseudo-first order approximation employing excess (10 equivalents) of the CN^- ions. The reaction was carried out at room temperature 25 ± 1 °C and the changes in the fluorescence intensity of the probe **2** were monitored at 637 nm (Figure 2.10B). The rate constant (k')²⁴ for nucleophilic addition of cyanide was calculated to be $k' = 0.522 \pm 0.063 \text{ s}^{-1}$

$$\ln [(F_{max}-F_t)/F_{max}] = -k't \quad (\text{Eq. 2.1.})$$

using the Eq. 2.1, wherein, F_t and F_{max} are the fluorescence intensities at 637 nm at time t and the maximum value obtained after the reaction was completed and k' is the pseudo-first-order rate constant. These results suggest that the probe **2** exhibits a high reactivity towards the cyanide ions and the completion of the reaction was observed within 15 s.

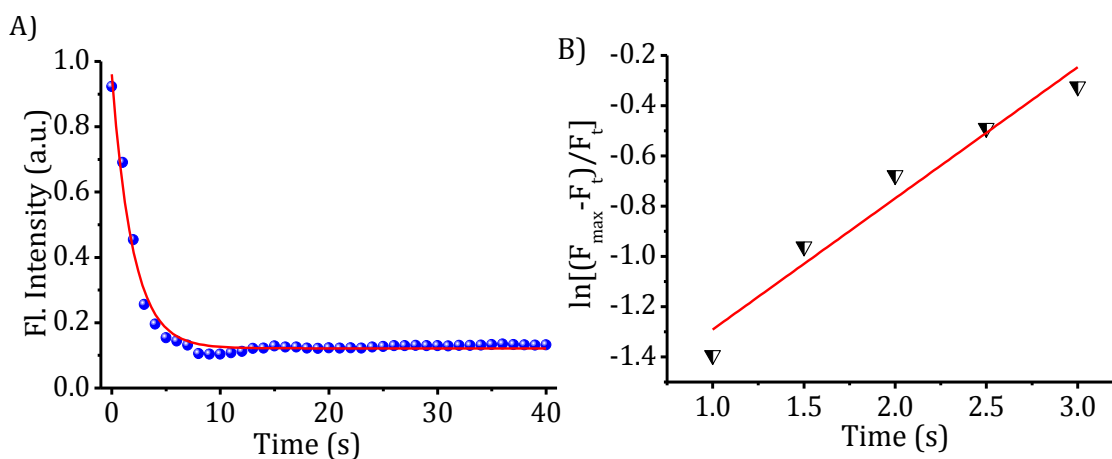


Figure 2.10. A) The emission changes monitored at 637 nm observed from the reaction between the probe **2** and cyanide anions. The experimental data points and theoretical fit (red) generated using $k' = 0.52 \pm 0.082 \text{ s}^{-1}$. B) Pseudo first-order kinetic plot for reaction of the probe **2** (11.8 μM) with the CN^- ions (120 μM). Slope = $0.522 \pm 0.063 \text{ s}^{-1}$.

2.3.4.3. Isothermal Titration Calorimetry

To understand the thermodynamic parameters involved in the reaction of CN^- with the probe **2**, we have carried out the isothermal titration calorimetric (ITC) measurements by the single injection method. Figure 2.11 shows the heat evolved

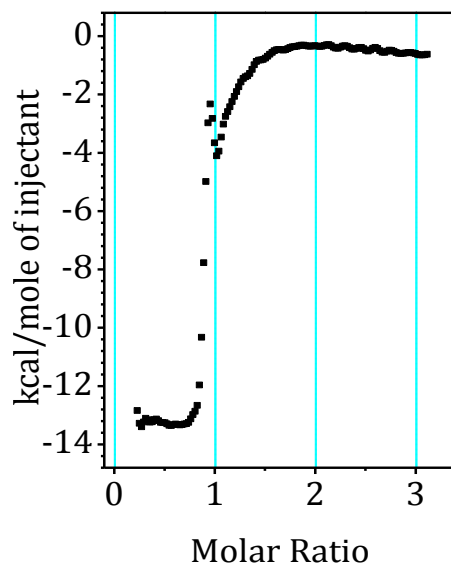


Figure 2.11. Isothermal Calorimetric titration of the probe **2** (1 mM) with the CN⁻ (15 mM) ions in acetonitrile at 303 K by single injection method. Figure shows the integration of area corresponding to amount of heat evolved as a function of molar ratio (the probe [2]/[CN⁻]).

TABLE 2.2. Binding and thermodynamic constants obtained from ITC (single injection method) experiments of the probe **2** (1 mM) with the CN⁻ (15 mM) ions.*

Parameters	Values ^a
Number of Sites (N)	0.913 ± 0.007 Sites
Association Constant (K)	1.65 ± 0.03 × 10 ⁵ M ⁻¹
Change in Enthalpy (ΔH)	-5.850 ± 0.087 × 10 ⁴ joules/mol
Change in Entropy (ΔS)	-93.0 joules/mol/deg
Change in Gibbs Free Energy (ΔG) ^b	-55.71 ± 0.71 × 10 ³ joules/mol

*^aAverage of more than three independent experiments. ^bCalculated using the equation, $\Delta G = \Delta H - T \Delta S$ (at 303 K).

per mole of the CN^- ions against molar ratio of the probe **2**. As can be seen from the figure, the change in enthalpy, ΔH was found to be $-5.850 \pm 0.086 \times 10^4 \text{ J/mol}$ with an association constant of $K=1.65 \pm 0.03 \times 10^5 \text{ M}^{-1}$, and from which the change in the Gibbs free energy has been calculated as $-55.71 \pm 0.71 \times 10^3 \text{ J/mol}$. The thermodynamic parameters involved in the reaction of the probe **2** with the CN^- ions were tabulated in Table 2.2.

2.3.4.4. Reversibility of the Detection

To investigate the reversibility of the detection of the CN^- ions by the probe **2**, we have analysed the 1,2-adduct formation and stability with the addition of trifluoroacetic acid (TFA). The changes in the emission spectra of the probe **2** in the presence of the CN^- ions and after the addition of TFA are shown in Figure 2.12A. Interestingly, when a drop of TFA was added to the probe **2** in the presence of the

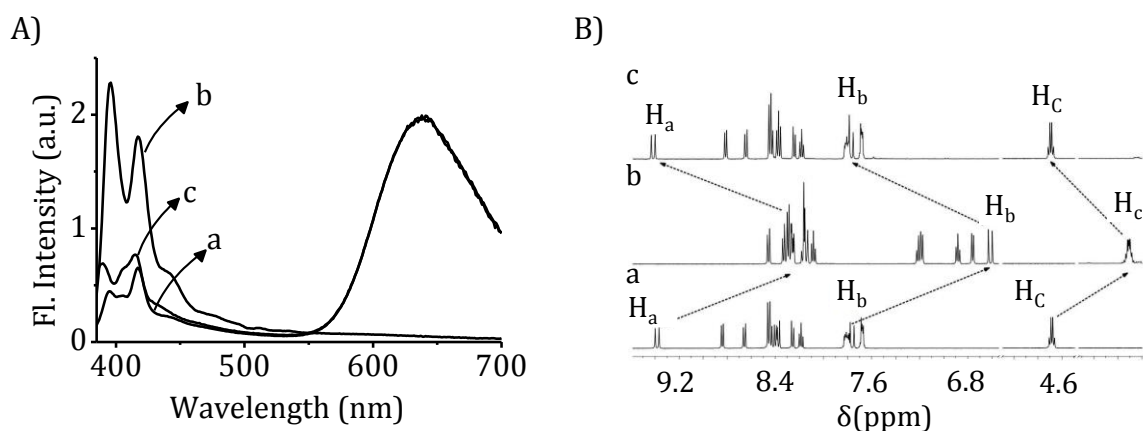


Figure 2.12. A) Emission and B) ^1H NMR spectra of the probe a) **2** alone, b) **2** + CN^- ions and c) after the addition of trifluoroacetic acid. Solvents CD_3CN and CF_3COOD were used for the ^1H NMR measurements.

CN⁻ ions, we obtained the fluorescence spectrum that is similar to that of the probe **2** without CN⁻ ions. Similarly, the evidence for the reversibility of the reaction was obtained through ¹H NMR measurements (Figure 2.12B). After the addition of deuterated TFA to the solution of the CN⁻ adduct of the probe **2** in CD₃CN, we obtained the spectrum that is similar to that of the probe **2** alone.

2.3.5. Design of a Prototype Device

To evaluate the versatility of the probe, we have developed a prototype device “dip-stick” containing the probe **2** adsorbed over alumina and the slurry was coated on a glass support. The ability of the dip-stick to detect the CN⁻ ions has been tested by dipping it in the alkaline solution (pH ~9.3) having various concentrations of the CN⁻ ions. We observed visual colour and fluorescence changes wherever the dip-stick came into contact with the solution of the cyanide ions (Figure 2.13). The visual colour changed from reddish pink to colourless while the fluorescence emission colour changed from red to bluish in the presence of the CN⁻ ions. Interestingly, when the dip-stick was dipped in a 10% (v/v) TFA solution, we observed the reversal of the colour changes, indicating the reversibility and reusability of the dip-stick for the detection of the CN⁻ ions in solution. In addition, we have also performed the dip-stick demonstration in the presence of potassium cyanide (KCN) in the aqueous medium. As shown in the Figure 2.14, we observed visual fluorescence colour changes of the probe **2**, which were found to be similar to those observed with tetrabutylammonium cyanide.

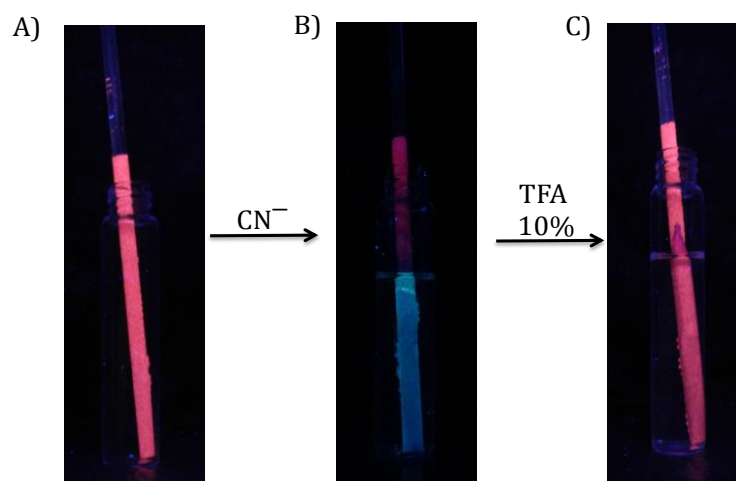


Figure 2.13. Photographs of alumina coated dip-stick containing the probe, A) **2** alone, B) **2** in presence of the CN^- ions (50 μM) and C) after exposure to trifluoroacetic acid in the aqueous medium (pH 9.3).

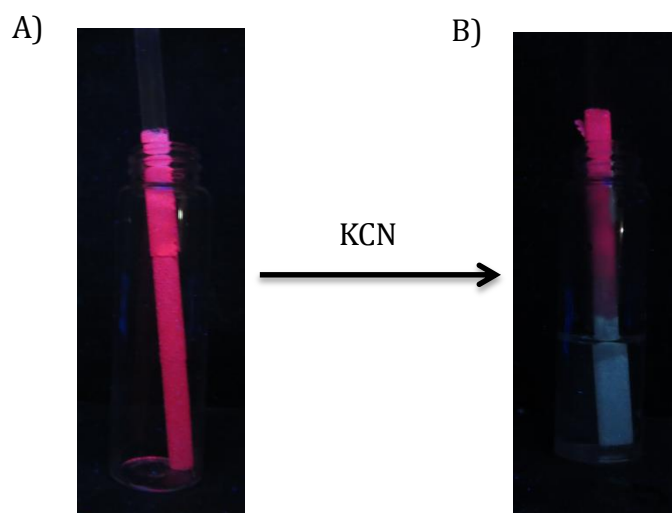


Figure 2.14. Photographs of alumina coated dip-stick containing the probe, A) **2** alone and B) **2** in the presence of KCN (50 μM) in water.

Furthermore, we have prepared the polymer films of poly(methylmethacrylate) (99.8% w/w) dissolved in CH_2Cl_2 and the probe **2** (0.2%

w/w) was added to it. This mixture was poured into a clean glass petri-dish and upon evaporation of the solvent at 25 °C gave a homogenous polymer film having the absorption and emission maxima at 517 and 627 nm, respectively (Figure 2.15). Subsequently, acetonitrile solution of the CN^- ions was applied onto the surface of the film with the aid of a capillary tube. Interestingly, the color of the film faded with

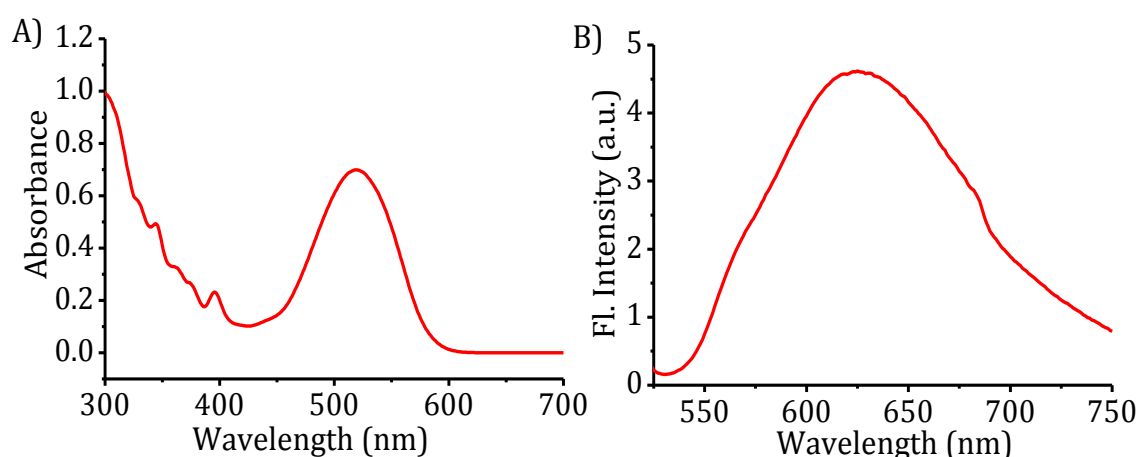


Figure 2.15. A) Absorption and B) emission spectra of the polymer films of PMMA, 99.8% (w/w) with the probe **2**, 0.2% (w/w) in the film state.

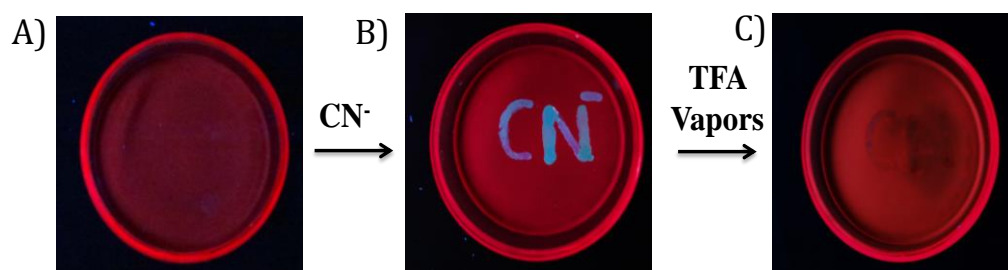


Figure 2.16. Photographs of polymer (PMMA) matrix containing the probe A) **2** alone, B) **2** in presence of the CN^- ions (50 μM) and C) after exposure to trifluoroacetic acid.

the simultaneous changes in the fluorescence features from red to bluish as observed in the solution and solid state (Figure 2.16). The reversibility of the detection has been achieved by exposing the polymeric film treated with the CN⁻ ions to the vapors of TFA as observed in the case of the dip-stick method.

To further explore the versatility of the probe, we have also developed a cheaper and easily accessible filter paper based prototype for the demonstration of the detection of the cyanide ions. We have developed this prototype by dipping a Whatman No.1 filter paper into a solution of dichloromethane containing the probe **2**, which was dried by exposing to atmospheric temperature. Then an aqueous solution of the CN⁻ ions was applied onto the surface of the filter paper with the aid of a capillary tube. As observed in the earlier cases, the colour of the filter paper got faded upon treating with the solution of CN⁻ ions and we observed concomitant visual changes in the fluorescence colour from red to bluish green (Figure 2.17). The reversibility of the detection was also achieved in this case by the exposure of the filter paper treated with the CN⁻ ions to the TFA vapors. These results demonstrate

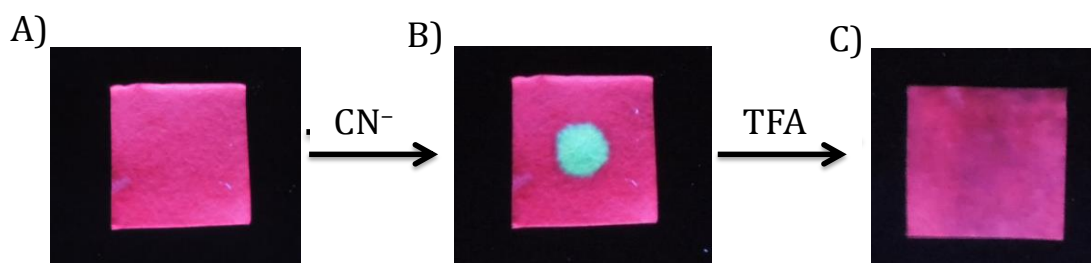


Figure 2.17. Photographs of Whatman No. 1 filter paper containing the probe A) **2** alone, B) **2** in presence of the CN⁻ ions (50 μ M) and C) after exposure to trifluoroacetic acid.

the fact that the filter paper coated with the probe **2** can be used for the detection of the CN⁻ ions as and when required as that of a laboratory pH paper.

2.3.6. Quantification of Endogenous Cyanide

By employing the probe **2**, we have subsequently investigated its ability to detect the endogenous CN⁻ ions in the seed of Indian almonds (*Terminalia catappa*). We prepared an extract of 0.02 M sodium bicarbonate aqueous solution from the degreased and dried freshly collected as well as commercially available almond seeds (Figure 2.18). The presence of cyanide in this extract was confirmed by the

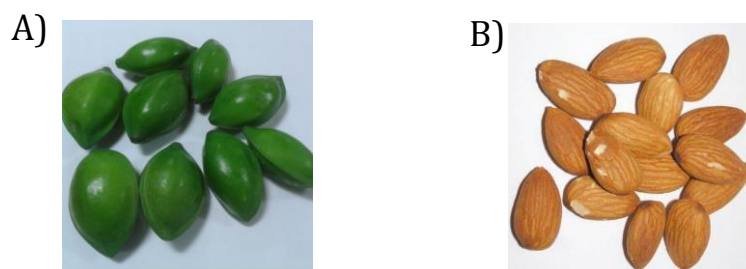


Figure 2.18. Photographs of A) freshly collected and B) commercially available Indian almonds, which were used for the extraction of the endogenous cyanide.

conventional ferric thiocyanate complexation using aqueous solution of sodium thiosulphate and ferric chloride, where in the colour changed from colourless to brownish yellow. Interestingly, upon gradual addition of the extract from the unripe almonds to the solution containing the probe **2** (10 μ M), we observed changes both in the absorption and ratiometric fluorescence intensity. In contrast, the extract from the degreased commercially available almonds showed negligible changes in photophysical properties of the probe. The amount of the endogenous cyanide ions

in the extract was determined by the standard addition method.^{20c,25} The spectral changes in the absorption and emission of the different solutions of the probe **2** with various known concentrations of tetrabutylammonium cyanide (TBACN) were measured. From the calibration curve, the concentration of the endogenous cyanide in the degreased and freshly collected, unripe almonds were calculated and the value is found to be *ca.* 100 ± 12 ppm (Figure 2.19). This value is in agreement with the values reported in the literature.²⁶

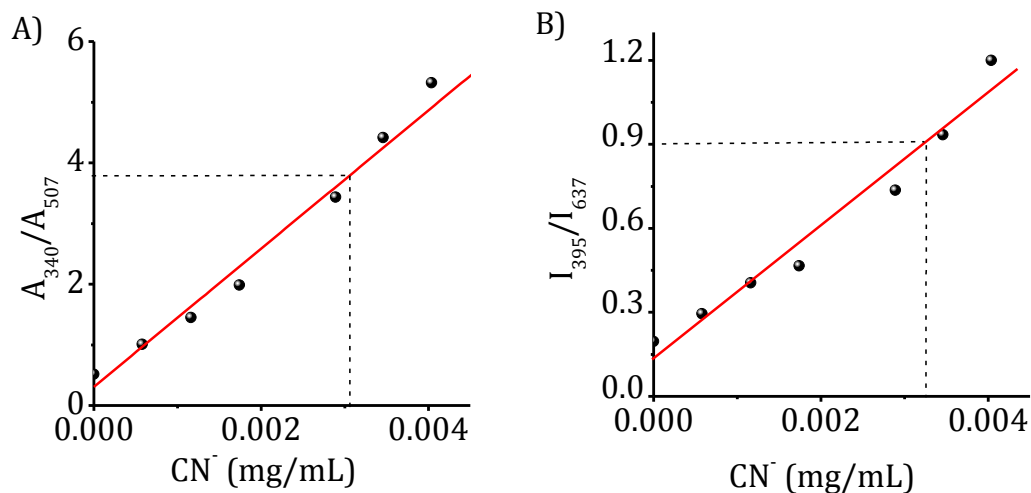


Figure 2.19. Quantitative estimation of the endogenous cyanide using the probe. Linear plot showing the changes in A) absorbance and B) fluorescence intensity vs the concentration of tetrabutylammonium cyanide in the aqueous medium.

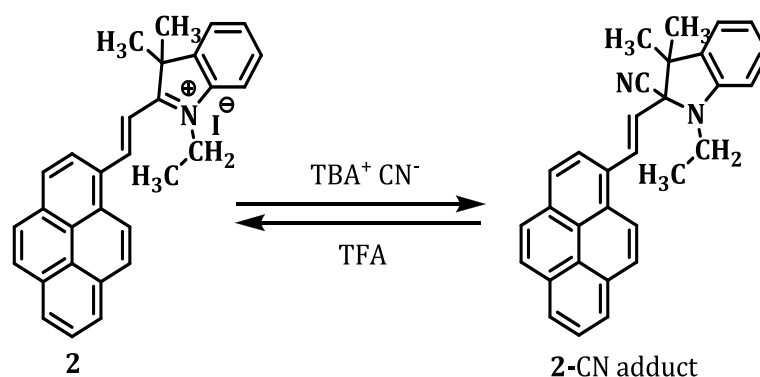
2.4. DISCUSSION

The indolium probes **1** and **2** under investigation showed favourable photophysical properties with well distinguished absorption and emission bands, owing to the charge transfer process from the aromatic chromophore to the

indolium moiety. Moreover, effect of the solvent polarity $E_T(30)$ on the emission maxima gave a linear correlation which confirmed that the charge transfer state in these cases is stabilized by the solvent.²² Both these conjugates showed selective interactions with the CN^- ions compared to other competent anions. Of these two systems, the anthracene analogue **1**, in the presence of the CN^- ions, showed negligible ratiometric changes in the emission spectra. On the other hand, the pyrene counterpart **2** showed significant fluorescence ratiometric changes with the CN^- ions, when excited at the isosbestic point of 375 nm. The ratiometric responses were evidenced with the decrement in the ICT emission at 637 nm, with the addition of the CN^- ions and with the simultaneous enhancement at 395 nm, corresponding to the pyrene monomeric emission. These changes were attributed due to the fact that the addition of the CN^- ions arrest the process of intramolecular charge transfer, with the disruption of the conjugation between the donor and acceptor groups. It is well reported in the literature that the CN^- ions are highly nucleophilic in nature and undergo reactions with the substrates like carbonyl, imidium groups.^{19e,f} However, in the case of the probes **1** and **2**, the CN^- ions can react with the imidium moiety either through 1,2 or 1,4-adduct formation. The formation of both these products can disrupt the conjugation and hence inhibit the intramolecular charge transfer between the donor anthracene/pyrene and the indolium acceptor moiety.

The observation of upfield shifts of the peaks corresponding to the vinylic protons as well as the methylene protons adjacent to the quaternized nitrogen of the indolium moiety corroborates the fact that the imidium group acts as the substrate

for the CN^- ions. However, the negligible changes observed in the coupling constant of vinylic protons suggest the formation of a 1,2-adduct over 1,4-adduct as shown in Scheme 2.2. The formation of the 1,2-adduct was unambiguously established through the isolation of the product, analytical and spectroscopic evidence. Moreover, owing to the bidentate nature of the cyano group, it is likely that such a reaction can also result in the formation of the isocyanide adduct. The ^{13}C NMR spectra of the 1,2-adduct of the probe **2** showed the absence of peak around *ca.* 155 ppm, corresponding to $-\text{N}^+\equiv\text{C}-$ functional group, which evidenced that the product formed is a CN^- adduct and not the isocyanide adduct.



Scheme 2.2. Probable mechanism for the formation of the 1,2-adduct upon reaction of the probe **2** with the CN^- ions.

The 1,2-adduct formed from the reaction of cyanide ions with the probe **2** can be categorized under the class of α -amino nitriles, which have been well exploited as versatile intermediates in a number of synthetic applications.²⁷ These α -amino nitriles serve as stable precursors to the iminium ions, whereby the loss of cyanide anion under a variety of conditions (e.g. use of Brønsted or Lewis acids)

generate the corresponding iminium intermediate. As documented in the literature,²⁸ the reversibility of the reaction was achieved by the acid mediated loss of the cyanide ion to give the starting material. We have thus demonstrated the potential of the probe **2** as a reversible chemodosimeter for the recognition and quantification of the cyanide ions through ratiometric fluorescence changes.

2.5. CONCLUSIONS

We synthesised two indolium based conjugates based on anthracene/pyrene moieties **1** and **2** and have systematically investigated their photophysical and anion binding properties under different conditions. Both these conjugates were characterised by involvement of intramolecular charge transfer (ICT) process and showed the corresponding distinguishable long wavelength absorption and fluorescence emission. Among the various anions tested, both these conjugates showed selective interactions with the CN⁻ ions with a limit of detection of 32 and 10 ppb, respectively. The recognition of the CN⁻ ions was characterised through the changes in the ICT induced absorption and emission bands. Of these two probes, the pyrene conjugate **2** can act as a selective and sensitive ratiometric fluorescent molecular probe for the detection of CN⁻ ions. The mechanism of the recognition of the CN⁻ ions by the probe **2** has been attributed to the formation of a 1,2-adduct, which was evidenced through various spectroscopic techniques as well as by the isolation of the resultant product. The reversibility of the reaction was investigated and the results were exemplified that the probe **2** acts as a reversible chemodosimeter for the detection of CN⁻ ions. The probe **2** can also be coated on the

solid support, filter paper strips as well as in the polymer matrix for the reversible and on-site analysis of the CN⁻ ions. Our results demonstrate that the probe **2** can be used not only for the quantification and analysis of the CN⁻ ions in solution but also for the endogenous concentration of CN⁻ ions in natural sources like Indian almonds.

2.6. EXPERIMENTAL SECTION

2.6.1. General Techniques

Melting points were determined on a Mel-Temp II melting point apparatus. The electronic absorption spectra were recorded on a Shimadzu UV-3101 or 2401PC UV-Vis-NIR scanning spectrophotometer. The fluorescence spectra were recorded on a SPEX-Fluorolog F112X and Perkin Elmer LS-55 spectrofluorimeters.²³ ¹H and ¹³C NMR spectra were recorded on 500 MHz Bruker advanced DPX spectrometer. The IR spectra were recorded on Perkin Elmer Model 882 and PRESTIGE-21 FTIR-84005 IR spectrometers. Quantum yields of fluorescence were calculated by the relative method using optically matching solutions using equation 2.1.,

$$\Phi_f = \frac{A_s F_u n_u^2}{A_u F_s n_s^2} \Phi_s \quad (\text{Eq. 2.1})$$

wherein, A_s and A_u are the absorbance of standard and unknown, respectively. F_s and F_u are the areas of fluorescence peaks of the standard and unknown and n_s and n_u are the refractive indices of the solvents used for the standard and unknown, respectively. Nile Red ($\Phi_F = 0.76$) and quinine sulphate ($\Phi_F = 0.55$) were used as the standards for determination of the fluorescence quantum yields. Isothermal titration

calorimetric (ITC) titrations were performed by using MicroCal iTC 200 calorimeter. All data were calculated with Origin ITC data-analysis software. All experiments were carried out using spectroscopic grade solvents and were carried out at room temperature (25 °C).

2.6.2. Materials and Methods

Starting materials. 9-Anthraldehyde, 1-pyrene carboxaldehyde and 2,3,3-trimethylindolenine were purchased from Sigma Aldrich. 2,3,3-Trimethyl-1-ethyl-3H-indolium iodide, mp 164–166°C (mixture mp 163–165 °C)²⁹ was synthesised as per the literature procedure.

2.6.3. Synthesis of the Aryl-Indolium Conjugates 1 and 2

General Procedure for the synthesis of the probes 1 and 2. A mixture of indolium iodide (0.97 mmol) and the corresponding aldehyde (0.97 mmol) was dissolved in 20 mL of dry ethanol. The reaction mixture was refluxed with stirring for a period of 4–5 h and the solvent was evaporated under vacuum. The resulted precipitate was dissolved in CH₂Cl₂. The organic layer was separated, washed three times with water and dried over anhydrous Na₂SO₄. The residue thus obtained was further purified by column chromatography on silica gel by eluting with a mixture of (49:1) CH₂Cl₂ and CH₃COCH₃ to give the corresponding products **1** or **2**.

(E)-2-(2-(Anthracen-9-yl)vinyl)-1-ethyl-3,3-dimethyl-3H-indolium iodide (1): 72%, mp 133–134°C; IR (KBr) ν_{\max} 3010, 1562, 1530, 1345, 1230 cm⁻¹; ¹H NMR (CDCl₃, 500 MHz) δ (ppm) 9.28 (1H, d, J=15 Hz), 8.65 (1H, s), 8.55 (2H, d, J=10 Hz),

8.11 (2H, d, J=10 Hz), 7.82-7.76 (2H, m), 7.68-7.59 (6H, m), 7.56 (1H, d, J=15 Hz), 4.90 (2H, q, J=7.5 Hz), 2.13 (6H, s), 1.60 (3H, t, J=7.5 Hz); ^{13}C NMR (CDCl_3 , 125MHz) δ (ppm) 180.89, 150.26, 143.41, 140.71, 133.03, 131.34, 130.39, 130.29, 129.98, 129.58, 129.10, 127.70, 126.20, 124.77, 123.59, 122.81, 120.88, 115.76, 52.98, 45.49, 27.17, 14.01, 11.35; HRMS (FAB) Calcd for $\text{C}_{28}\text{H}_{26}\text{N}^+$: 376.21, Found 376.19. CHN Anal. Calcd for $\text{C}_{28}\text{H}_{26}\text{IN}$: C, 66.80; H, 5.21; N, 2.78; Found: C, 67.02; H, 5.50; N, 2.55.

(E)-2-(2-(Pyren-1-yl)vinyl)-1-ethyl-3,3-dimethyl-3H-indolium iodide (2):

86%, mp 204–205°C; IR (KBr) ν_{max} 3004, 1571, 1522, 1310, 1225 cm^{-1} ; ^1H NMR (CDCl_3 , 500 MHz) δ (ppm) 9.40 (1H, d, J=15 Hz), 8.84 (1H, d, J=8 Hz), 8.66 (1H, d, J=9.5 Hz), 8.46-8.36 (5H, m), 8.26 (1H, d, J=9.5 Hz), 8.20 (1H, t, J=7.5 Hz), 7.82-7.78 (2H, m), 7.77 (1H, d, J=15 Hz), 7.68-7.66 (2H, m), 4.69 (2H, q, J=7.5 Hz), 1.95 (6H, s), 1.65 (3H, t, J=7.5 Hz); ^{13}C NMR (CDCl_3 , 125 MHz) δ (ppm) 180.57, 149.7, 143.26, 140.47, 135.94, 131.86, 131.06, 131.01, 130.71, 130.14, 129.78, 129.73, 127.75, 127.71, 127.62, 127.39, 126.70, 126.56, 126.33, 124.50, 124.09, 122.95, 120.88, 114.64, 113.04, 52.33, 44.46, 27.83, 14.49; HRMS (FAB) Calcd for $\text{C}_{30}\text{H}_{26}\text{N}^+$: 400.21; Found 400.55. CHN Anal. Calcd for $\text{C}_{30}\text{H}_{26}\text{IN}$: C, 68.32; H, 4.97; N, 2.66; Found: C, 68.57; H, 4.76; N, 2.63.

2.6.4. Preparation of the Dip-stick Probe

To a solution of the probe **2** (5 mg) dissolved in CH_2Cl_2 (5 ml), finely powdered neutral alumina (1 g) was added and allowed for the solvent to partial evaporation at room temperature. The probe **2** containing slurry of alumina

exhibited red fluorescence emission. The alumina slurry was bound to one end of the glass rod from its bottom, such that the part coated with the probe **2** can be dipped into the sample solution for the detection purpose.

2.6.5. Preparation of the Polymer Films

Polymethylmethacrylate (PMMA) polymer [500 mg, 99.8% (w/w)] was dissolved in dichloromethane, and mixed with the probe **2** [1 mg, 0.2% (w/w)] and poured onto a clean, glass petridish. The solvent was evaporated to dryness and the polymer film thus obtained showed red fluorescence emission.

2.6.6. Isothermal Titration Calorimetric Studies

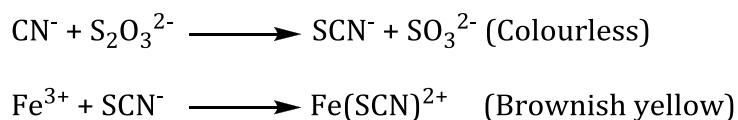
Isothermal titration calorimetric (ITC) experiments were performed at (30 ± 0.1) °C using a MicroCal iTC200 calorimeter. The anion titrant (CN^- , 15.0 mM) and the probe **2** solution (1 mM, 200 μL) were made from the same acetonitrile solvent. The solution in the sample cell was stirred at 1000 rpm by the injection syringe to ensure rapid mixing. Typically, the titrant (2.0 μL) was delivered in little spurts without time interval. The data were shown as the peak-integrated, concentration-normalized heat of reaction versus the molar ratio of the cyanide ions to dyad was presented in the bottom panel. The ITC data was analysed with the models using the Origin software package (MicroCal LLC ITC program) supplied by MicroCal. A nonlinear least-square algorithm (minimization of χ^2) was used to provide an equilibrium binding model and the best-fit values of the stoichiometry (n), change in enthalpy (ΔH), and binding constant (K).

2.6.7. Kinetic Fluorescence Studies

Kinetic studies were performed at 25 ± 1 °C using Perkin Elmer LS-55. The experiment was carried out using the kinetic mode of the instrument, where the emission of the probe **2** ($11.8 \mu\text{M}$) at 637 nm was monitored with respect to time, after the addition of the CN^- ions ($120 \mu\text{M}$).

2.6.8. Extraction of Endogenous Cyanide from Seeds of Indian Almonds

Seeds commercially available as well as unripe Indian almonds (*Terminalia catappa*) were collected and grounded to give fine powder. This was further degreased with hexane for a period of 24 h. The residue, thus obtained, was then extracted with 0.02 M sodium bicarbonate aqueous solution for 24 h. The extract was filtered and centrifuged and used for the detection of the endogenous cyanide. The presence of the cyanide content in the extract was confirmed using the common qualitative analysis. The aqueous almond extract was added to a solution of sodium thiosulphate, which was further treated with a solution of ferric chloride. An intense brownish yellow colouration was observed, which is a confirmation for the presence of the cyanide ions.



2.6.9. Quantification of the Endogenous Cyanide Using Probe **2**

The aqueous extract ($30 \mu\text{L}$) was added to a solution containing the probe **2** ($10 \mu\text{M}$) and the corresponding absorption and emission spectra were recorded. The

content of endogenous cyanide in the extract was measured with the probe **2** by using the standard addition method.²⁵ Tetrabutylammonium cyanide (TBACN) of various concentrations were added to the probe **2** (10 μ M) taken in different volumetric flasks and the absorption and emission spectra were recorded. A calibration curve was plotted (A_{340}/A_{508} or I_{395}/I_{637} vs concentration of TBACN). Subsequently, the unknown concentration of the cyanide in the 30 μ L of the aqueous extract was calculated to be 100 ± 12 ppm from the calibration curve.

2.7. REFERENCES

1. a) P. D. Beer and P. A. Gale, *Angew. Chem., Int. Ed.*, **2001**, *40*, 486; b) R. Martínez-Máñez and F. Sancenón, *Chem. Rev.*, **2003**, *103*, 4419; c) W. W. H. Wong, M. S. Vickers, A. R. Cowley, R. L. Paul and P. D. Beer, *Org. Biomol. Chem.*, **2005**, *3*, 4201; d) V. Amendola, L. Fabbrizzi and L. Mosca, *Chem. Soc. Rev.*, **2010**, *39*, 3889; e) P. A. Gale, *Chem. Commun.*, **2011**, *47*, 82; f) V. Amendola, D. Esteban-Gómez, L. Fabbrizzi and M. Licchelli, *Acc. Chem. Res.*, **2006**, *39*, 343.
2. a) R. M. Duke and T. Gunnlaugsson, *Tet. Lett.*, **2010**, *51*, 5402; b) J. Park, H. Kim, Y. Choi and Y. Kim, *Analyst*, **2013**, *138*, 3368; c) M.-Y. Wu, T. He, K. Li, M.-B. Wu, Z. Huanga and X.-Qi Yu, *Analyst*, **2013**, *138*, 3018; d) P. P. Neelakandan, M. Hariharan and D. Ramaiah, *J. Am. Chem. Soc.*, **2006**, *128*, 11334. e) D. Ramaiah, P. P. Neelakandan, A. K. Nair and R. R. Avirah, *Chem. Soc. Rev.*, **2010**, *39*, 4158.
3. a) A. Ishii, H. Seno, K. Watanabe-Suzuki, O. Suzuki and T. Kumazawa, *Anal. Chem.*, **1998**, *70*, 4873; b) Z. Xu, X. Chen, H. N. Kim and J. Yoon, *Chem. Soc. Rev.*, **2010**, *39*, 127; c) F. Pedro, M. Daniel, V. C. Jose, G. V. Maria and T. Tomas, *Chem.*

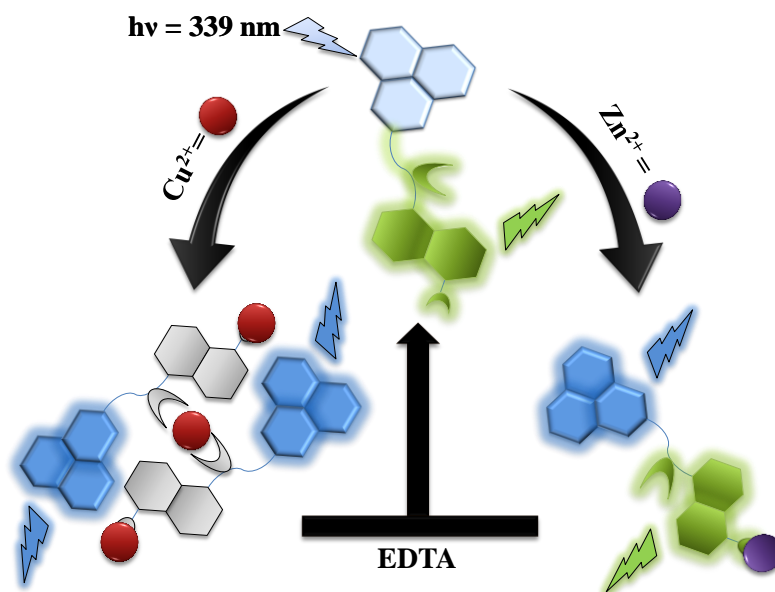
- Asian J.*, **2010**, *5*, 1692; d) S. Basurto, D. Miguel, D. Moreno, A. G. Neo, R. Quesada and T. Torrobac. *Org. Biomol. Chem.*, **2010**, *8*, 552; e) P. C. do Nascimento, D. Bohrer and L. M. de Carvalho, *Analyst*, **1998**, *123*, 1151.
4. Guidelines for Water Reuse, U.S. Environmental Protection Agency, EPA/625/R-04/108-2004; Washington, DC.
 5. a) C. Young, L. Tidwell, C. Anderson in Cyanide: Social, Industrial, and Economic Aspects, Minerals, Metals, and Materials Society, Warrendale, **2001**; b) E. Palomares, M. V. Martinez-Diaz, T. Torres and E. Coronado, *Adv. Funct. Mater.*, **2006**, *16*, 1166.
 6. Z. Xu, X. Chen, H. N. Kim and J. Yoon, *Chem. Soc. Rev.*, **2010**, *39*, 127.
 7. a) N. Kumari, S. Jha and S. Bhattacharya *J. Org. Chem.*, **2011**, *76*, 8215; b) H.- J. Mo, Y. Shen and B.- H. Ye *Inorg. Chem.*, **2012**, *51*, 7174; c) N. Kumari, S. Jha and S. Bhattacharya, *Chem. Asian J.*, **2012**, *7*, 2805; d) X. Lou, J. Qina and Z. Li *Analyst*, **2009**, *134*, 2071.
 8. a) R. Badugu, J. R. Lakowicz and C. D. Geddes, *J. Am. Chem. Soc.*, **2005**, *127*, 3635; b) L. Shang, C. Qin, L. Jin, L. Wang and S. Dong, *Analyst*, **2009**, *134*, 1477; c) R. Guliyev, S. Ozturk, E. Sahin and E. U. Akkaya, *Org. Lett.*, **2012**, *14*, 1528; d) Z. Ekmekci, M. D. Yilmaz and E. U. Akkaya, *Org. Lett.*, **2008**, *10*, 461;
 9. a) A. Wild, A. Winter, M. D. Hager and U. S. Schubert, *Analyst*, **2011**, *137*, 2333; b) X. Lou, J. Qin and Z. Li, *Analyst*, **2009**, *134*, 2071; c) Y. -H. Jeong, C. -H. Lee, W. -D. Jang and *Chem. Asian J.*, **2012**, *7*, 1562; d) T. Agou, M. Sekine, J. Kobayashi and T. Kawashima, *Chem. Eur. J.*, **2009**, *15*, 5056; e) F. H. Zelder, *Inorg. Chem.*, **2008**, *47*, 1264.

10. a) Y. Yang, Q. Zhao, W. Feng and F. Li, *Chem. Rev.*, **2013**, *113*, 192; b) J. Du, M. Hu, J. Fan and X. Peng, *Chem. Soc. Rev.*, **2012**, *41*, 4511; c) Z. Xu, X. Chen, H. N. Kim and J. Yoon, *Chem. Soc. Rev.*, **2010**, *39*, 127; c) Q. Lin, X. Liu, T. -B. Wei and Y. -M. Zhang, *Chem. Asian J.*, **2013**, *8*, 3015.
11. a) J. V. Ros-Lis, R. Martínez-Máñez and J. Soto, *Chem. Commun.*, **2005**, 5260; b) R. Badugu, J. R. Lakowicz and C. D. Geddes, *Dyes Pigm.*, **2005**, *64*, 49; c) Y. Kim, H.-S. Huh, M. H. Lee, I. L. Lenov, H. Zhao and F. P. Gabbai, *Chem.-Eur. J.*, **2011**, *17*, 2057.
12. a) Y. H. Kim and J. I. Hong, *Chem. Commun.*, **2002**, 512; b) X. Chen, S.-W. Nam, G.-H. Kim, N. Song, Y. Jeong, I. Shin, S. K. Kim, J. Kim, S. Park and J. Yoon, *Chem. Commun.*, **2010**, *46*, 8953; c) C.-F. Chow, M. H. W. Lam and W.-Y. Wong, *Inorg. Chem.*, **2004**, *43*, 8387.
13. W. J. Jin, M. T. Fernández-Argüelles, J. M. Costa-Fernández, R. Pereiro and A. Sanz-Medel, *Chem. Commun.*, **2005**, 883.
14. a) A. P. de Silva, H. Q. N. Gunaratne, T. Gunnlaugsson, A. J. M. Huxley, C. P. McCoy, J. T. Rademacher and T. E. Rice, *Chem. Rev.*, **1997**, *97*, 1515; b) X. -L. Liu, X.-Y. Duan, X.-J. Du, Q. -H. Song *Chem. Asian J.*, **2012**, *7*, 2696; c) B. H. Shankar and D. Ramaiah, *J. Phys. Chem B*, **2011**, *115*, 13292; d) P. P. Neelakandan and D. Ramaiah, *Angew. Chem., Int. Ed.*, **2008**, *47*, 8407; e) V. S. Jisha, K. T. Arun, M. Hariharan and D. Ramaiah, *J. Am. Chem. Soc.*, **2006**, *128*, 6024; f) P. C. Nandajan, P. P. Neelakandan and D. Ramaiah, *RSC Adv.*, **2013**, *3*, 5624; g) E. Kuruvilla and D. Ramaiah, *J. Phys. Chem. B*, **2007**, *111*, 6549; h) X. Yuan, Z. Luo, Y. Yu, Q. Yao

- and J. Xie, *Chem. Asian J.*, **2013**, *8*, 858; h) C. Wang, L. Xu, Y. Wang, D. Zhang, X. Shi, F. Dong, K. Yu, Q. Lin and B. Yang, *Chem. Asian J.*, **2012**, *7*, 1652.
15. a) M. E. Jun, B. Roy and K. H. Ahn, *Chem. Commun.*, **2011**, *47*, 7583; b) J. Du, M. Hu, J. Fan and X. Peng, *Chem. Soc. Rev.*, **2012**, *41*, 4511; c) J. Chan, S. C. Dodani and C. J. Chang, *Nat. Chem.*, **2012**, *4*, 973.
16. a) L. Yuan, W. Lin, Y. Yang, J. Song and J. Wang, *Org. Lett.*, **2011**, *13*, 3730; b) K.-S. Lee, H. J. Kim, G.-H. Kim, I. Shin and J.-I. Hong, *Org. Lett.*, **2008**, *10*, 49; c) J. Jin, J. Zhang, L. Zou and H. Tian, *Analyst*, **2013**, *138*, 1648.
17. a) J. L. Sessler and D. G. Cho, *Org. Lett.*, **2008**, *10*, 73; b) D. G. Cho, J. H. Kim and J. L. Sessler, *J. Am. Chem. Soc.*, **2008**, *130*, 12163.
18. M. Jamkratoke, V. Ruangpornvisuti, G. Tumcharern, T. Tuntulani and B. Tomapatanaget, *J. Org. Chem.*, **2009**, *74*, 3919.
19. a) H. J. Kim, K. C. Ko, J. H. Lee, J. Y. Lee and J. S. Kim, *Chem. Commun.*, **2011**, *47*, 2886; b) X. Lv, J. Liu, Y. Liu, Y. Zhao, Y. -Q. Sun, P. Wang and W. Guo, *Chem. Commun.*, **2011**, *47*, 12843; c) Z. Liu, X. Wang, Z. Yang and W. He, *J. Org. Chem.*, **2011**, *76*, 10286; d) Z. Cheng, R. Tang, H. Jia, J. Feng, J. Qin and Z. Li, *ACS Appl. Mater. Interfaces*, **2012**, *8*, 4387; e) J. Zhang, S. Zhu, L. Valenzano, F. -T. Luob and H. Liu, *RSC Adv.*, **2013**, *3*, 68; f) J. Jin, J. Zhang, L. Zou and H. Tian *Analyst*, **2013**, *138*, 1641.
20. a) C. Mannel-Croise, B. Probst and F. Zelder, *Anal. Chem.*, **2009**, *81*, 9493; b) K. P. Divya, S. Sreejith, B. Balakrishna, P. Jayamurthy, P. Anees and A. Ajayaghosh, *Chem. Commun.*, **2010**, *46*, 6069; c) T. Gómez, D. Moreno, B. D. de Greñu, A. C.

- Fernández, T. Rodríguez, J. Rojo, J. V. Cuevas and T. Torroba *Chem. Asian J.*, **2013**, *8*, 1271.
21. a) L. Sanguinet, J.-L. Pozzo, V. Rodriguez, F. Adamietz, F. Castet, L. Ducasse and B. Champagne, *J. Phys. Chem. B*, **2005**, *109*, 11139; b) E. Deniz, M. Tomasulo, J. Cusido, I. Yildiz, M. Petriella, M. L. Bossi, S. Sortino and F. M. Raymo, *J. Phys. Chem. C*, **2012**, *116*, 6058.
22. a) J. Hicks, M. Vandersall, Z. Babaogic, and K. B. Eisenthal, *Chem. Phys. Lett.*, **1985**, *116*, 18.
23. a) V. S. Jisha, A. J. Thomas and D. Ramaiah, *J. Org. Chem.*, **2009**, *74*, 6667; b) R. R. Avirah, K. Jyothish and D. Ramaiah, *Org. Lett.*, **2007**, *9*, 121; c) A. K. Nair, P. P. Neelakandan and D. Ramaiah, *Chem. Commun.*, **2009**, 6352.
24. a) T. J. Dale and J. Rebek, *J. Am. Chem. Soc.*, **2006**, *128*, 4500; b) Y. D. Lin, Y. S. Pen, W. Su, K. L. Liau, Y. S. Wen, C. H. Tu, C. H. Sun and T. J. Chow, *Chem. Asian J.*, **2012**, *7*, 2864.
25. W. R. Kelly, K. W. Pratt, W. F. Guthrie and K. R. Martin, *Anal. Bioanal. Chem.*, **2011**, *400*, 1805.
26. A. S. Ekop and N. O Eddy, *Chem Class J.*, **2005**, *2*, 74.
27. D. Enders and J. P. Shilvock, *Chem. Soc. Rev.*, **2000**, *29*, 359.
28. a) A. D. S. Goes, C. Ferroud and J. Santamaria, *Tet. Lett.*, **1995**, *36*, 2235; b) J. Santamaria, M. T. Kaddachi and C. Ferroud, *Tet. Lett.*, **1992**, *33*, 781.
29. L. Yuan, W. Lin and J. Song, *Chem. Commun.*, **2010**, *46*, 7930.

DANSYL-NAPHTHALIMIDE DYADS: STUDY OF THEIR METAL ION RECOGNITION PROPERTIES



3.1. ABSTRACT

We synthesised few dansyl-naphthalimide conjugates **1–5** linked through polymethylene spacer groups to explore their potential as molecular probes, and have investigated their interactions with various metal ions. The characteristic feature of these dyads is that they exhibited competing singlet-singlet energy transfer (SSET) and photoinduced electron transfer (PET) processes; both of these processes decreased with the increase in spacer length. Depending on the spacer group, these dyads showed selective interactions with the Cu^{2+} and Zn^{2+} ions, as

compared to other mono- and divalent metal ions. Jobs plot analysis showed that these dyads form 2:3 complexes with the Cu^{2+} ions, while 1:1 complexes were observed with Zn^{2+} ions. The association constants were determined and which were found to be in the range 10^3 – 10^5 M^{-1} . Furthermore, these dyads acted as ratiometric fluorescence molecular probes irrespective of the length of the spacer group for the Cu^{2+} ions by altering the emission intensity of both the dansyl and naphthalimide chromophores. In contrast, only the fluorescence intensity of the naphthalimide chromophore of the lower homologues (**1–3**) was altered by the Zn^{2+} ions. ^1H NMR and ITC measurements confirmed the involvement of both the sulphonamide and dimethylamine groups in the complexation with the Cu^{2+} ions, while the Zn^{2+} ions interact with only the latter functional group.

Nanosecond flash photolysis studies of these dyads were carried out which showed the transient absorption, which can be attributed to the radical anion of the naphthalimide chromophore. In contrast, only the triplet excited state of the dyads was observed in the presence of the Cu^{2+} ions. Uniquely, the complexation of the dyads **1–5** with the Cu^{2+} ions affected both PET and SSET processes, while, only the PET process was partially inhibited by the Zn^{2+} ions in the lower homologues (**1–3**); while the higher homologues (**4–5**) exhibited negligible changes in their fluorescence intensity. Our results demonstrate the spacer length dependent variation of the photophysical properties of these novel conjugates, which enabled not only selective recognition of the Cu^{2+} and Zn^{2+} ions, but also aid in discriminating these two important metal ions through ratiometric fluorescence changes.

3.2. INTRODUCTION

Development of chemosensors for essential metal ions,¹ especially copper and zinc ions, has gained increasing importance in recent years because these ions play important roles in living systems and have an extremely toxic impact on the environment.² For instance, the Cu^{2+} ions are important in maintaining many biological processes, but excess concentrations of these ions can be highly toxic.³ The Cu^{2+} ions are also capable of retarding many enzyme-catalyzed reactions by displacing other metal ions and acting as a cofactor.^{3d} Deficiency of the Cu^{2+} ions leads to Menkes disease,^{4a} while high levels cause Alzheimer^{4b,c} or Wilson disease,^{4d} gastrointestinal disorders and kidney damage. The Zn^{2+} ions, on the other hand, play central role in various biological processes including signal transduction, metabolism of RNA and DNA, gene expression and numerous other cellular functions.⁵ The overdose of Zn^{2+} ions can result in clinical conditions, some of which are similar to those observed with the Cu^{2+} ions deficiency. Due to these reasons, the development of the molecular probes that can, not only signal the presence of these two metal ions, but also differentiate between them is important. Of the various techniques employed, the optoelectronic detection has several advantages and the fluorescence based techniques, in particular, offer high sensitivity.⁶

The most commonly adopted approach in the design of a fluorescence based chemosensor is to incorporate a fluorophore (signaling unit) with ion-receptor unit that can bind to various metal ions. The binding of the metal ions with the receptor unit can cause variations in the fluorescence of the fluorophore moiety either by

altering photoinduced electron transfer (PET)⁷ or fluorescence resonance energy transfer (FRET)⁸ mechanism, resulting in the sensing of the metal ions. An alternative approach is to employ two different fluorescent chromophores linked *via* a suitable spacer group characterised by PET and/or singlet–singlet energy transfer (SSET) mechanisms, so that the metal ion binding results in blockade of either one or both of these mechanisms such that a selective fluorescence signaling can be achieved. However, if the binding site in the ligand has affinity towards more than one metal ion, such a sensor will suffer from selectivity. Nevertheless, if the binding of one of the metal ion can selectively alter or exclusively hinder one relaxation pathway over the other, such a sensor can be employed to discriminate different metal ions under similar conditions.

Recently, Miranda and coworkers⁹ have reported few dansyl–naphthalimide dyads linked through a sulphonamide bridging group. The interesting feature of these bichromophoric systems is the presence of two competing relaxation processes: PET from the dansyl chromophore to the naphthalimide moiety and SSET from the naphthalimide moiety to the dansyl entity. The estimated rates of PET and SSET processes indicate that both these relaxation processes decrease with the increase in the length of the spacer group. These dyads contained two potential metal ion binding sites: the sulphonamide as well as the dimethylamine group. It can, therefore, be expected that the interactions of such dyads with different metal ions can in principle would alter the photophysical properties and thus, enable the detection of specific metal ions. In this context, we designed a series of the dansyl–naphthalimide dyads **1-5** bridged through polymethylene spacer group (Chart 3.1).

In these cases, two binding processes can be envisaged in the presence of the metal ions: one pertains to the interaction of the metal ion at the dimethylamino group, while the other corresponding to the deprotonation of the sulphonamide bridging unit. Depending on the nature, the metal ion can, thus, partially or completely, either perturb PET or hinder the SSET process, or inhibit both of these processes. In the present study, we have systematically investigated the potential of the dyads **1–5** as selective molecular probes for different metal ions and also the role of the spacer group in the metal ion binding properties. Our results demonstrate that the lower homologues (**1–3**) of the dyad series show interactions with both the Cu^{2+} and Zn^{2+} ions, while the dyads with longer spacer groups (**4** and **5**) interact only with the Cu^{2+} ions and thereby act as sensitive ratiometric fluorescence probes.

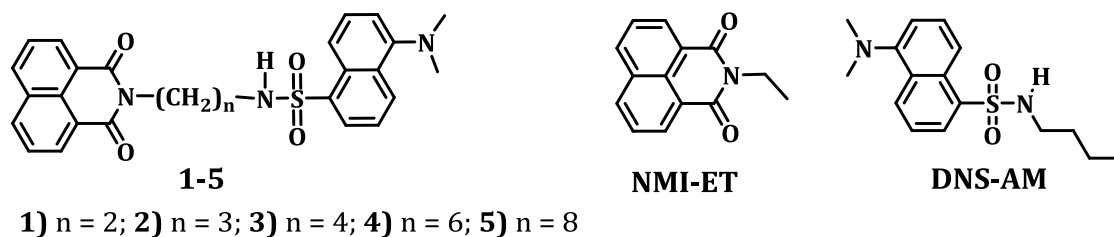


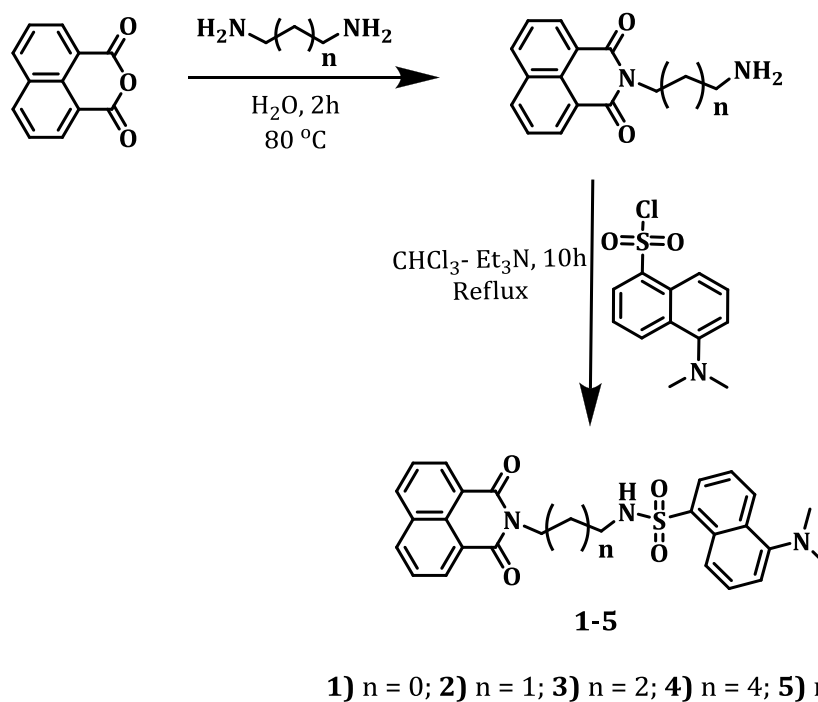
Chart 3.1

3.3. RESULTS

3.3.1. Synthesis of the Dansyl–Naphthalimide Dyads

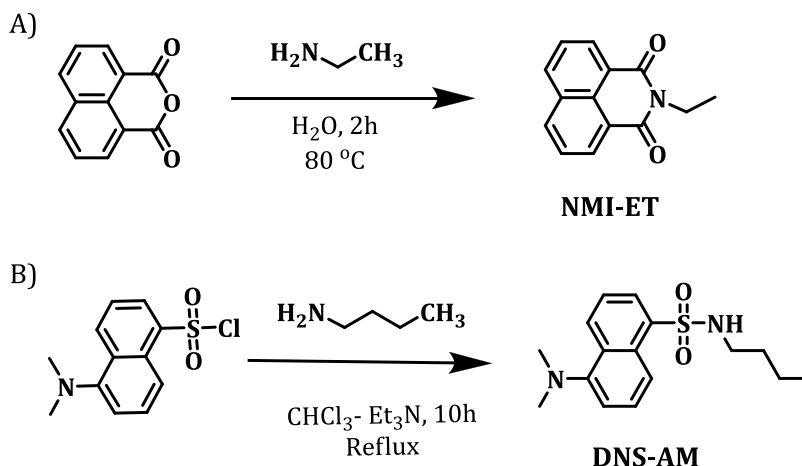
As shown in Scheme 3.1, the synthesis of dansyl–naphthalimide dyads **1–5**, linked through varying spacer groups has been achieved in good yields (*ca.* 60–66%) by the reaction of the corresponding *N*-(ω -aminoalkyl)-1,8-naphthalimides with

dansyl chloride, whereas the model derivatives **NMI-ET** and **DNS-AM** were synthesised as per the reported procedures.¹⁰ These products were purified through column chromatography as well as recrystallization from different solvents. The starting materials and products were characterised on the basis of spectral data and analytical results. For example, the ¹H NMR spectrum of the dyad **1** in CD₃CN, showed the -NH protons of the sulfonamide group of dansyl moiety as a triplet at δ 5.95 ppm, while the six *N*-CH₃ protons appeared as a singlet at δ 2.66 ppm and the methylene protons as triplet and quartet at δ 4.12 and 3.29 ppm, respectively. The aromatic peaks of the dansyl appeared in the region δ 6.74 – 7.96 ppm, whereas the naphthalimide proton signals are observed multiplets at δ 7.72 and 8.29 ppm. The ¹³C NMR spectrum of the dyad **3**, on the other hand, consisted of signals δ 39.2–42.8



Scheme 3.1. Synthesis of the dansyl-naphthalimide dyads **1–5**.

ppm, corresponding to the aliphatic sp^3 carbons of the methylene spacer group and carbon of N-CH₃ group appeared at 45.6 ppm. Similarly, the aromatic carbons of the probe **3** appeared in the region 114.5–151.6 and the carbonyl carbon at 165.0 ppm.



Scheme 3.2. Synthesis of the model derivatives, A) **NMI-ET** and B) **DNS-AM**.

3.3.2. Absorption and Fluorescence Properties

The absorption spectra of the dyads **1–5** in acetonitrile are shown in Figure 3.1A. These dyads showed the absorption maximum at 332 nm with a shoulder at 339 nm. The absorption spectra of these naphthalimide–dansyl dyads is similar to that of the model derivative **NMI-ET**, implying that there are no ground state interactions exist between the these two chromophores. The emission spectra of these dyads were characterised by two well spaced maxima at 378 and 525 nm, when excited at 339 nm (where more than 80% of the incident photons are absorbed by the naphthalimide moiety).^{9a} The emission peak observed at 378 nm can be attributed to the naphthalimide chromophore, while the peak at 525 nm was assigned to the dansyl moiety, which arises due to the excited state energy transfer

from the naphthyl chromophore to the dansyl moiety. This observation has been corroborated by the excitation spectral analysis as shown in Figure 3.2.

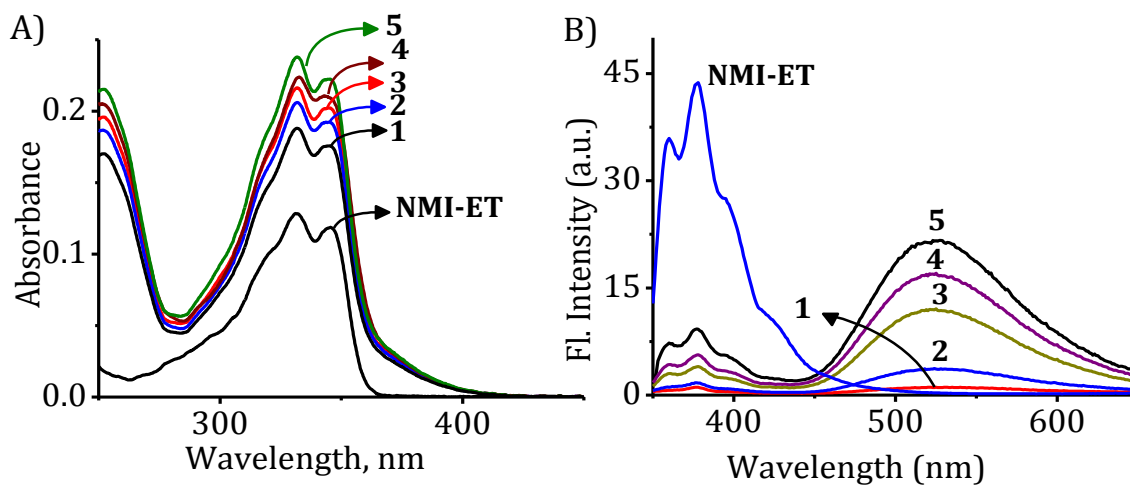


Figure 3.1. A) Absorption and B) emission spectra of the dyads **1-5** (12 μM) and **NMI-ET** (12 μM) in acetonitrile. Excitation wavelength, 339 nm.

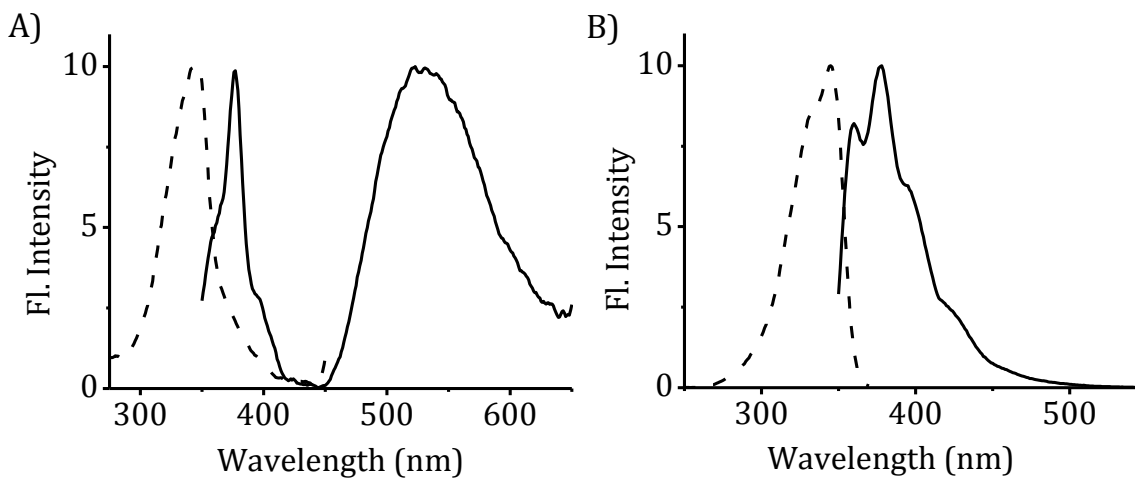


Figure 3.2. Normalized excitation (dashed line) and emission spectra (solid line) of A) **1** (12 μM) and B) **NMI-ET** (12 μM) in acetonitrile. Excitation wavelength, 339 nm. Excitation spectra were collected for the emission wavelengths, A) 525 and B) 378 nm, respectively.

To understand the mechanism of the energy transfer, we have carried out the AM1 theoretical calculations to generate the optimized structures. Based on these structures, we have determined the distance between the dansyl chromophore and the naphthalimide moiety. We observed the values of distances in the range 5.6 to 12.01 Å with the increase in the spacer length for the dyads 1-5 (Figure 3.3). The observed range of distances is quite below the estimated critical energy transfer distance (R_0) of *ca.*14.4 Å.¹¹ The theoretically calculated values as well as the photophysical properties of these dyads are summarised in Table 3.1. Results indicate that the energy transfer process thus observed can be attributed to occur through a Coulombic mechanism,¹¹ which was corroborated by the existence of a large spectral overlap integral ($J_{\text{Coulombic}} = 3.1 \times 10^{-12} \text{ cm}^6 \text{ mol}^{-1}$) for these dyads.

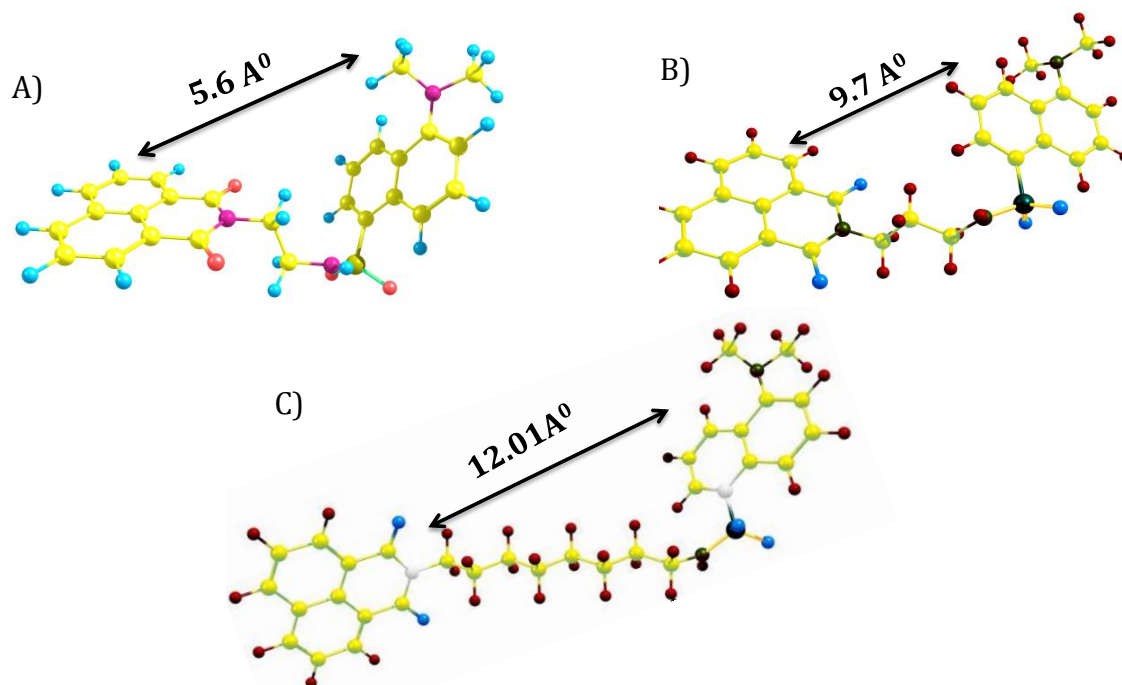


Figure 3.3. AM1 optimized structures of the dyads A) 1 B) 3 and C) 5.

Table 3.1. Photophysical properties of various dyads **1-5**.^a

Dyad	Molar Extinction Coefficient (ϵ) at 345 nm ($M^{-1}cm^{-1}$)	Fluorescence quantum yield (ϕ_F)	Distance between naphthalimide and dansyl moieties ^c (\AA)
1	1.416×10^4	0.01 ± 0.005^b	5.6
2	1.562×10^4	0.06 ± 0.007^b	8.4
3	1.656×10^4	0.09 ± 0.002^b	9.7
4	1.742×10^4	0.12 ± 0.009^b	11.1
5	1.813×10^4	0.18 ± 0.01^b	12.0
NMI-ET	0.935×10^4	0.016 ± 0.003	-

^aAverage of more than three independent experiments. ^bCalculated using **DNS-AM** in acetonitrile ($\Phi_F=0.3$) as the reference standard. ^cCalculated by theoretical calculations using AM1 method.

3.3.3. Recognition of the Metal Ions

The dyads **1-5** having suitable binding sites for the metal ions showed characteristic dual emission and hence it was our interest to investigate their potential as molecular probes. With this view, we have carried out their interactions with various mono and divalent metal ions. For example, Figure 3.4A shows the changes in the absorbance of the dyad **1** with the addition of the Cu^{2+} ions in acetonitrile. Upon increasing in concentration of the Cu^{2+} ions, we observed a gradual decrease in the absorption band at 340 nm, with the concomitant increase in

the band at 287 nm, and exhibited isosbestic points at 265 and 320 nm.

Interestingly, in the emission spectra, with the addition of the Cu^{2+} ions resulted in

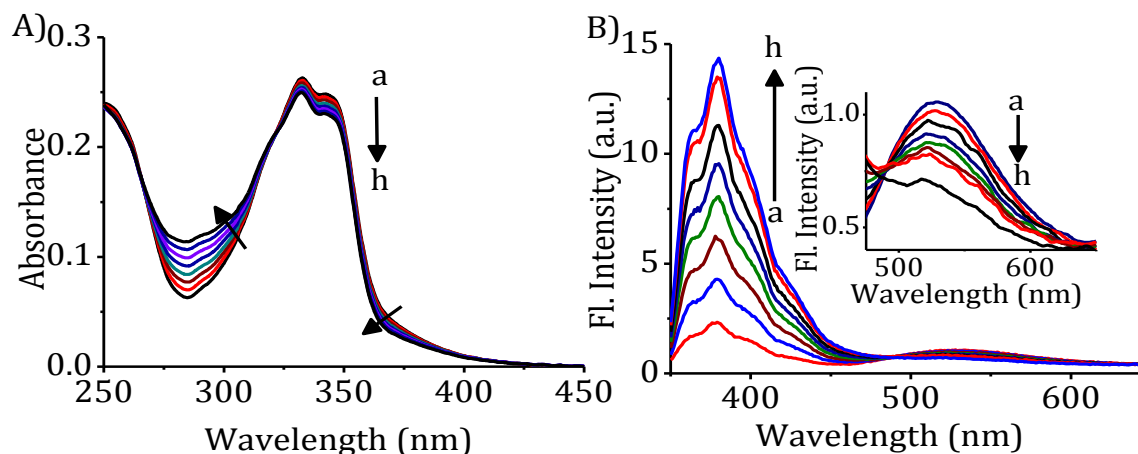


Figure 3.4. Changes in the A) absorption and B) emission spectra of the dyad **1** (16 μM) in acetonitrile with the addition of the Cu^{2+} ions. $[\text{Cu}^{2+}]$ (a) 0 and (h) 32 μM . Excitation wavelength, 339 nm. Inset of B shows the corresponding changes in the emission spectra at 525 nm.

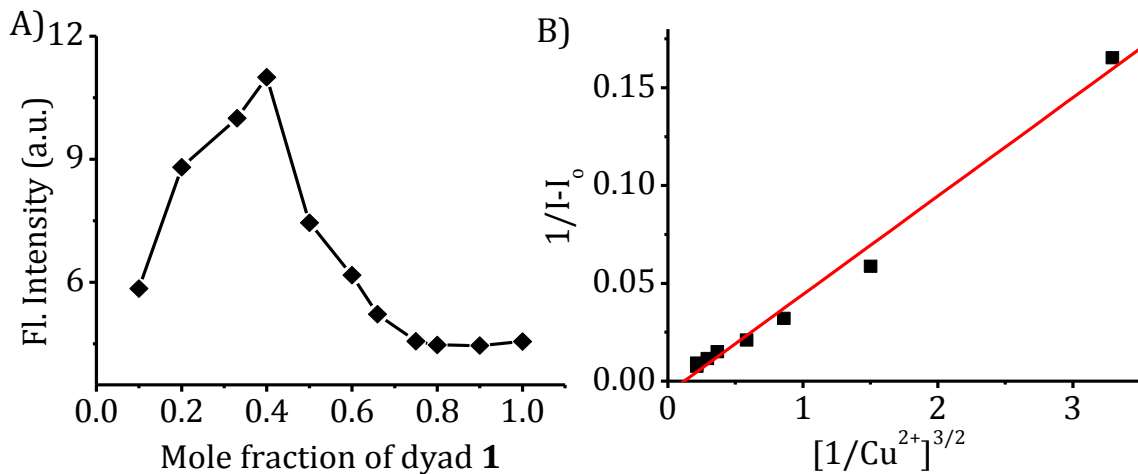


Figure 3.5. A) Jobs plot and B) Benesi-Hilderbrand plot for the complexation of the dyad **1** with A) Cu^{2+} ions in acetonitrile. The ratio of changes at the emission wavelengths, I_{378}/I_{525} . Excitation wavelength, 339 nm.

the decrease in intensity of SSET mediated dansyl emission at 525 nm (Figure 3.4B). Simultaneously, we could observe the growth of the emission band corresponding to the naphthalimide at 378 nm with an isoemissive point at 485 nm. The addition of 12 μM of the Cu^{2+} ions resulted in significant increase in the ratio of $I_{378/525}$ to *ca.* 20, thereby indicating its potential as a ratiometric sensor for the Cu^{2+} ions. The fluorescence changes of the dyad **1** in the presence of the Cu^{2+} ions were analysed through Jobs and Benesi-Hildebrand plots¹² (Figure 3.5), which gave a 2:3 stoichiometry for the complexation between the dyad **1** and Cu^{2+} ions and exhibited the association constant value of $K = 1.19 \pm 0.23 \times 10^5 \text{ M}^{-1}$.

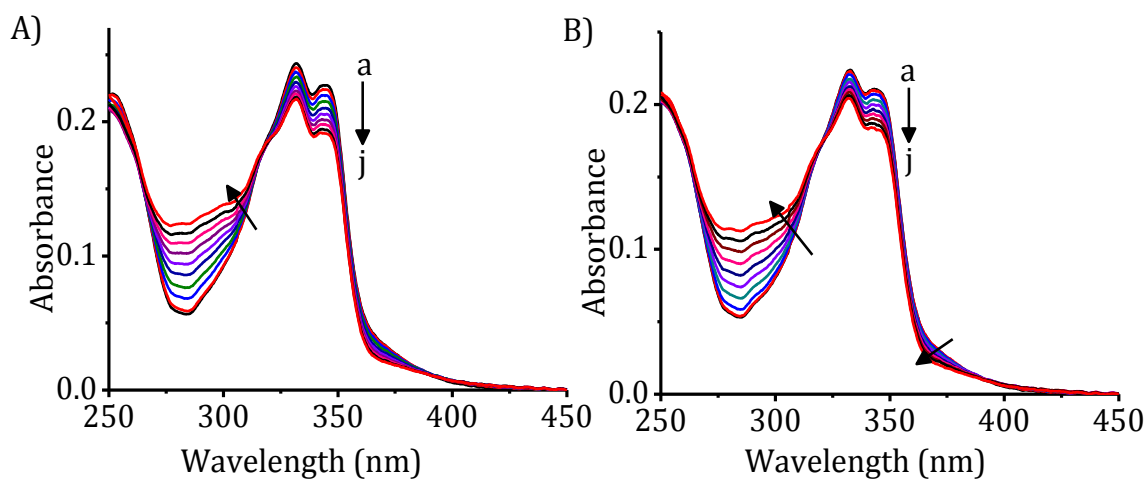


Figure 3.6. Changes in the absorption spectra of the dyads A) **2** (16 μM) and B) **3** (16 μM) in acetonitrile with the addition of the Cu^{2+} ions. [Cu^{2+}] (a) 0, and (j) 32 μM .

To study how the variation of the spacer group affects rates of energy and electron transfer processes,¹³ the interaction of the dansyl-naphthalimide dyads **2-5** with the Cu^{2+} ions was investigated. Figure 3.6 shows the changes in the absorption

spectra of dyads **2** and **3** with the addition of the Cu^{2+} ions. As observed for the dyad **1**, we observed a regular decrease in the emission intensity at 525 nm for **2**, with the concomitant increase in the emission corresponding to the naphthalimide chromophore at 378 nm with the addition of the Cu^{2+} ions (Figure 3.7A). We observed the saturation at 1.5 equivalents; with the ratiometric fluorescence change ratio $I_{378/525}$, of *ca.* 20-fold. Interestingly, the dyad **3** having tetramethylene spacer, also showed a fluorescence ratiometric ($I_{378/525}$) change of *ca.* 20-fold, indicating thereby the negligible influence of the spacer length on the interaction of the Cu^{2+} ions with the dyads (Figure 3.7B). Similarly and also as observed in the case of the dyad **1**, the Jobs plot analysis gave a stoichiometry value of 2:3 for the complexes [dyad- Cu^{2+}] formed between the dyads **3-5** and the Cu^{2+} ions.

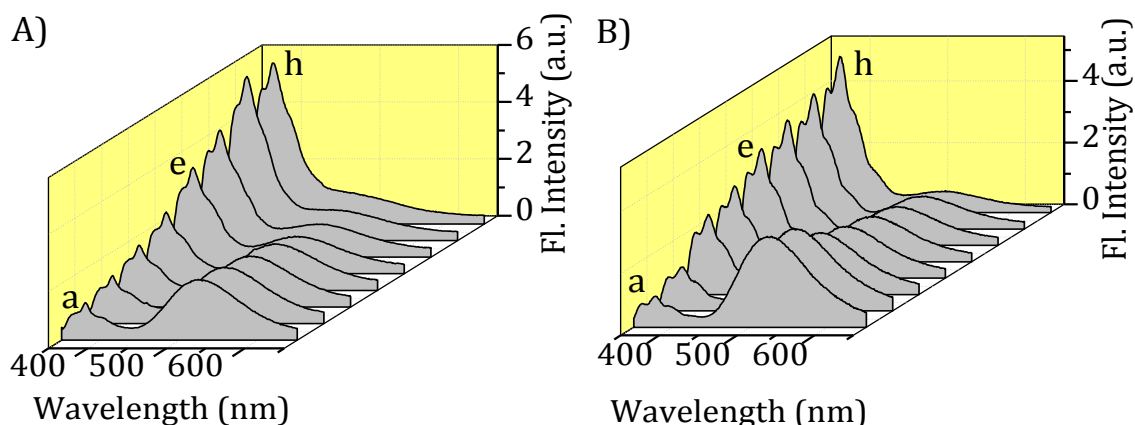


Figure 3.7. Changes in the emission spectra of the dyads, A) **2** (16 μM) and B) **3** (16 μM) in acetonitrile with the addition of the Cu^{2+} ions. [Cu^{2+}] (a) 0, (e) 6, and (h) 32 μM . Excitation wavelength, 339 nm.

3.3.4. Selectivity and Reversibility of the Recognition

To investigate the selectivity of the dyads **1-5** for the Cu^{2+} ions, we have investigated their interactions with other important monovalent and divalent metal ions such as Na^+ , Li^+ , K^+ , Pb^{2+} , Hg^{2+} , Co^{2+} , Fe^{2+} , Cd^{2+} , Mg^{2+} , Ba^{2+} and Zn^{2+} ions under identical conditions. Notably, all the metal ions, except Zn^{2+} ions, showed negligible interactions towards these dyads. The addition of the Zn^{2+} ions caused negligible changes in the absorption properties of the dyad **1** (Figure 3.8A). However, in the emission spectrum of the dyad **1**, we observed an enhancement in the fluorescence intensity at 378 nm, corresponding to the naphthalimide chromophore (Figure 3.8B). At the same time, the SSET mediated emission band of the dansyl group of the dyad **1** at 525 nm, showed negligible changes. The changes in the emission of the naphthalimide reached saturation with the addition of 2 equivalents of the Zn^{2+} ions,

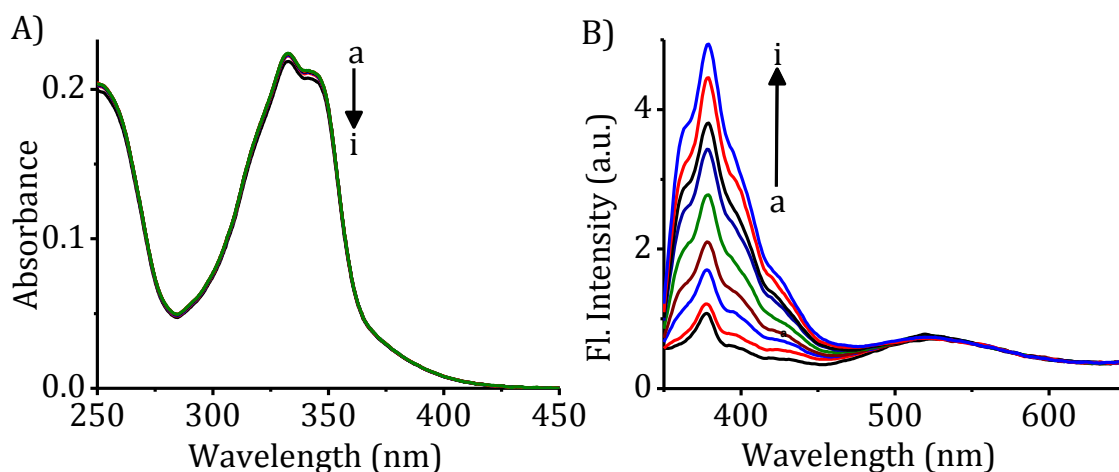


Figure 3.8. Changes in the A) absorption and B) emission spectra of the dyad **1** (16 μM) in acetonitrile with the addition of the Zn^{2+} ions. $[\text{Zn}^{2+}]$ (a) 0, and (i) 32 μM . Excitation wavelength, 339 nm.

with an overall enhancement of *ca.* 4.6-fold of the fluorescence ratiometric ratio of I_{378}/I_{525} . The Jobs plot analysis of the complexation between the dyad **1** and the Zn^{2+} ions indicated the formation of a 1:1 complex (Figure 3.9), with an association constant of $7.26 \pm 0.52 \times 10^4 M^{-1}$.

To understand the effect of spacer group, we have monitored the interactions of the dyads **2-5** with the Zn^{2+} ions. For example, Figure 3.10A shows the changes in the emission spectrum of the dyad **2** in presence of the Zn^{2+} ions. As observed in the case of the dyad **1**, the addition of the Zn^{2+} ions resulted in the enhancement in the emission band at 378 nm, corresponding to the naphthalimide chromophore with negligible changes in the SSET mediated emission band of the dansyl moiety at 525 nm. However, the extent of enhancement of the naphthalimide emission was found to be low i.e., *ca.* 2.3-fold for the dyad **2**, as compared to *ca.* 4.6-

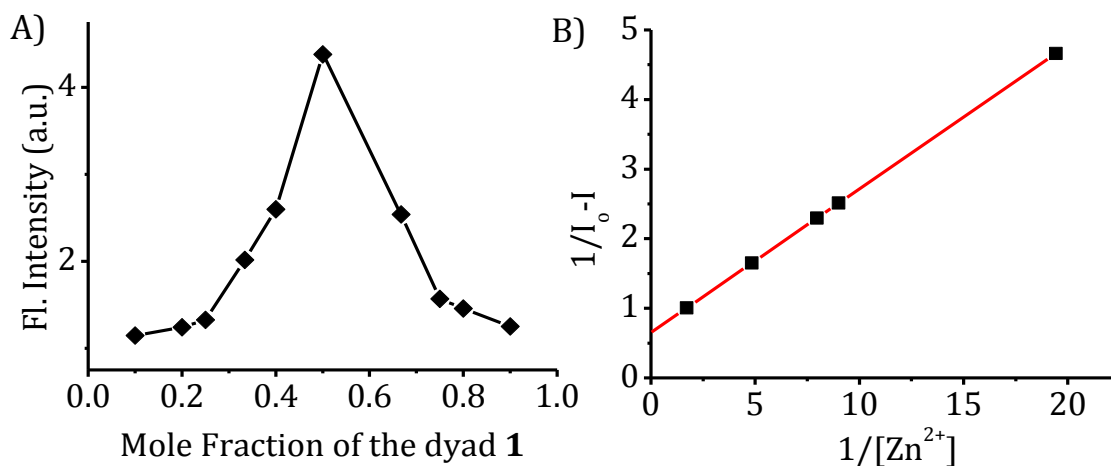


Figure 3.9. A) Jobs plot and B) Benesi-Hilderbrand plot for the complexation of the dyad **1** with the Zn^{2+} ions in acetonitrile. Emission wavelength monitored is the ratio of I_{378}/I_{525} . Excitation wavelength, 339 nm.

fold enhancement observed for the dyad **1**. Similar changes in the emission spectra were observed for the dyad **3** in the presence of the Zn^{2+} ions, albeit with much lowered (*ca.* 1.5 fold) enhancement of the naphthalimide emission band (Figure 3.10B). Further increase in the length of the spacer to the hexa and octa-methylene groups, as in the case of the dyads **4** and **5**, respectively, caused negligible changes in the emission bands of these dyads.

Figure 3.11A shows the relative changes in the fluorescence intensity of the dyads **1-5** with the addition of different metal ions. As evident from the figure, the addition of equimolar concentrations of other metal ions caused negligible changes in the fluorescence emission of all the dyads. The interaction of the dyad **1** towards the Cu^{2+} and Zn^{2+} ions can readily be monitored because the fluorescence intensity of the dyad **1** remained unchanged in the presence of the other metal ions. In contrast, we observed significant increment in the fluorescence ratio of I_{378}/I_{525} in the presence of the Cu^{2+} and the Zn^{2+} ions. Interestingly, it is also possible to employ the dyads, **1-3**, to distinguish between the Cu^{2+} and Zn^{2+} ions, since the Zn^{2+} ions altered only the fluorescence emission intensity at 378 nm.

To investigate the reversibility of the complexation of the dyad **1** with the Cu^{2+} and Zn^{2+} ions, ethylenediamine tetraacetic acid (EDTA)¹⁴ was used as the ligand for the metal ions. The dyad **1**, initially, showed dual emission bands with emission maxima at 378 and 525 nm. However, with the addition of the Cu^{2+} ions, a significant increase in the fluorescence intensity at 378 nm was observed. When EDTA was added to the solution of the [**1**- Cu^{2+}] complex, we observed the decrease in the

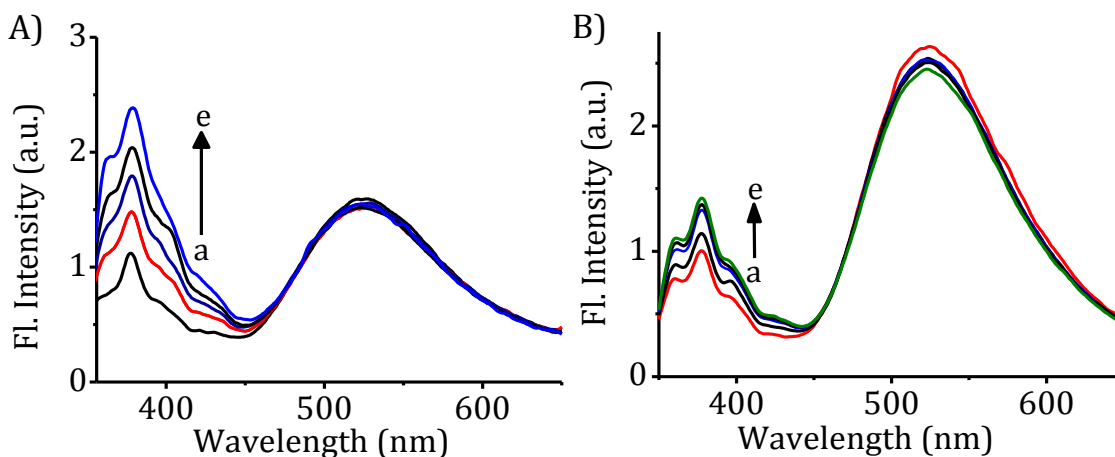


Figure 3.10. Changes in the emission spectra of A) **2** (6 μM) **3** (16 μM) in acetonitrile with the addition of Zn^{2+} ions. $[\text{Zn}^{2+}]$ (a) 0, and (e) 32 μM . Excitation wavelength, 339 nm.

fluorescence intensity, corresponding to the naphthalimide chromophore (Figure 3.11B). These results demonstrate the reversible binding of the Cu^{2+} ions with the dyads. Similar observations were made in the case of the [dyad- Zn^{2+}] complexes with the addition of EDTA.

3.3.5. Nature of the Metal Ion Complexation

The complexation between the dyads and Cu^{2+} and Zn^{2+} ions was further studied through ^1H NMR and isothermal titration calorimetric (ITC) experiments. Interestingly, the addition of Cu^{2+} ions resulted in significant broadening and the downfield shift of $N\text{-H}$ peak by $\Delta\delta = 0.05$ ppm, while the peaks corresponding to the $N\text{-CH}_3$ protons showed a shift of $\Delta\delta = 0.12$ ppm. The peaks at δ 7.11 ppm assigned to the aromatic protons of the dansyl moiety showed broadening as well as downfield

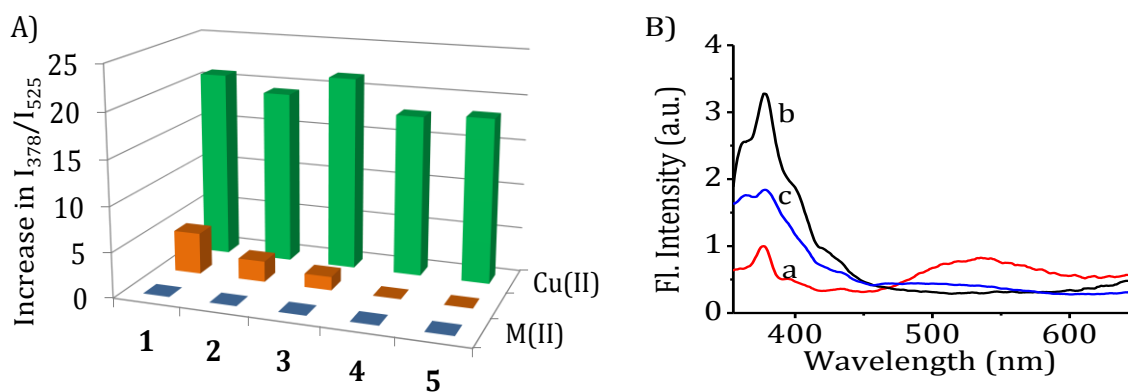


Figure 3.11. A) Relative plot showing the increase in I_{378}/I_{525} vs dyads in the presence of various metal ions; Cu^{2+} , Zn^{2+} and $M(II)$: Pb^{2+} , Hg^{2+} , Co^{2+} , Fe^{2+} , Cd^{2+} , Mg^{2+} , Ba^{2+} ions. Excitation wavelength, 339 nm. B) Emission spectra of the dyad **1** (16 μM) in the presence of the Cu^{2+} ions (32 μM) in acetonitrile. a) **1** alone, b) [**1**- Cu^{2+}] complex, and c) [**1**- Cu^{2+}] complex after the addition of aqueous solution of EDTA (16 μM). Excitation wavelength, 339 nm.

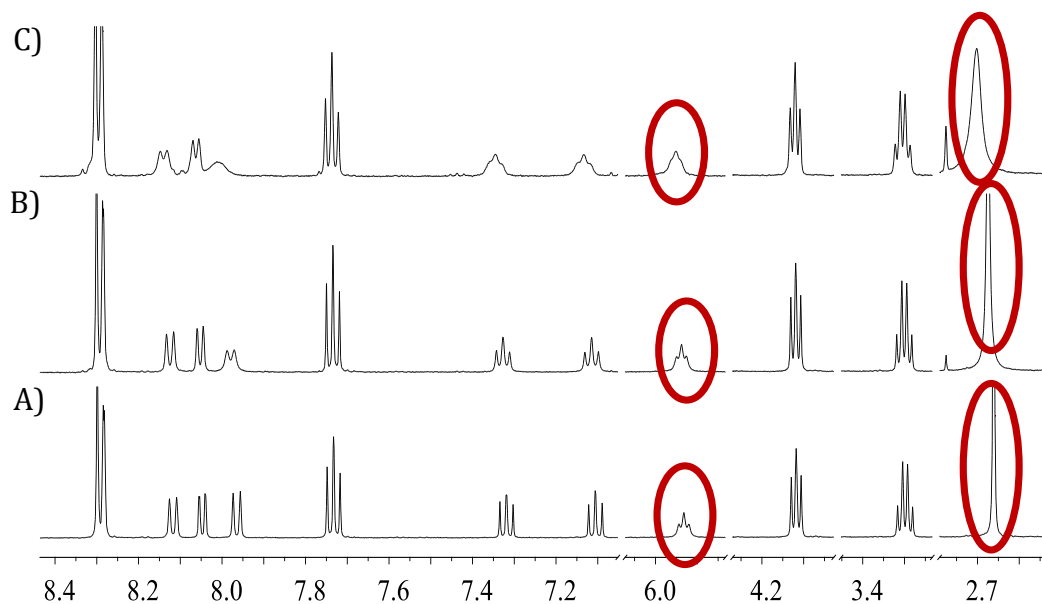


Figure 3.12. 1H NMR spectra of the dyad **1** (8 mM) with the addition of the Cu^{2+} ions in CD_3CN . [Cu^{2+}] A) 0, B) 5, and C) 15 mM.

shift of $\Delta\delta = 0.03$ ppm (Figure 3.12). In contrast, negligible changes were observed in the case of the naphthalimide protons. The association constant values calculated from the Benesi-Hildebrand analysis of changes in δ corresponding to $N\text{-CH}_3$ was found to be $8.0 \pm 0.1 \times 10^5 \text{ M}^{-1}$, respectively, and which is in agreement with the K value obtained from the emission changes.

The addition of the Zn^{2+} ions to the dyad **1**, on the other hand, caused less significant changes for the peak at δ 5.95 ppm, corresponding to the sulphonamide. As observed in the presence of the Cu^{2+} ions, the Zn^{2+} ions also caused a shift in the N -methyl protons, though to a lesser extent of $\Delta\delta = 0.06$ ppm (Figure 3.13). Furthermore, we observed significant broadening of the peaks corresponding to the dansyl aromatic protons in the ^1H NMR spectrum, indicating that the Zn^{2+} ions interact with the dyads at the dansyl moiety. The association constant calculated

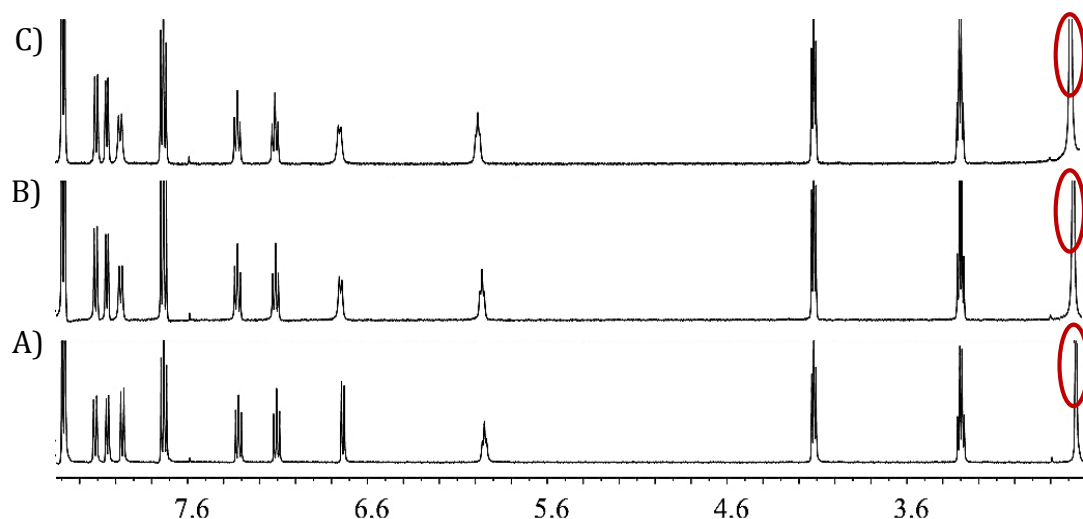


Figure 3.13. ^1H NMR spectra of the dyad **1** (8 mM) with the addition of the Zn^{2+} ions in CD_3CN . [Zn^{2+}] A) 0, B) 4, and C) 10 mM.

from the shift of the $N\text{-CH}_3$ peak was found to be $6.0 \pm 0.3 \times 10^4 \text{ M}^{-1}$, which is in good agreement with the value obtained from the emission changes.

Isothermal titration calorimetric (ITC) measurements allow the direct determination of the association constant (K), the binding enthalpy (ΔH) and stoichiometry (n , number of binding sites) and provide insights in understanding the involvement of various types of interactions. Figure 3.14A shows the heat evolved per injection plotted against the molar ratio for the calorimetric titration of the dyad **1** with the Cu^{2+} ions. By this, the thermodynamic parameters involved in the

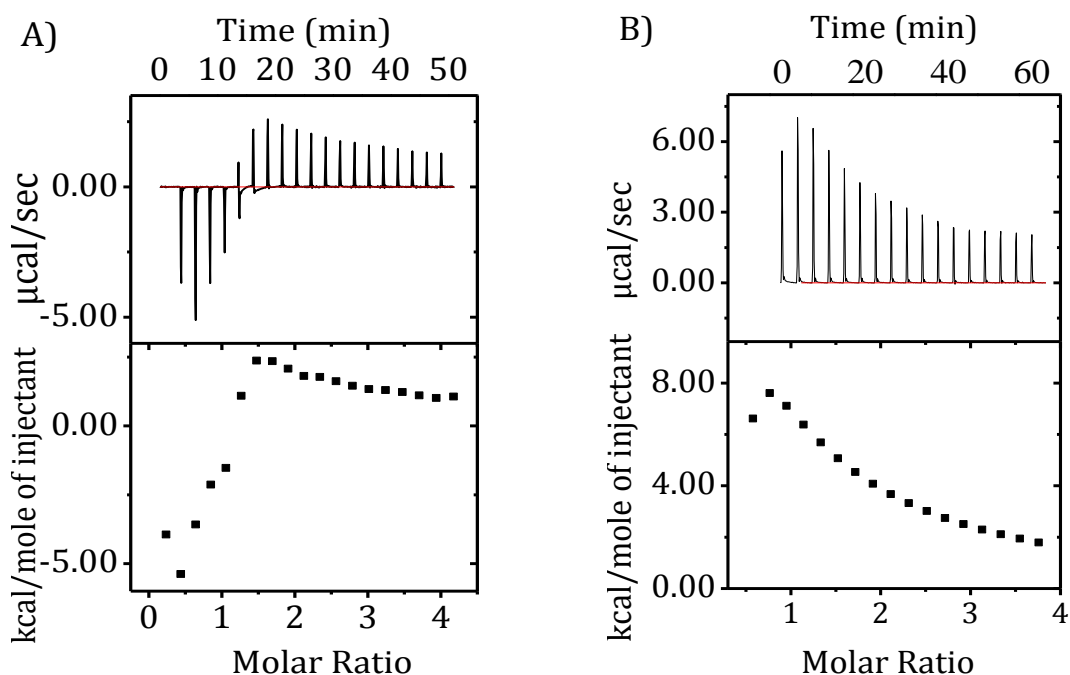


Figure 3.14. ITC titration of the dyad **1** (0.25 mM) with A) Cu^{2+} (5.0 mM), B) Zn^{2+} (2.5 mM) ions in acetonitrile at 303 K. (Top) Differential power recorded in the experiment; (Bottom) Integration of areas under peaks corresponding to the amount of heat released upon addition of the Cu^{2+} or Zn^{2+} ions to the dyad **1** as a function of the molar ratio ($[\mathbf{1}]/[\text{M}^{2+}]$). $\text{M} = \text{Cu}^{2+}$ or Zn^{2+} ions.

complexation were determined by fitting the ITC data to either one or two independent binding sites model using non-linear least-square fitting. As can be seen from the figure, an initial exothermic process was observed with the addition of the Cu^{2+} ions, which correspond to a 1:1 complexation with an association constant of $K_1 = 8.03 \pm 0.05 \times 10^5 \text{ M}^{-1}$. This is followed by an endothermic event with $K_2 = 2.10 \pm 0.14 \times 10^3 \text{ M}^{-1}$. The calculated ΔG values for these processes show that both these binding events are highly feasible; with $\Delta G_1 = -8.15 \pm 0.02 \times 10^3$ and $\Delta G_2 = -4.58 \pm 0.01 \times 10^3 \text{ cal/mol}$, respectively. In contrast, the addition of the Zn^{2+} ions to a dilute solution of dyad **1**, showed a regular endothermic response at 30 °C as shown in Figure 3.14B. The heat changes, fitted to a one site binding model, which gave an

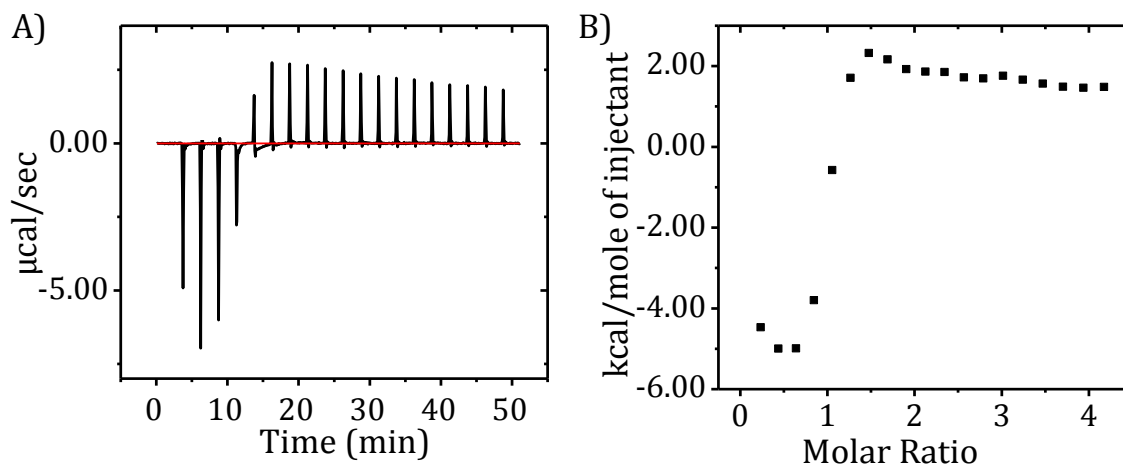


Figure 3.15. ITC titration of the dyad **2** ($0.25 \mu\text{M}$) with the Cu^{2+} ($5.0 \mu\text{M}$) ions in acetonitrile at 303 K. A) Differential power recorded in the experiment; B) Integration of areas under peaks corresponding to the amount of heat released upon the addition of the Cu^{2+} ions to dyad **2** as a function of the molar ratio of ($[\mathbf{2}]/[\text{Cu}^{2+}]$).

association constant of $1.70 \pm 0.07 \times 10^4 \text{ M}^{-1}$ and n value of 1.05. The [**1**-Zn²⁺] complex, on the other hand showed a free energy change of $-5.84 \pm 0.23 \times 10^3 \text{ cal mol}^{-1}$. Similar observations were made with the other dyads, **2–4** (Figure 3.15) and various thermodynamic parameters obtained for the interactions of these dyads with the Cu²⁺ and Zn²⁺ ions are summarised in Table 3.2.

Table 3.2. Binding and thermodynamic parameters obtained from isothermal titration calorimetric experiments of the dyads **1-4** with the Cu²⁺ and Zn²⁺ ions.^a

	No. of sites, n	Association constant, $K, \text{ M}^{-1}$	ΔH cal/mol, 10^4	ΔG^b cal/mol, 10^3
1 + Cu ²⁺	0.99	$8.03 \pm 0.05 \times 10^5 (K_1)$	-0.53 ± 0.02	-8.15 ± 0.02
	0.52	$2.10 \pm 0.14 \times 10^3 (K_2)$	2.88 ± 0.32	-4.58 ± 0.01
2 + Cu ²⁺	0.95	$7.30 \pm .03 \times 10^5 (K_1)$	-0.56 ± 0.01	-8.09 ± 0.01
	0.56	$2.81 \pm 0.17 \times 10^3 (K_2)$	2.93 ± 0.07	-4.76 ± 0.20
3 + Cu ²⁺	0.98	$4.06 \pm 0.17 \times 10^5 (K_1)$	-0.54 ± 0.02	-7.74 ± 0.11
	0.55	$1.01 \pm 0.41 \times 10^3 (K_2)$	1.71 ± 0.45	-4.15 ± 0.02
4 + Cu ²⁺	0.97	$1.85 \pm 0.81 \times 10^5 (K_1)$	-0.57 ± 0.37	-7.27 ± 0.03
	0.58	$2.14 \pm 0.96 \times 10^3 (K_2)$	1.18 ± 0.09	-4.60 ± 0.01
1 + Zn ²⁺	1.05	$1.70 \pm 0.07 \times 10^4$	13.50 ± 0.03	-5.84 ± 0.23
2 + Zn ²⁺	0.98	$1.51 \pm 0.01 \times 10^4$	5.51 ± 0.11	-5.77 ± 0.61
3 + Zn ²⁺	1.01	$0.41 \pm 0.01 \times 10^4$	3.73 ± 0.14	-4.99 ± 0.22

^aAverage of more than three independent experiments. ^bCalculated using the equation $\Delta G = -RT \ln K$.

3.3.6. Laser Flash Photolysis Studies

With a view to understand the transients involved, we have carried out the nanosecond laser flash photolysis studies of the dyads in the presence and absence of the metal ions. Excitation of the dyad **1**, by 355 nm pulse gave a transient spectrum having absorption maximum at 410 nm. Based on literature reports¹⁵ we assigned this peak to the naphthalimide radical anion formed as a result of PET process from the dansyl chromophore to the naphthalimide moiety (Figure 3.16A). With the addition of the Cu^{2+} ions to a solution of the dyad **1**, the peak corresponding to the naphthalimide radical anion disappeared with the concomitant appearance of new peaks maxima at 360, 440 and 470 nm. This transient absorption was readily quenched by dissolved oxygen, suggesting that the transient absorption could be due to the triplet excited state of the dyad. The transient absorption spectrum obtained for the $[\mathbf{1}-\text{Cu}^{2+}]$ complex was characteristic of the T_1-T_n triplet excited

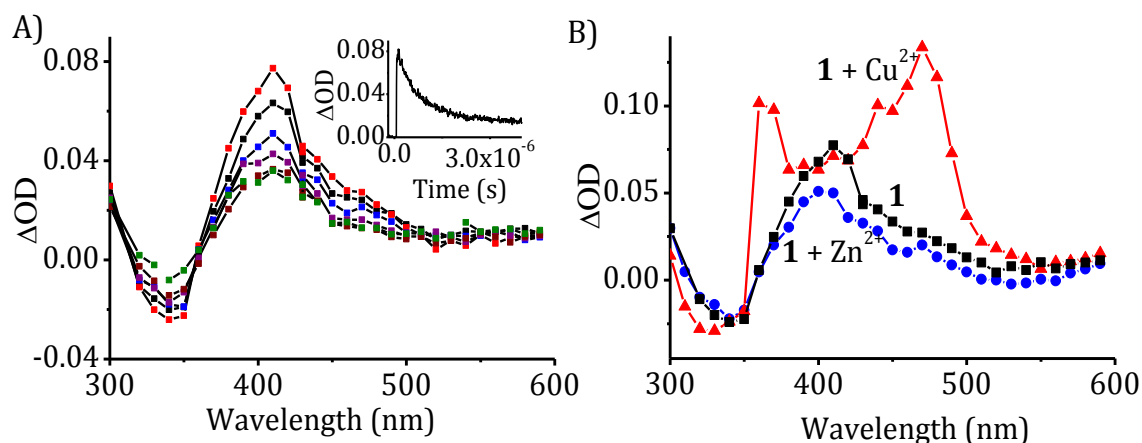


Figure 3.16. Transient absorption spectra obtained following 355 nm laser pulse excitation of de-aerated solution of a) dyad **1** (18 μM), b) Cu^{2+} (27.6 μM) and c) Zn^{2+} (27.6 μM) ions in acetonitrile.

state absorption of the naphthalimide chromophore (trace b in Figure 3.16B).¹⁵ Interestingly, the formation of the triplet excited state of the naphthalimide chromophore has been observed for all the dyads, irrespective of the spacer group, in the presence of the Cu^{2+} ions. In contrast, we observed, only the transient absorption of the naphthalimide radical anion, in the presence of the Zn^{2+} ions, albeit with low intensity, indicating thereby the partial inhibition of the photoinduced electron transfer process (trace c in Figure 3.16B) under these conditions.

3.4. DISCUSSION

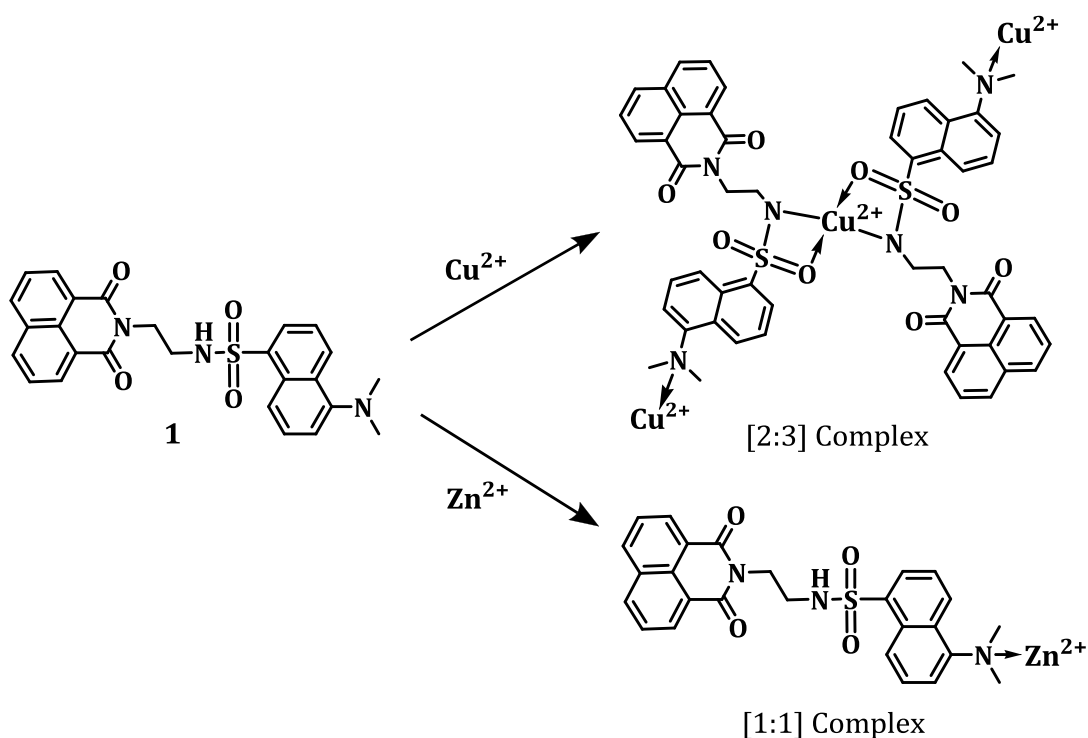
The dyads **1-5**, under investigation exhibited both mechanisms such as SSET and PET processes. These processes can be easily visualized from the emission spectra of the dyads with characteristic dual bands at 378 nm and 525 nm, which correspond to the naphthalimide chromophore and the SSET mediated dansyl emission, respectively. It is noteworthy to mention that both these processes vary with the spacer groups; the dyads with the longest spacer group having the lowest rate of SSET/PET.¹⁶ Moreover, the existence of distance between the two chromophores in these dyads is within the critical distance of 14.4Å, and hence these systems can undergo energy transfer process as confirmed through changes in their photophysical properties.¹²

Furthermore, these dyads **1-5** showed selective interactions with the Cu^{2+} and Zn^{2+} ions, when compared to other mono and divalent metal ions. In the presence of the Cu^{2+} ions, we observed the formation of a new band, that could be attributed to the deprotonation of the sulphonamide group.¹⁷ Notably, such

deprotonation led to the inhibition of the energy transfer process (SSET) in all the dyads. As a result we observed negligible SSET mediated emission of the dansyl moiety and which enabled the monitoring of the presence of Cu²⁺ ions through ratiometric fluorescence changes.

The evidence for this hypothesis was obtained through NMR, ITC and laser flash photolysis experiments. In the ¹H NMR spectra, we observed broadening and downfield shift of the peaks corresponding to the sulphonamide and *N*-methyl protons, upon interaction with the Cu²⁺ ions. This indicates fact that both these groups act as potential sites to interact with the Cu²⁺ ions (Scheme 3.3). Such a proposition was also consistent with the observed stoichiometry of 2:3 through the Jobs plot analysis for all [dyad-Cu²⁺] complexes. Further evidence was obtained through the results of the ITC experiments, which showed the existence of two distinct binding events; an exothermic and an endothermic process with the addition of the Cu²⁺ ions. The exothermic process with a *n* value of *ca.* 1 can be attributed to the formation of a 1:1 complex between the Cu²⁺ ions and the dyads involving the *N,N*-dimethylamine group of the dansyl moiety. The association constant for this binding interaction, and the associated free energy change, decreased considerably with the increasing in spacer group [$8.03 \pm 0.05 \times 10^5 \text{ M}^{-1}$ for **1** (*n*=2) and $1.85 \pm 0.81 \times 10^5 \text{ M}^{-1}$ for **4** (*n*=6)]. Nevertheless, the enthalpy change for this process remained more or less constant for all the dyads.

The second binding event, as seen from the ITC measurements was an enthalpy driven process, which could be attributed to the deprotonation of the sulphonamide group. The *n* value obtained for this process, *ca.* 0.5; pertains to the



Scheme 3.3. Structure of the complexes formed between **1** and the $\text{Cu}^{2+}/\text{Zn}^{2+}$ ions.

formation of a 2:1 complex, with respect to the dyad. Expectedly, the deprotonation process was not significantly affected by the spacer length as well as in ΔG values across the dyad series. However, both these processes were found to be favourable as indicated by the negative ΔG values (Table 3.2). Thus, the overall binding stoichiometry was two ligands to three Cu^{2+} ions, which is in agreement with the observations made with the analysis of the Jobs plot and photophysical measurements. Furthermore, the observation of higher value of the association constants, calculated from the ^1H NMR and ITC changes, for the interaction of the Cu^{2+} ions at the *N,N*-dimethylamine group suggest a much stronger affinity for this site, when compared to the binding at the sulphonamide group.

On the basis of these observations, we propose that the interaction of the Cu^{2+} ions at the *N,N*-dimethylamine group prevents the PET process (from dansyl to the naphthalimide moiety), while the deprotonation of the sulphonamide group disrupts the SSET process (from naphthalimide to the dansyl moiety), which results in the alteration of both these processes for all dyads in the presence of Cu^{2+} ions. This hypothesis was evidenced through the nanosecond laser flash photolysis studies, wherein, we observed the negligible formation of the transient absorption, corresponding to the radical anion of the naphthalimide chromophore in the presence of the Cu^{2+} ions. Under these conditions, we observed only the triplet excited state of the naphthalimide moiety due to the perturbation of both PET as well as SSET processes. The Cu^{2+} ions thus caused the complete disruption of both the processes, and hence the ratio of I_{378}/I_{525} remained the same for all the dyads.

The interaction of the Zn^{2+} ions with the dyads, on the other hand, caused negligible changes in their absorption spectra revealing the non-perturbation of the electronic levels of the dyads. Interestingly, the Zn^{2+} ions significantly enhanced the emission of the naphthalimide chromophore at 378 nm, with negligible alterations of the SSET mediated dansyl emission intensity. The Jobs plot analysis indicated the formation of a 1:1 complex as shown in Scheme 3.2; with the Zn^{2+} ions interacting only at the dimethylamino functionality. This interaction was evidenced by the shift observed in the peaks corresponding to the N-CH_3 protons at δ 2.66 ppm. The observation of lower value of the association constant ($6 \times 10^4 \text{ M}^{-1}$) obtained for this interaction, as compared to that of the Cu^{2+} ions ($8 \times 10^5 \text{ M}^{-1}$), confirms the existence of only weak interactions between the Zn^{2+} ions and the dyads. This hypothesis was

evidenced through the ITC experiments, which confirmed the formation of a 1:1 complex with association constants of the order of 10^4 M^{-1} . Notably, a significant decrease in the K values observed with increase in the spacer length and this trend was also reflected in the photophysical studies. The extent of the fluorescence intensity enhancement of the naphthalimide chromophore (378 nm) was found to decrease considerably from **1** to **5**, in the order $1 > 2 > 3 > 4 > 5$.

More importantly, the interaction of the Zn^{2+} ions with the dyads at the dimethylamino group showed negligible influence on the SSET reaction, but partially affected the PET process. This was, in turn, reflected in the negligible changes observed in the energy transfer mediated dansyl emission intensity in the presence of the Zn^{2+} ions. The observation of the transient absorption of the naphthalimide radical anion even in the presence of the Zn^{2+} ions, furthermore confirms the fact that the electron transfer process is only partially inhibited, rather than a complete inhibition as observed in the presence of the Cu^{2+} ions. In contrast, the negligible emission changes observed for the higher homologues (**4** and **5**) in the presence of the Zn^{2+} ions as compared to the lower series (**1-3**) demonstrates the lower values of the rate of PET for the former series over the latter. Thus, these dyads uniquely interact only with the Cu^{2+} and Zn^{2+} ions and further can also be effectively utilized for their differentiation through changes in ratiometric fluorescence intensity.

3.5. CONCLUSIONS

The dansyl-naphthalimide dyads (**1-5**) linked through spacer groups of different lengths have exhibited characteristically both PET and SSET processes and

irrespective of the spacer group, they acted as selective ratiometric fluorescence probes for the recognition of the Cu^{2+} ions. Both these mechanisms i.e., PET and SSET were inhibited upon the addition of the Cu^{2+} ions. In contrast, these dyads exhibited spacer length dependent interactions with the Zn^{2+} ions; wherein the lower homologues (**1–3**) exhibited the maximum affinity. The interactions with the Zn^{2+} ions resulted only in partial inhibition of PET process and while un-altering the SSET process. All these interactions were found to be reversible as evidenced through EDTA titrations. The uniqueness of this study is that, although these dyads interact effectively and selectively with both the Cu^{2+} and Zn^{2+} ions, as compared to other mono and divalent metal ions, due to their contrary redox character, these two metal ions affected the photophysical processes in the dyads differently. As a result, these dyads can be effectively utilized for differentiating the Cu^{2+} ions even in the presence of the Zn^{2+} ions and signal the event through the changes in ratiometric fluorescence intensity.

3.6. EXPERIMENTAL SECTION

3.6.1. General Techniques

The melting points were determined on a Mel-Temp II melting point apparatus. The electronic absorption spectra were recorded on a Shimadzu UV-3101 or 2401PC UV-Vis-NIR scanning spectrophotometer. The fluorescence spectra were recorded on a SPEX-Fluorolog F112X spectrofluorimeter. ^1H and ^{13}C NMR spectra were recorded on a 500 MHz Bruker advanced DPX spectrometer with chemical

shifts reported relative to TMS. The transient absorption studies were carried out using a nanosecond laser flash photolysis system by employing an Applied Photophysics model LKS-20 laser kinetic spectrophotometer using OCR-12 Series Quanta Ray Nd:YAG laser. The analyser and laser beams were fixed at right angles to each other. The laser energy was 60-65 mJ at 355 nm. Quantum yields of fluorescence were measured by the relative method using optically matching solutions. Isothermal titration calorimetric titrations were carried out using a Microcal iTC200 microcalorimeter. All data were calculated with Origin ITC data-analysis software. All experiments were carried out at room temperature (25 °C) using spectroscopic grade solvents.

3.6.2. Materials and Methods

Starting Materials. 1,8-Naphthalic anhydride, dansyl chloride, diaminoalkanes, ethylamine and butylamine were purchased from Aldrich and S. D. Fine Chemicals, India. All the solvents used were purified and distilled before use by the standard methods.

3.6.3. Synthesis of the Dansyl-Naphthalimide Dyads 1-5

General procedure for the synthesis of the dyads 1-5. Dansylchloride (5.0 mmol) was added to a stirred solution of the corresponding *N*-(ω -aminoalkyl)-1, 8-naphthalimide (4.2 mmol) and triethylamine (5.4 mmol) in dry chloroform (15 mL). The reaction mixture was refluxed for 10 h. After cooling the reaction mixture to room temperature (25 °C), the precipitate thus obtained was filtered off. The

clear filtrate solution was evaporated to dryness under vacuum to give a pale yellow residue, which was chromatographed over silica gel. Elution with a mixture (1:9) of ethyl acetate and hexane gave the dyads **1-5** in good yields. The dyads thus obtained were further purified through recrystallization from acetonitrile.

5-(Dimethylamino)-N-(2-(1,3-dioxo-1H-benzo[de]isoquinolin-2(3H)-yl)ethyl)naphthalene-1-sulfonamide (1). 63%, mp 152–153 °C; ¹H-NMR (500 MHz, CD₃CN) δ (ppm) 2.66 (s, 6H), 3.29 (q, 2H, J=5 Hz), 4.12 (t, 2H, J=5.5 Hz), 5.95 (t, J = 5.5 Hz, 1H), 6.74 (d, 1H, J = 5.5 Hz), 7.11 (t, 1H, J = 8.5 Hz), 7.32 (t, 1H, J = 8 Hz), 7.72 (t, 2H, J = 8 Hz), 7.96 (d, 1H, J = 8.5 Hz), 8.05 (d, 1H, J = 8.5 Hz), 8.11 (d, 1H, J = 8 Hz), 8.29 (d, 4 H, J = 8.5 Hz); ¹³C-NMR (125 MHz, CD₃CN) δ (ppm) 39.2, 42.8, 45.6, 100.0, 114.5, 118.6, 122.4, 123.3, 127.2, 128.4, 129.4, 129.7, 130.4, 130.4, 130.6, 131.7, 134.2, 134.5, 151.6, 165.0; HRMS (FAB) Calcd for C₂₆H₂₃N₃O₄S: 473.14; Found: 473.30.

5-(Dimethylamino)-N-(3-(1,3-dioxo-1H-benzo[de]isoquinolin-2(3H)-yl)propyl)naphthalene-1-sulfonamide (2). 66%, mp 142–144 °C; ¹H-NMR (500 MHz, CD₃CN) δ (ppm) 1.68-1.74 (m, 2H), 2.82 (s, 6H), 2.87 (q, 2H, J = 5 Hz), 3.99 (t, 2H, J = 5 Hz), 6.07 (t, 1H, J = 5 Hz), 7.22 (d, 1H, J = 7.5 Hz), 7.43 (t, 1H, J = 7.5 Hz), 7.59 (t, 1H, J = 7.5 Hz), 7.79 (t, 2H, J = 8.5 Hz), 8.12 (d, 1H, J = 8 Hz), 8.29 (d, 1H, J = 8.5 Hz), 8.32 (d, 2 H, J = 8.5 Hz), 8.45 (t, 3H, J = 8.5 Hz); ¹³C-NMR (125 MHz, CD₃CN) δ (ppm) 28.5, 37.4, 40.4, 45.8, 115.5, 119.6, 122.6, 123.6, 127.4, 128.5, 128.6, 129.7, 130.1, 130.3, 130.6, 131.9, 131.9, 134.7, 135.9, 152.2, 165.0; HRMS (FAB) Calcd for C₂₇H₂₅N₃O₄S: 487.15; Found: 487.25.

5-(Dimethylamino)-N-(4-(1,3-dioxo-1H-benzo[de]isoquinolin-2(3H)-yl)butyl)naphthalene-1-sulfonamide (3). 62%, mp. 134–135 °C; ¹H-NMR (500 MHz, CD₃CN) δ (ppm) 1.36-1.42 (m, 2H), 1.47-1.53 (m, 2H), 2.76 (s, 6H), 2.87 (q, 2H, J = 7.3 Hz), 3.94 (t, 2H, J = 7.3 Hz, 2H), 5.86 (t, 1H, J = 6 Hz), 7.11 (d, 1H, J = 7.5 Hz), 7.48-7.54 (m, 2H), 7.80 (t, 2H, J = 8.5 Hz), 8.14 (d, 1H, J = 8.5 Hz), 8.24 (d, 1H, J = 8.5 Hz), 8.33 (d, 2H, J = 8.5 Hz), 8.44 (d, 1H, J = 9 Hz), 8.49 (d, 2H, J = 8.5 Hz); ¹³C-NMR (125 MHz, CD₃CN) δ (ppm) 25.4, 27.1, 39.7, 43.2, 45.8, 115.4, 119.2, 122.9, 123.6, 127.3, 128.5, 128.7, 130.0, 130.1, 130.3, 130.8, 131.7, 132.0, 134.4, 135.1, 152.3, 164.6; HRMS (FAB) Calcd for C₂₈H₂₇N₃O₄S: 501.14; Found: 501.07.

5-(Dimethylamino)-N-(6-(1,3-dioxo-1H-benzo[de]isoquinolin-2(3H)-yl)hexyl)naphthalene-1-sulfonamide (4). 60%, mp 121–122 °C; ¹H-NMR (500 MHz, CD₃CN) δ (ppm) 1.1-1.12 (m, 4H), 1.12-1.13 (m, 4H), 1.25 (d, 2H, J=4Hz), 2.80 (s,6H), 3.93 (t, 2H, J=7.5 Hz), 5.7 (t, 1H, J=5.5 Hz), 7.20 (d, 1H, J=7.5 Hz), 7.53-7.59 (m, 2H), 7.78-7.81(m, 2H), 8.14-8.15 (dd, 1H), 8.25 (d, 1H, J=8.5 Hz), 8.31-8.33 (dd, 2H), 8.47-8.51 (m, 3H); ¹³C-NMR (125 MHz, CD₃CN) δ (ppm) 25.3, 25.7, 27.1, 28.5, 29.0, 39.4, 42.40, 44.3, 114. 8, 118.7, 122.5, 123.0, 126.7, 127.6, 127.7, 128.7, 129.1, 129.3, 129.6, 130.3, 131.4, 133.7, 135.4, 151.7, 163.6; HRMS (FAB) Calcd for C₃₀H₃₁N₃O₄S: 531.21; Found: 531.23.

5-(Dimethylamino)-N-(8-(1,3-dioxo-1H-benzo[de]isoquinolin-2(3H)-yl)octyl)naphthalene-1-sulfonamide (5). 65%, mp 108–109 °C; ¹H-NMR (500 MHz, CD₃CN) δ (ppm) 1.05-1.08 (m, 8H), 1.18-1.21 (m, 4H), 1.53-1.59 (m, 2H), 2.80 (s, 6H), 4.01 (t, 2H, J=7.5 Hz), 5.75 (t, 1H, J=6 Hz), 7.21 (d, 1H, J=7.5Hz), 7.52-7.59 (m,

2H), 7.76-7.80 (m, 2H), 8.14-8.16 (dd, 1H), 8.25 (d, 1H, J=8.5 Hz), 8.29-8.31(m, 2H), 8.47-8.49 (d, 3H, J=8.5 Hz). ¹³C-NMR (125 MHz, CD₃CN) δ (ppm) 27.2, 27.9, 28.9, 29.7, 30.0, 30.1, 41.2, 44.0, 46.0, 116.4, 120.3, 124.1, 124.6, 128.3, 129.3, 130.4, 130.7, 130.9, 131.2, 131.9, 132.9, 135.3, 137.0, 153.3, 165.2; HRMS (FAB) Calcd for C₃₂H₃₅N₃O₄S: 559.23; Found: 559.11.

3.6.4. Calculation of Association Constants

The association between the dyads and the Cu²⁺ ions was analysed using the fluorescence data. The association constants were calculated employing Benesi-Hildebrand method and employing equations 3.1 and 3.2,

$$\frac{1}{(I - I_0)} = \frac{1}{(I - I_{fc})} + \frac{1}{K (I - I_{fc}) [\text{Cu}^{2+}]^{3/2}} \quad (\text{Eq 3.1})$$

$$\frac{1}{(I - I_0)} = \frac{1}{(I - I_{fc})} + \frac{1}{K (I - I_{fc}) [\text{Zn}^{2+}]} \quad (\text{Eq 3.2})$$

where, *K* is the association constant, *I* is the fluorescence intensity of the free dyad, *I*₀ is the observed fluorescence intensity of the [dyad-M²⁺] complex, and *I*_{fc} is the fluorescence intensity at the saturation.

3.6.5. Isothermal Titration Calorimetry (ITC) Measurements

ITC experiments were performed at 30 °C using a MicroCal iTC200 calorimeter. The metal ions (Cu²⁺, 5.0 mM; Zn²⁺, 2.5 mM) and the dyad solutions (0.25 mM, 200 μL) were made from acetonitrile solution. The solution in the sample cell was stirred at 1000 rpm, while injecting the metal ion solution to ensure rapid

mixing. Typically, the injection of the metal ions from the syringe (2.0 μL) was delivered in 4 s with an interval of 3 min between two injections to ensure the complete equilibration. The data were shown as the baseline-adjusted raw data in the top panel. The peak-integrated and the concentration-normalized heat of reaction versus the molar ratio of the metal ions to the dyad were presented in the bottom panel. The ITC data was analysed with the models using the Origin software package (MicroCal LLC ITC program) supplied by MicroCal.¹⁸ A nonlinear least-square algorithm (minimization of χ^2) was used to obtain an equilibrium binding model and the best-fit values of the stoichiometry (n), change in enthalpy (ΔH), and binding constant (K).

3.7. REFERENCES

1. a) A. P. de Silva, H. Q. Gunaratne, T. Gunnlaugsson, A. J. M. Huxley, C. P. McCoy, J. T. Rademacher and T. E. Rice, *Chem. Rev.*, **1997**, *97*, 1515; b) B. Valeur and I. Leray, *Coord. Chem. Rev.*, **2000**, *205*, 3; c) L. Fabbrizzi, M. Licchelli, F. Mancin, M. Pizzeghello, G. Rabaioli, A. Taglietti, P. Tecilla and U. Tonellato, *Chem. Eur. J.*, **2002**, *8*, 94; d) A. P. de Silva and S. Uchiyama, *Nature Nanotechnol.*, **2007**, *2*, 399; e) Y. Shiraishi, K. Ishizumi, G. Nishimura and T. Hirai, *J. Phys. Chem. B*, **2007**, *111*, 8812; f) K. Jyothish, R. R. Avirah and D. Ramaiah, *Org. Lett.*, **2006**, *8*, 111.
2. a) J. V. Ros-Lis, B. Garcia, D. Jimenez, R. Martinez-Manez, F. Sancenon, J. Soto, F. Gonzalvo and M. C. Valdecabres, *J. Am. Chem. Soc.*, **2004**, *126*, 4064; b) G. W.

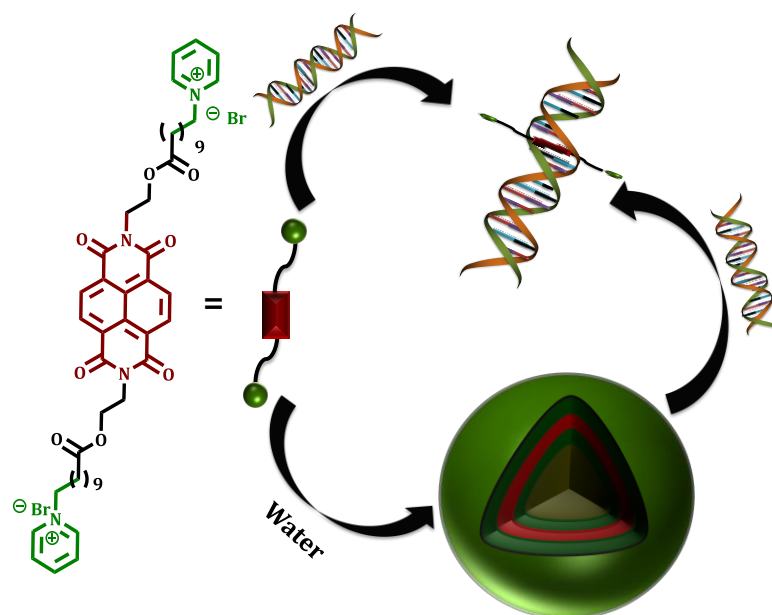
- Gokel, W. M. Leevy and M. E. Weber, *Chem. Rev.*, **2004**, *104*, 2723; c) D. Montvydiene and D. Marciulioniene, *Environ. Toxicol.*, **2004**, *19*, 351.
3. a) R. Kramer, *Angew. Chem., Int. Ed.*, **1998**, *37*, 772; b) A. Torreggiani, J. Domènech, R. Orihuela, C. Ferreri, S. Atrian, M. Capdevila and C. Chatgililoglu, *Chem. Eur. J.*, **2009**, *15*, 6015; c) I. A. Koval, P. Gamez, C. Belle, K. Selmeczi, J. Reedijk, *Chem. Soc. Rev.*, **2006**, *35*, 814.
4. a) C. Vulpe, B. Levinson, S. Whitney, S. Packman and J. Gitschier, *Nat. Genet.*, **1993**, *3*, 7; b) K. J. Barnham, C. L. Masters, A. I. Bush, *Nat. Rev. Drug Discovery*, **2004**, *3*, 205; c) Y. Jiao and P. Yang, *J. Phys. Chem. B*, **2007**, *111*, 7646; d) A. Rodriguez-Granillo, A. Crespo, P. Wittung-Stafshede, *J. Phys. Chem. B*, *114*, 1836.
5. a) J. M. Berg and Y. Shi, *Y. Science*, **1996**, *271*, 1081; b) L. Zhang, R. J. Clark and L. Zhu, *Chem. Eur. J.*, **2008**, *14*, 2894; c) C. E. Outtenand and T. V. O'Halloran, *Science*, **2001**, *292*, 2488; d) P. Jiang and Z. Guo, *Coord. Chem. Rev.*, **2004**, *248*, 205; e) R. J. McMahon and R. J. Cousins, *Proc. Natl. Acad. Sci. U.S.A.*, **1998**, *95*, 4841; f) T. Dudev and C. Lim, *J. Phys. Chem. B*, **2001**, *105*, 10709.
6. a) R. Métivier, I. Leray and B. Valeur, *Chem. Eur. J.*, **2004**, *10*, 4480; b) E. C. Constable, R. Martinez-Manez, A. M. W. Cargill Thompson and J. V. J. Walker, *J. Chem. Soc., Dalton Trans.*, **1994**, 1585; c) A. J. Weerasinghe, C. Schmiesing, S. Varaganti, G. Ramakrishna and E. Sinn, *J. Phys. Chem. B*, **2010**, *114*, 9413; d) Z. Xu, J. Yoon and D. R. Spring, *Chem. Soc. Rev.*, **2010**, *39*, 1996; e) V. S. Jisha, K. T.

- Arun, M. Hariharan, and D. Ramaiah, *J. Am. Chem. Soc.*, **2006**, *128*, 6024; f) P. P. Neelakandan, M. Hariharan, and D. Ramaiah, *J. Am. Chem. Soc.*, **2006**, *128*, 11334; g) K. T. Arun, and D. Ramaiah, *J. Phys. Chem. A*, **2005**, *109*, 5571.
7. a) L. Fabbrizzi and A. Poggi, *Chem. Soc. Rev.*, **1995**, *24*, 197; b) J. S. Kim and D. T. Quang, *Chem. Rev.*, **2007**, *107*, 3780; c) M. R. Wasielewski, *Acc. Chem. Res.*, **2009**, *42*, 1910; d) K. Hanaoka, Y. Muramatsu, Y. Urano, T. Terai and T. Nagano, *Chem. Eur. J.*, **2010**, *16*, 568; e) *Photoinduced Electron Transfer*; M. A. Fox, M. Channon, Eds.; Elsevier: Amsterdam, **1988**; f) X. Lu, W. Zhu, Y. Xie, X. Li, Y. Gao, F. Li and H. Tian, *Chem. Eur. J.*, **2010**, *16*, 8355.
8. a) H. J. Kim, J. Hong, A. Hong, S. Ham, J. H. Lee and J. S. Kim, *Org. Lett.*, **2008**, *10*, 1963; b) M. Arduini, F. Felluga, F. Mancin, P. Rossi, P. Tecilla, U. Tonellato and N. Valentinuzzi, *Chem. Commun.*, **2003**, 1606; c) E. M. W. M. Van Dongen, L. M. Dekkers, K. Spijker, E. W. Meijer, L. W. J. Klomp and M. Merckx, *J. Am. Chem. Soc.*, **2006**, *128*, 10754; d) C. Ma, F. Zeng, L. Huang and S. Wu, *J. Phys. Chem. B*, **2011**, *115*, 874; e) K. S. Sanju, P. P. Neelakandan and D. Ramaiah, *Chem. Commun.*, **2011**, *47*, 1288.
9. a) S. Abad, M. Kluciar, M. A. Miranda and U. Pischel, *J. Org. Chem.*, **2005**, *70*, 10565; b) M. H. Lee, H. J. Kim, S. Yoon, N. Park, and J. S. Kim, *Org. Lett.*, **2008**, *10*, 213; c) G. G. Battistuzzi, G. Grandi, L. Menabue, G. C. Pellacani, M. Sola, *J. Chem. Soc., Dalton Trans.*, **1985**, 2363.

10. a) P. Ceroni, I. Laghi, M. Maestri, V. Balzani, S. Gestermann, M. Gorka and F. Vögtle, *New. J. Chem.*, **2002**, 26, 66; b) M. Licchelli, A. Orbelli Biroli, A. Poggi, D. Sacchi, C. Sangermani and M. J. Zema, *Chem. Soc., Dalton Trans.*, **2003**, 4537.
11. S. Speiser, *Chem. Rev.*, **1996**, 96, 1953.
12. a) H. A. Benesi and J. H. Hildebrand, *J. Am. Chem. Soc.*, **1949**, 71, 2703; b) L. L. Yannis, *J. Phys. Chem. B*, **1997**, 101, 4863; c) H. J. Kim, J. Hong, A. Hong, S. Ham, J. H. Lee and J. S. Kim, *Org. Lett.*, **2008**, 10, 1963; d) R. R. Avirah, K. Jyothish, and D. Ramaiah, *J. Org. Chem.*, **2008**, 73, 274.
13. a) V. K. Vadim, *J. Phys. Chem.*, **1992**, 96, 2609; b) J. Joseph, N. V. Eldho, and D. Ramaiah, *Chem. Eur. J.*, **2003**, 9, 5926; c) E. E. Neuteboom, P. A. Van Hal and R. A. J. Janssen, *Chem. Eur. J.*, **2004**, 10, 3907; d) W. C. Tsoi, M. O'Neill, M. P. Aldred, S. P. Kitney, P. and S. M. Kelly, *Chem. Mater.*, **2007**, 19, 5475; e) S. Murata, M. Tachiya, *M. J. Phys. Chem.*, **1996**, 100, 4064; f) H. Langhals, A. Obermeier, Y. Floredo, A. Zanelli and L. Flamigni, *Chem. Eur. J.*, **2009**, 15 12733.
14. a) E. Arunkumar, P. Chithra and A. Ajayaghosh, *J. Am. Chem. Soc.*, **2004**, 126, 6590; b) M. A. Zaitoun and C. T. Lin, *J. Phys. Chem. B*, **1997**, 101, 1857.
15. a) V. Wintgens, P. Valat, J. Kossanyi, L. Biczok, A. Demeter and T. Berces, *J. Chem. Soc., Faraday Trans.*, **1994**, 90, 411; b) G. Jones, S. J. Kumar, *Photochem. Photobiol. A: Chem*, **2003**, 160, 139.
16. a) C. F. Portela, J. Brunckova, J. L. Richards, B. Schöllhorn, Y. Iamamoto, D. Magde, T. G. Traylor and C. L. Perrin, *J. Phys. Chem. A*, **1999**, 103, 10540; b) K.

- Pettersson, K. Kilså, J. Mårtensson and B. Albinsson, *J. Am. Chem. Soc.*, **2004**, *126*, 6710; c) M. Kuragaki and M. Sisido, *J. Phys. Chem.*, **1996**, *100*, 16019.
17. a) T. Koike, T. Watanabe, S. Aoki, E. Kimura and M. Shiro, *J. Am. Chem. Soc.*, **1996**, *118*, 12696; b) S. Deo and H. A. Godwin, *J. Am. Chem. Soc.* **2000**, *122*, 174; c) J. S. Kim, D. T. Quang, *Chem. Rev.*, **2007**, *107*, 3780.
18. a) Y. Zhang, S. Akilesh and D. E. Wilcox, *Inorg. Chem.*, **2000**, *39*, 3057; b) N. E. Grossoehme, S. Akilesh, M. L. Guerinot, D. E. Wilcox, *Inorg. Chem.*, **2006**, *45*, 8500; c) N. E. Grossoehme, S. B. Mulrooney, R. P. Hausinger and D. E. Wilcox, *Biochemistry*, **2007**, *46*, 10506.

NOVEL NAPHTHALENE IMIDE SYSTEMS: STUDY OF THEIR SELF-ASSEMBLY AND DNA BINDING ASPECTS



4.1. ABSTRACT

We synthesised two novel amphiphilic conjugates **1** and **2** based on naphthalene di- and monoimide chromophores and have investigated their photophysical, self-assembly and DNA binding aspects. Both these conjugates exhibited good solubility in the aqueous medium and showed characteristic absorption and fluorescence bands of the naphthalene di- and monoimide chromophores at the wavelengths 382 and 390 nm; 344 and 378 nm, respectively. Of these two conjugates, the bolamphiphile **1** was found to undergo self-assembly to

form vesicular structures of size *ca.* 220 nm in the aqueous medium at and above critical aggregation concentration of 0.4 mM as confirmed through microscopic techniques. In contrast, the naphthalimide conjugate **2**, exhibited the formation of lamellar flake like structures at and above the CAC of *ca.* 0.25 mM. Furthermore, the vesicular structures of the conjugate **1** thus formed exhibited strong affinity for the hydrophobic molecules such as Nile red through encapsulation as confirmed through changes in photophysical properties and fluorescence microscopic images.

To understand the affinity of these conjugates **1** and **2** for biomolecules, we have studied their interactions with proteins, (for example, BSA), ct-DNA and synthetic polynucleotides such as poly(dG.dC)-poly(dG.dC) and poly(dA.dT)-poly(dA.dT). Both these conjugates exhibited less efficient interactions with the albumins. In contrast, with the addition of ct-DNA, the conjugate **1** exhibited significant hypochromicity (*ca.* 42%) in its absorption spectrum. Further, we observed a regular decrement in the fluorescence intensity at 390 nm with a concomitant enhancement in intensity at 510 nm. Similar observations have been made with the amphiphilic conjugate **2**. The mode of interaction of these systems with DNA was evaluated through photophysical and biophysical techniques. Results of these studies have revealed that the conjugates **1** and **2** interact with DNA through intercalation with association constants in the order of $\sim 5-8 \times 10^4 \text{ M}^{-1}$. Uniquely, when interacted with DNA, we observed the disassembly of the vesicles of the conjugate **1** and such a transformation could be utilized for the encapsulation and release of the hydrophobic molecules, employing DNA as stimuli.

4.2. INTRODUCTION

The study of self-assembly of the amphiphilic conjugates has been an active area of interest in recent years due to their medicinal and material applications.¹ Thus, the small-molecule based amphiphiles such as surfactants, bolamphiphiles, gemini surfactants, etc. have been employed to generate diverse nanostructures, varying from micelles, vesicles, fibres to nanotubes.² Most of these amphiphiles constitute hydrophobic and hydrophilic segments and which are known to form various supramolecular assemblies in the organic medium involving various non-covalent interactions.³ However, there has been a great challenge in creating well defined nanostructures in the aqueous medium for their efficient biological applications. In this context, the study of supramolecular assemblies of appropriately substituted chemical building blocks such as the amphiphilic and bolamphiphilic systems have attracted much attention in recent years.⁴

Recently, increasing efforts are also being made towards the development of stimuli-responsive units containing well-defined nanostructures, because of their added advantages over the conventional structures. In general, the stimuli can be of a change in temperature, pH, light, magnetic field and ionic strength of the medium, which can be employed to generate the desired nanoarchitectures.⁵ Among the various stimuli investigated, the materials that respond to biological stimuli such as proteins and nucleic acids have been less explored.⁶ Therefore, the design of functional chromophores, which undergo supramolecular assemblies in the aqueous

medium and whose architectures can be stimulated by biomolecules is quite challenging. Of the various chromophores, the conjugates based on naphthalene diimides and naphthalimides are very attractive since these systems have extended π -core and are also belong to an important class of DNA binding agents.⁷

In this context, we have designed two amphiphilic conjugates **1** and **2** (Chart 4.1) and have investigated their photophysical, self-assembly and DNA responsive properties. The uniqueness of these conjugates is that they are amphiphilic in nature and the presence of the π -extended and planar aromatic surface in these systems makes them as interesting candidates to explore their supramolecular assemblies. Our investigations have revealed that both these conjugates exhibited good solubility in the aqueous medium and strong affinity for DNA and polynucleotides through intercalation. Of these two conjugates, the bolamphiphile **1** showed formation of vesicular structures at above critical aggregates concentration of 0.4 mM and which subsequently were found to be efficient in encapsulating the hydrophobic dyes. Interestingly, the vesicular structures of **1** exhibited disassembly in the presence of DNA and such a transformation can be effectively utilized to release the encapsulated dyes employing DNA as stimuli.

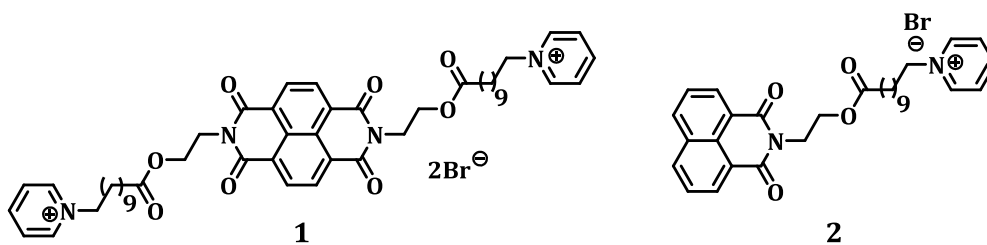
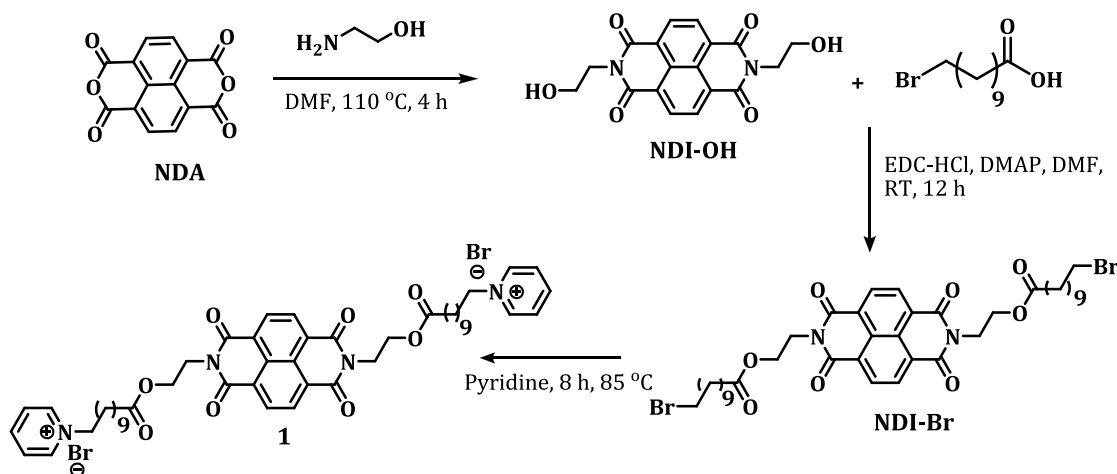


Chart 4.1. Structures of the naphthalene imide conjugates **1** and **2**.

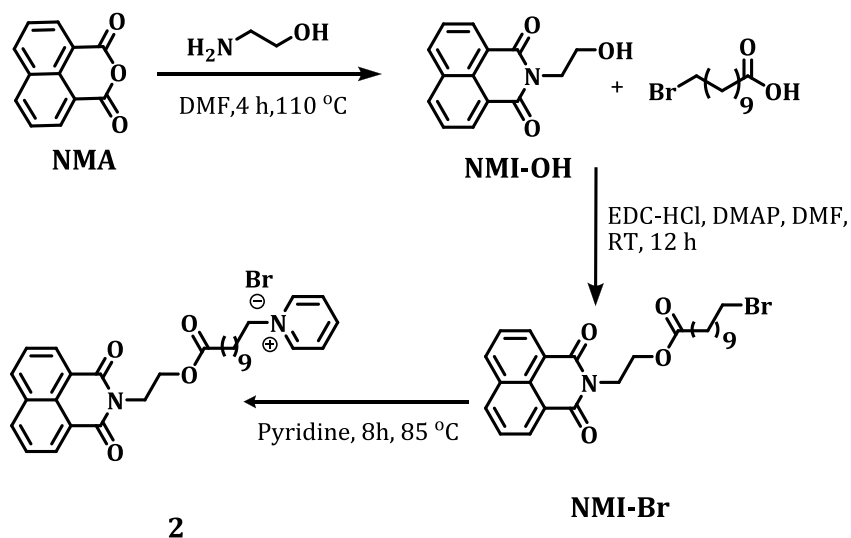
4.3. RESULTS

4.3.1. Synthesis of the Amphiphilic Conjugates

The synthesis of the symmetric bolamphiphile **1** was achieved starting from the 1,4,5,8-naphthalenetetracarboxylic dianhydride derivative (NDA) in three steps (Scheme 4.1). The reaction of NDA with ethanolamine afforded the corresponding alcohol derivative, which on successive esterification with two equivalents of 11-bromoundecanoic acid and the quaternization with pyridine gave the bolamphiphile **1** in moderate yields (*ca.* 66%). Similarly, the synthesis of the amphiphilic naphthalimide derivative **2** was achieved in moderate yields (*ca.* 55%) as shown in Scheme 4.2. The naphthalic anhydride (NMA), upon amination with ethanolamine followed by esterification and subsequent quaternization with pyridine gave the conjugate **2** in good yields. All these products were purified and unambiguously characterised through various analytical and spectroscopic techniques.



Scheme 4.1. Synthesis of the naphthalene diimide based bolamphiphile **1**.



Scheme 4.2. Synthesis of the naphthalimide based amphiphile **2**.

4.3.2. Photophysical and Self-Assembly Aspects

We have investigated the photophysical properties including the time-resolved fluorescence spectral analysis of both the conjugates under different conditions. For example, the ground-state absorption spectrum of the conjugate **1** in the aqueous medium, showed characteristic vibrationally resolved spectral bands of the naphthalene diimide chromophore having maximum at 382 nm ($\epsilon = 2.33 \pm 0.1 \times 10^4 \text{ M}^{-1} \text{ cm}^{-1}$) (Figure 4.1). Similarly, in the case of the conjugate **2**, we observed the characteristic absorption maximum at 344 nm ($\epsilon = 1.42 \pm 0.1 \times 10^4 \text{ M}^{-1} \text{ cm}^{-1}$). In the fluorescence spectra, both these conjugates **1** and **2** showed maxima at 390 and 378 nm, respectively. The fluorescence quantum yields (Φ_F) of these conjugates were determined in the aqueous medium. We observed significantly quenched values for the diimide conjugate **1** ($\Phi_F=0.005$), when compared to the monoimide derivative **2**

($\Phi_F=0.29$), indicating existence of efficient fluorescence quenching mechanism in the former case as reported in the literature.⁸

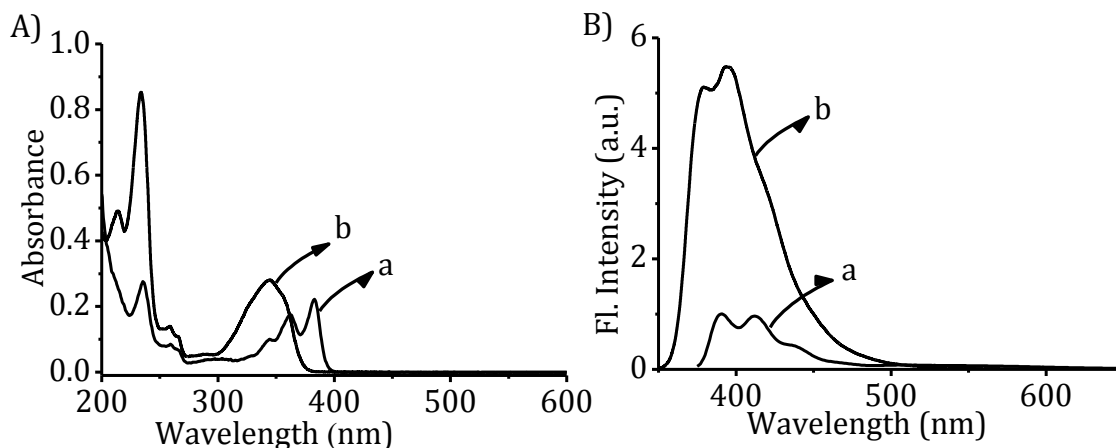


Figure 4.1. A) Absorption and B) fluorescence spectra of the conjugates, a) **1** (10 μM) and b) **2** (20 μM) in the aqueous medium. Excitation wavelength, 360 nm and 345 nm, respectively.

To determine the excited state behaviour of the conjugates **1** and **2**, we have carried out picosecond time-resolved fluorescence measurements. The fluorescence lifetime, in the case of the conjugate **1**, was found to be very short lived (<0.1 ns), which is the characteristic feature of the N-substituted NDI chromophore.⁹ In contrast, the fluorescence decay profile of the conjugate **2**, when excited at 335 nm, showed a mono-exponential decay profile, with a lifetime of *ca.* 2.2 ± 0.3 ns. The observed lifetime can be attributed to the locally excited state (monomer) emission of the naphthalimide chromophore¹⁰ (Figure 4.2).

To understand the propensity of the conjugates under investigation for aggregation, we have monitored their absorption and fluorescence properties at

higher concentrations. Figure 4.3 shows the concentration dependent absorption and fluorescence spectra of the conjugate **1**. With increase in the concentration from 0.046 to 1.1 mM, we observed a deviation from the linearity at concentrations greater than *ca.* 0.4 mM. The critical aggregation concentration of **1** was estimated from the concentration dependent molar extinction coefficient (ϵ) changes at 382 nm, and the value is found to be 0.4 mM (inset of Figure 4.3A). In the emission spectrum, upon increasing the concentration, we observed a gradual increase in emission at 510 nm, with I_{510}/I_{390} ratio varying from 0.2 to 0.9. Similar observations were made with the conjugate **2** and which gave a CAC value of *ca.* 0.25 mM. In the emission studies, we observed the formation of a new band at 510 nm. When monitored at 510 nm, the conjugate **1** (at CAC), showed a biexponential decay with an average fluorescence lifetime $\langle\tau\rangle$ of 3.3 ± 0.2 ns, which can be attributed to the

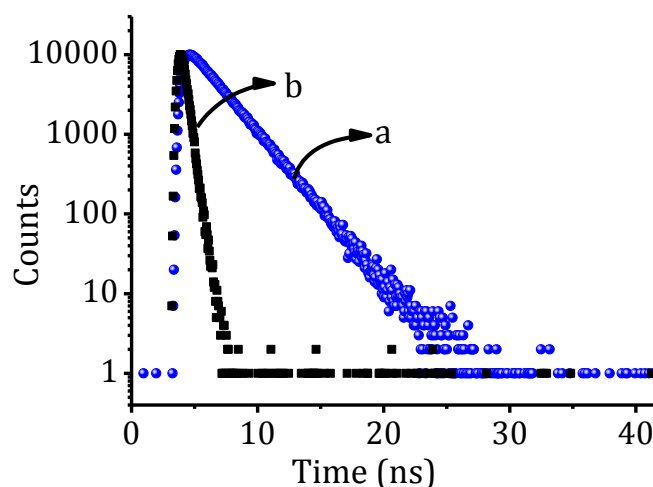


Figure 4.2. Fluorescence decay of a) the conjugate **2** (20 μ M) and b) the corresponding lamp profile in aqueous medium monitored at 378 nm. Excitation wavelength, 335 nm.

formation of intermolecular excimer of the naphthalene diimide (Figure 4.4A). On the other hand, the conjugate **2**, at CAC, showed a biexponential decay with emission lifetimes of 22.6 ± 0.1 (90%) and 4.11 ± 0.2 ns (10%), which can be attributed to the emission from the intermolecular excimer and the monomer of the naphthalimide chromophore, respectively.

To understand the formation of excimer emission at higher concentrations and also to evaluate the supramolecular assemblies formed, we have carried out the morphological analysis of the conjugates **1** and **2** through dynamic light scattering (DLS), scanning electron (SEM) and transmission electron (TEM) microscopic techniques. At lower concentrations (<0.4 mM i.e., below CAC), the bolamphiphile **1** showed negligible formation of the nano-aggregates as analysed by the particle size

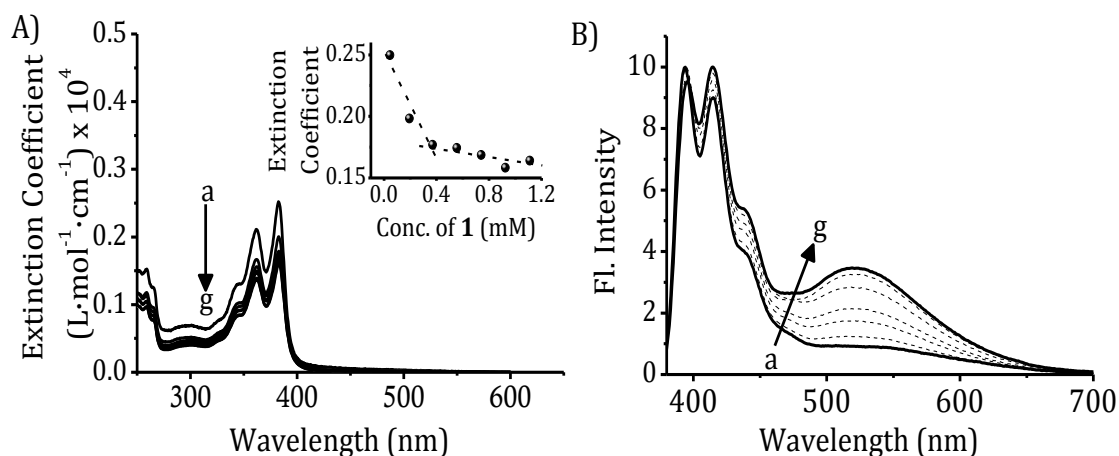


Figure 4.3. Concentration dependent A) absorption and B) emission spectra (normalized) of the conjugate **1** in aqueous medium with varying concentrations, a) 0.046 mM to g) 1.1 mM. Inset of A shows the variation of extinction coefficient at 382 nm as a function of concentration of the conjugate **1**. Path length of the cell, $l = 0.1$ cm, Excitation wavelength, 360 nm.

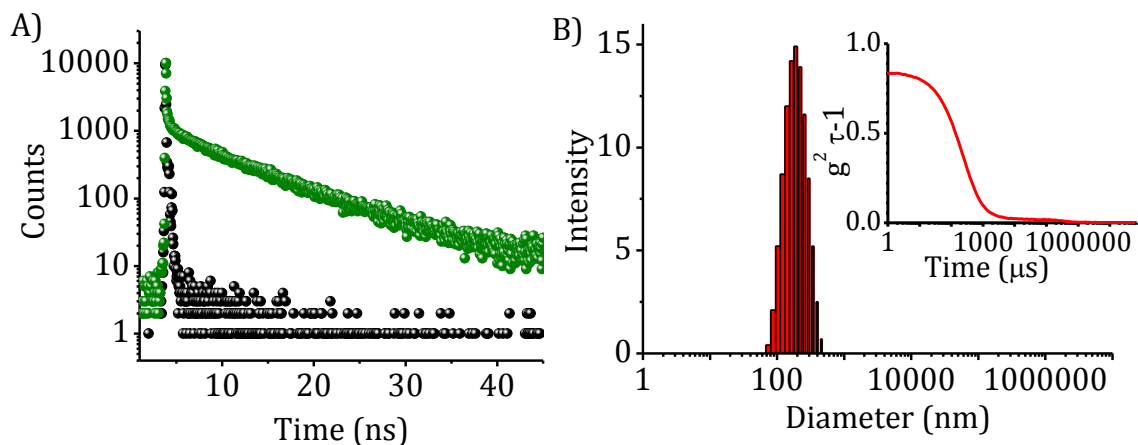


Figure 4.4. Fluorescence decay profiles of the conjugate **1** (0.4 mM) (green trace) and lamp (black trace) in aqueous medium monitored at 510 nm. Excitation wavelength, 375 nm. B) Size distribution and correlogram (inset) of the conjugate **1** (0.4 mM) in the aqueous medium.

analyser. Interestingly, upon increasing the concentration to CAC (0.4 mM), we observed aggregates of Z-average hydrodynamic diameter of 240 nm, with a good correlation data (Figure 4.4B). In contrast, the amphiphilic conjugate **2** at CAC showed the correlation data which confirm that the aggregates formed from this system were not of spherical in nature. To evidence these observations, we have carried out SEM and TEM analysis. The images of both these techniques have confirmed the formation of the self-assembled structures with diameter in the range *ca.* 220 ± 5 nm from the conjugate **1** under these conditions.

To get more insights on nature of the self-assembled structures of the conjugate **1**, we have carried out the TEM analysis after negative staining with phosphotungstic acid (pH 7.4). The images obtained by the TEM analysis have

revealed the presence of spherical particles with distinctive walls of width *ca.* 5 nm and solid interior (Figure 4.5A and 4.5B), confirming thereby that the self-assembled structures formed were of vesicular in nature. The thickness of the walls closely matched with the theoretically calculated extended aliphatic chain length of the conjugate **1** (Figure 4.5C). In contrast, the amphiphilic conjugate **2**, showed the formation of lamellar flakes as analysed through SEM and TEM (Figure 4.6) images, which is in agreement with those results obtained using the particle analyser.

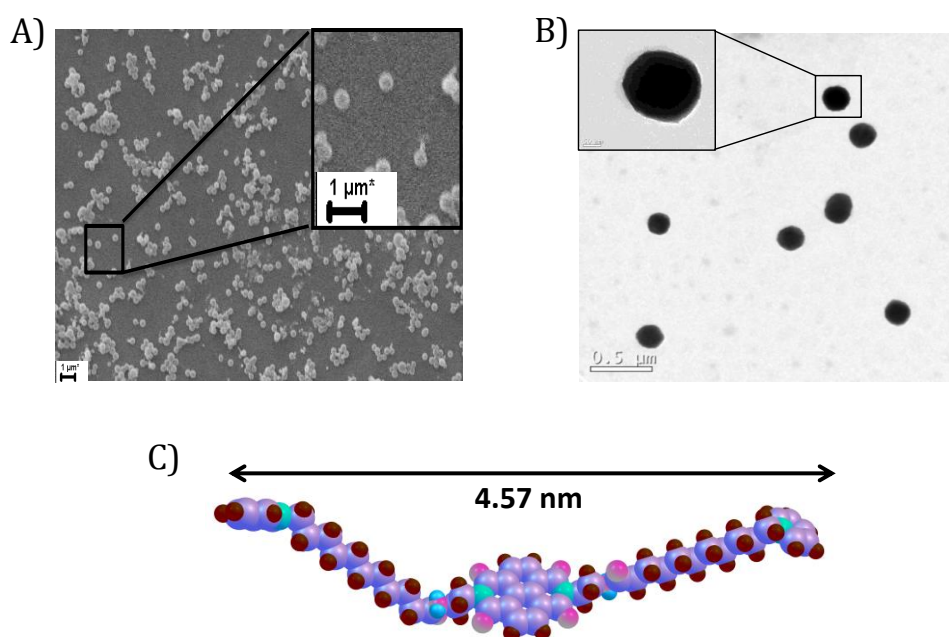


Figure 4.5. A) Scanning (SEM) and B) transmission (TEM) electron microscopic images of the vesicular solution of the conjugate **1** (at CAC of 0.4 mM). Inset shows the magnified images of the portion marked by the black box in the respective image. C) Energy minimized structure of the conjugate **1** by Gaussian 09W using 6-31G/B3LYP basis set.

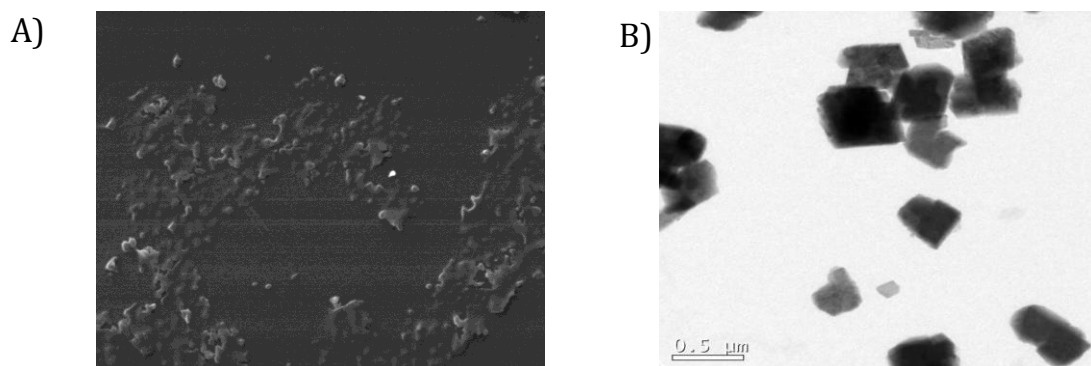


Figure 4.6. A) Scanning (SEM) and B) transmission electron (TEM) microscopic images of the conjugate **2** (0.25 mM).

To evaluate the potential utility of the vesicular structures as drug carrier systems, we have studied their interactions with a hydrophobic dye, Nile red, which has negligible solubility in the aqueous medium. The emission spectrum of Nile red (at a fixed conc. 100 μM) was monitored for a series of solutions of varying the concentration of the conjugate **1**. At and above a specific concentration of the conjugate **1**, we observed a strong emission at 630 nm, corresponding to Nile red dye (Figure 4.7) due to its encapsulation in the vesicular structures of the conjugate **1**. Furthermore, the emission intensity of Nile red at 630 nm was monitored as a function of the concentration of **1** (Figure 4.8). From the inflection point of the plot, we obtained a CAC value of 0.4 mM, which is in agreement with the value of CAC obtained for **1** from the absorption studies. The encapsulated Nile red in the vesicles showed a biexponential emission decay profile with lifetimes values of 10.05 ± 0.2 ns and 2.1 ± 0.1 ns, when compared to that of THF (4.1 ± 0.4 ns). These observations confirm the fact that Nile red undergoes effective encapsulation in the hydrophobic

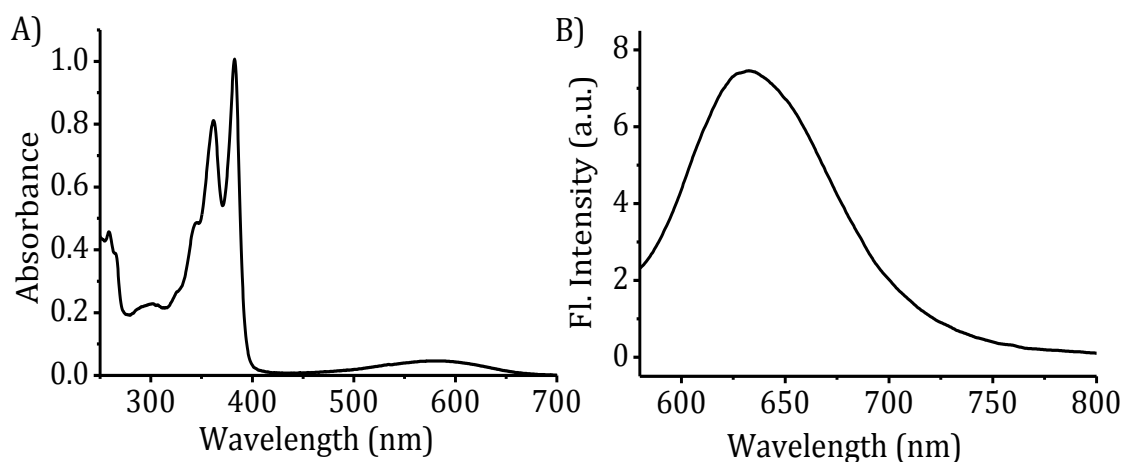


Figure 4.7. A) Absorption and B) emission spectra of the aqueous solution of the conjugate **1** (at CAC of 0.4 mM) containing hydrophobic dye, Nile red (100 μ M). Excitation wavelength, 530 nm.

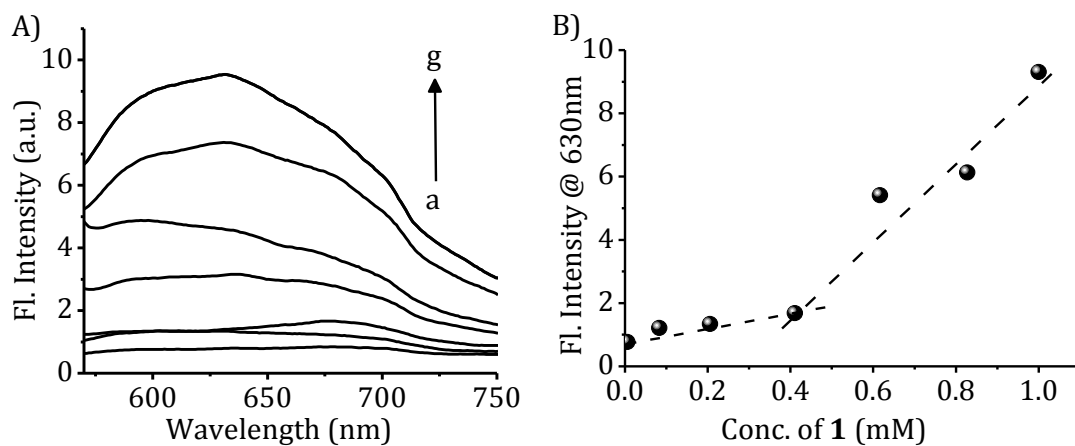


Figure 4.8. A) Changes in the emission spectra of the individual solutions containing Nile red (100 μ M) with varying concentrations of the conjugate **1**. a) 80 μ M and g) 1 mM. B) Variations in the emission intensity of Nile red at 630 nm as a function of the concentration of the conjugate **1**. Excitation wavelength, 530 nm.

microenvironment of the vesicles (Figure 4.9A). Further evidence was obtained for the encapsulation of the dye through fluorescence microscope. We observed red-light-emitting spherical particles when the Nile-red-encapsulated vesicular solution of **1** was examined under a fluorescence microscope as shown in Figure 4.9B.

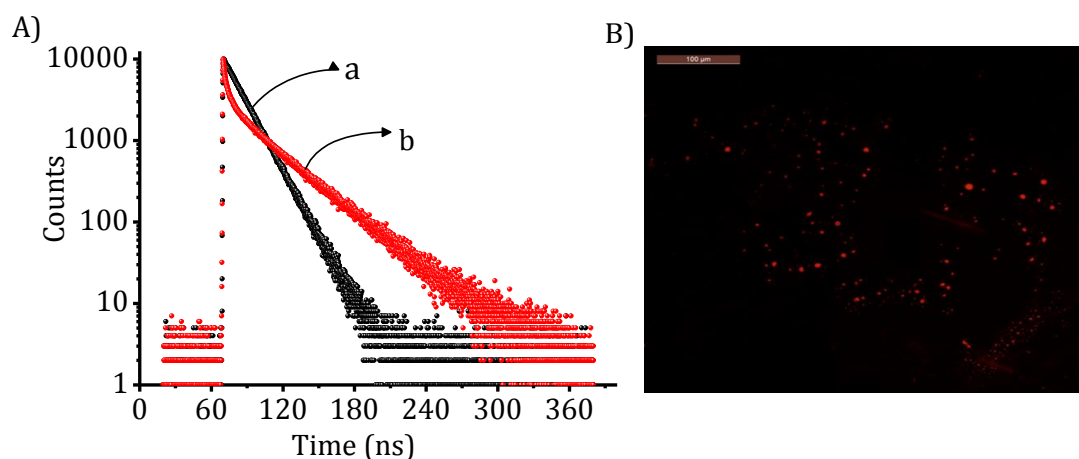


Figure 4.9. A) Fluorescence decay profiles of Nile red (100 μM), a) in THF alone, b) Nile red encapsulated in the vesicles of the conjugate **1** (at CAC of 0.4 mM). B) Fluorescence microscopic images of encapsulated Nile red in the vesicles of **1** in aqueous medium under similar conditions. Excitation wavelength, 530 nm.

4.3.3. Interaction with Biomolecules

To investigate the potential of the biomolecules as stimuli, we have studied the interactions of the conjugates with proteins, (for example, BSA), ct-DNA and synthetic polynucleotides under different concentrations. The successive addition of BSA (0 – 50 μM) led to negligible changes in the absorption and fluorescence spectra of the conjugate **1** (10 μM) in buffer (Figure 4.10). Similar observations were made with the conjugate **2**. These observations indicate the fact that both these conjugates

show less efficient interactions with the albumins. In contrast, the addition of calf thymus (ct) DNA (0-50 μM) in small aliquots to the buffer solution of the conjugate **1** (10 μM), resulted in gradual decrease in the absorbance at 382 nm, corresponding to the naphthalene diimide chromophore (Figure 4.11A). We observed the maximum hypochromicity of *ca.* 42% at 50 μM of DNA, along with a bathochromic shift of *ca.* 3 nm, with isosbestic points at 389 and 313 nm. The intrinsic binding constant (K_{DNA}) was determined through half-reciprocal analysis and the value is found to be $8.61 \pm 0.03 \times 10^4 \text{ M}^{-1}$, indicating the strong binding affinity of the conjugate **1** towards DNA.

In the emission spectrum of the conjugate **1**, with the increase in the concentration of DNA, we observed a regular and significant decrement in the emission intensity at 390 nm, corresponding to the naphthalene diimide monomer. We observed a concomitant enhancement in the emission intensity at 510 nm, which

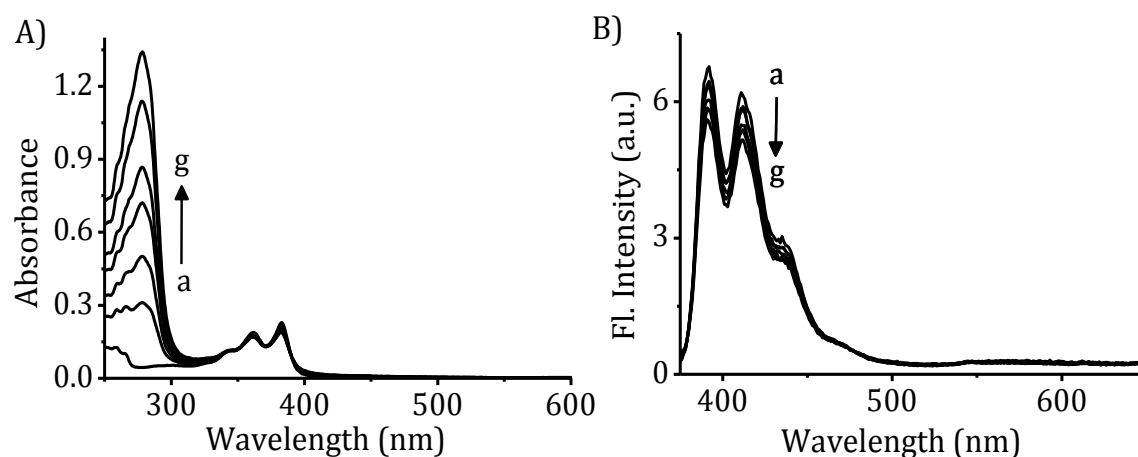


Figure 4.10. Changes in A) absorption and B) emission spectra of the conjugate **1** (10 μM) with addition of BSA, a) 0, and g) 50 μM in phosphate buffer (10 mM, pH 7.4). Excitation wavelength, 362 nm.

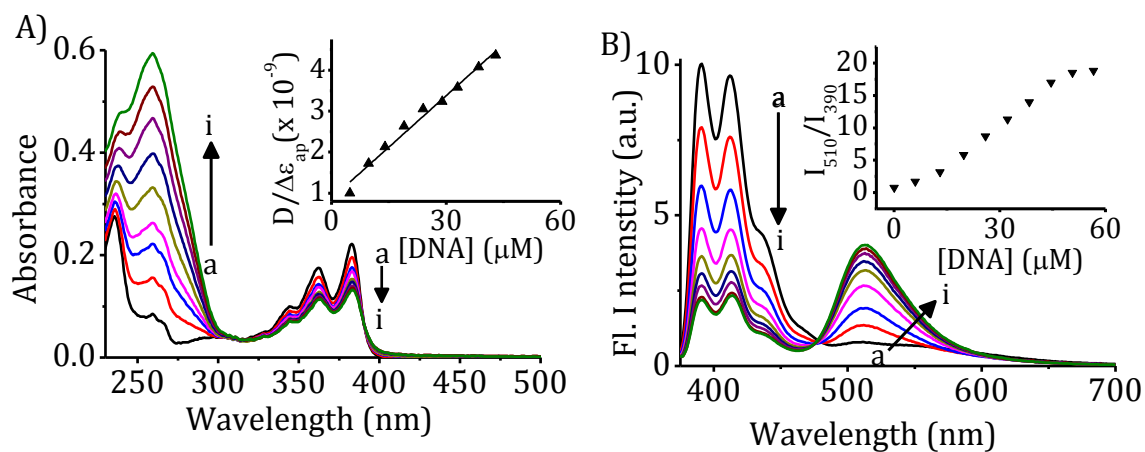


Figure 4.11. A) Changes in A) absorption and B) emission spectra of the conjugate **1** (10 μM) in presence of ct-DNA in phosphate buffer (10 mM, pH 7.4) containing 2 mM NaCl. [DNA], (a) 0 and (i) 50 μM. Insets of A and B show the half-reciprocal analysis for the binding of **1** with DNA and the ratiometric plot between emission maxima at 510 and 390 nm, respectively. Excitation wavelength, 362 nm.

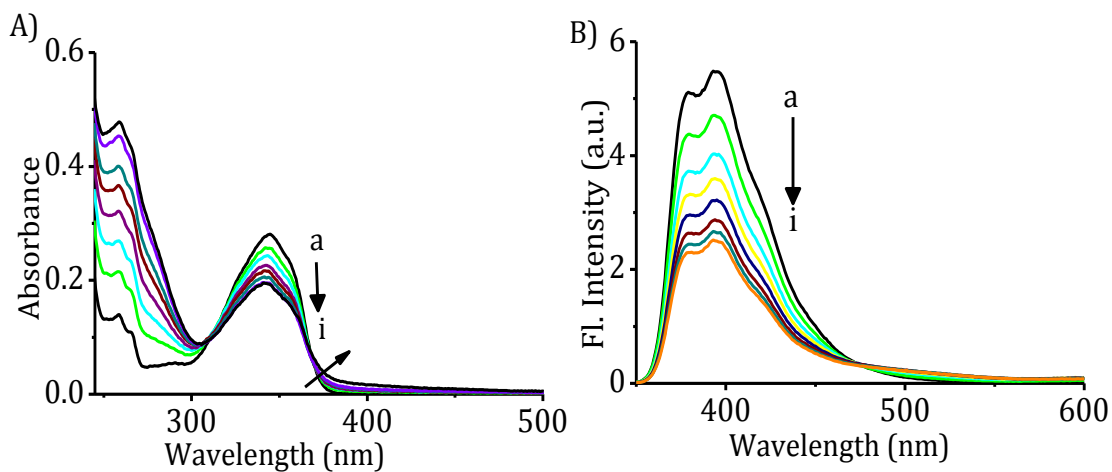


Figure 4.12. Changes in A) absorption and B) emission spectra of the conjugate **2** (20 μM) in presence of ct-DNA in phosphate buffer (10 mM, pH 7.4) containing 2 mM NaCl. [DNA], (a) 0 and (i) 73 μM. Excitation wavelength, 310 nm.

can be attributed to the formation of the excimer (Figure 4.11B). At 50 μM of DNA, we observed *ca.* 30-fold enhancement in the ratio of I_{510}/I_{390} , which led to the recognition of DNA in buffer medium through excimer emission of the conjugate **1**. Similarly, we observed a significant hypochromicity (*ca.* 39%) in the absorption spectra of the conjugate **2** (20 μM), upon addition of 73 μM of DNA. In the emission spectrum, we observed prominent and gradual decrease in the emission intensity of the conjugate **2** at 378 nm, with a concomitant enhancement at 500 nm (Figure 4.12). The association constant (K_{DNA}) between **2** and DNA was determined through half-reciprocal analysis¹¹ and the value is found to be $5.56 \pm 0.1 \times 10^4 \text{ M}^{-1}$.

To evaluate the effect of DNA on the excited state properties, we have analysed the fluorescence decay profiles of the conjugates **1** and **2** under different conditions. The successive additions of DNA to a solution of the conjugate **1** resulted in gradual increase in the lifetimes, when monitored at 510 nm (Figure 4.13A). We

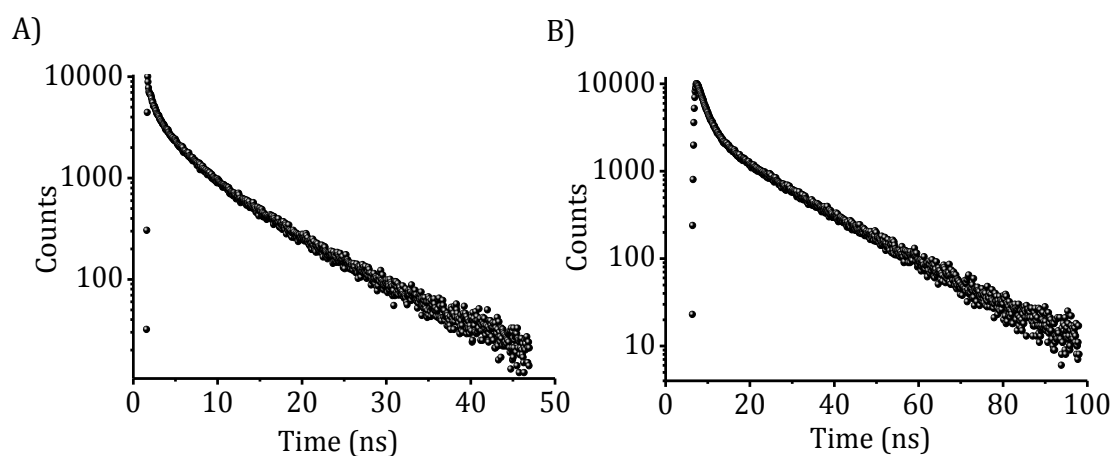


Figure 4.13. Fluorescence decay profiles of the conjugates, A) **1** (10 μM) and B) **2** (20 μM) in the presence of DNA (50 μM) in phosphate buffer (10 mM, pH 7.4) monitored at 510 and 500 nm, respectively. Excitation wavelengths, 375 or 335 nm.

observed a significant enhancement in the lifetime to 2.49 ns in the presence of 50 μM DNA (Figure 4.13A), when compared to its initial average lifetime of $\langle\tau\rangle = 0.1$ ns in buffer. In contrast, we observed negligible changes in the fluorescence lifetimes of the conjugate **2**, corresponding to the monomeric emission at 378 nm, even at 50 μM of DNA. However, when we monitored at 500 nm for the conjugate **2**, we observed a biexponential fluorescence decay profile with lifetime values of 2.5 ± 0.02 (31%) and 17.2 ± 0.07 ns (69%), which correspond to the monomer and excimer of the naphthalimide chromophore, respectively (Figure 4.13B).

To understand the origin of the excimer emission, we have employed time-resolved emission spectroscopy (TRES). The TRES analysis of the conjugate **1** showed a single peak at 395 nm, corresponding to the NDI monomer, immediately after excitation (7 ps) (Figure 4.14A). However, in the presence of 50 μM of DNA, the

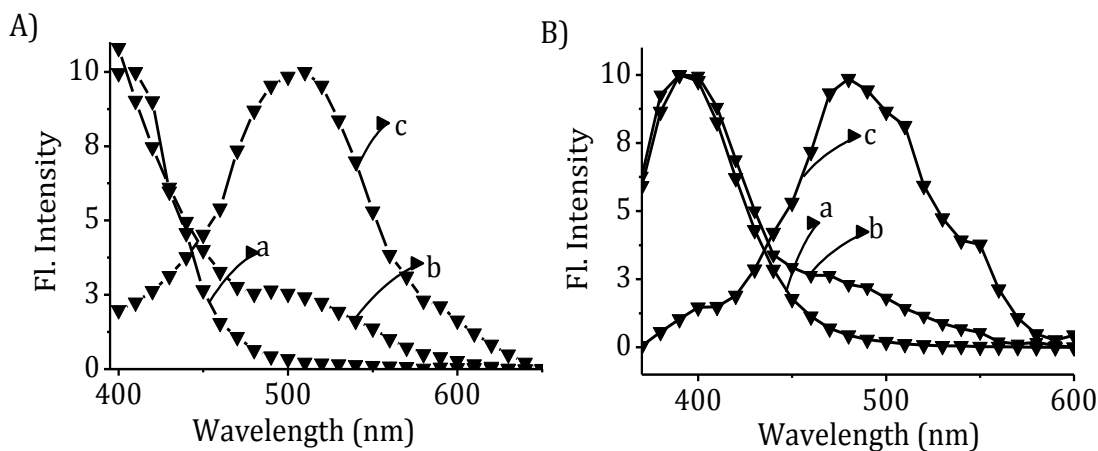


Figure 4.14. Time-resolved emission spectra (TRES) of the conjugates A) **1** (10 μM) and B) **2** (20 μM) in the presence of DNA (50 μM) in phosphate buffer (10 mM, pH 7.4), monitored after excitation pulse (a) 7 ps; 0.5 ns, (b) 63 ps; 1.4 ns, and (c) 1.4 ns; 13.8 ns. Excitation wavelengths, 375 and 335 nm, respectively.

formation of the excimer was observed even at 63 ps and it showed an enhancement in the intensity as a function of time. After 1 ns of excitation pulse, the spectrum dominated exclusively with the excimer emission having maximum at 510 nm. Similar observations were made with the conjugate **2** in the presence of DNA (Figure 4.14 B). The photophysical and DNA binding properties of the conjugates in buffer and under different conditions are summarized in Table 4.1.

Table 4.1. Photophysical and DNA binding properties of the conjugates **1** and **2** in 10 mM phosphate buffer (pH 7.4) containing 2 mM NaCl.

Photophysical aspects	Conjugate 1	Conjugate 2
λ_{\max} (nm)	382	344
Hypochromicity (%)	42%	39%
Isosbestic points	389, 313	366, 310
λ_{em} (nm)	390	378
Lifetime (τ) (ns)	< 0.1 ns	2.2
Lifetime (plus DNA) (ns)	< 0.1 (at 390 nm)	2.5 (at 378 nm)
	2.49 (< τ >) (at 510 nm)	17.2 (at 500 nm)
K_{DNA}^a	$8.61 \pm 0.03 \times 10^4 \text{ M}^{-1}$	$5.56 \pm 1 \times 10^4 \text{ M}^{-1}$

^aBinding constant values were determined using half-reciprocal analysis of the absorbance changes as reported in the literature.¹¹

To evaluate the DNA sequence selectivity, we have investigated the interactions of the conjugates **1** and **2** with the synthetic poly-oligonucleotides; poly(dG.dC)–poly(dG.dC) and poly(dA.dT)–poly(dA.dT) under similar conditions.

Upon increasing the concentration of poly(dG.dC)-poly(dG.dC) to a solution of the conjugate **1** in buffer showed an enhancement in the excimer emission intensity at 510 nm (Figure 4.15) with the concomitant decrease in the monomer emission. We have determined the association constants as in the case of ct-DNA and obtained a value of $3.52 \pm 0.2 \times 10^5 \text{ M}^{-1}$. Similar observations were made with the conjugate **2**, wherein, we observed K_{DNA} of $1.71 \pm 0.1 \times 10^5 \text{ M}^{-1}$. The presence of the poly(dA.dT)-poly(dA.dT), too exhibited similar changes, albeit with low affinity of K_{DNA} $1.4 \pm 0.2 \times 10^4 \text{ M}^{-1}$ for **1**. These results indicate that the conjugates **1** and **2** show sequence dependency, and the affinity was found to be in the order; poly(dG.dC)-poly(dG.dC) > ct-DNA > poly(dA.dT)-poly(dA.dT). The observed sequence dependency can be attributed to the rather low ionization potential of the GC sequences over the AT pair as reported in the literature for several DNA binding agents.¹²

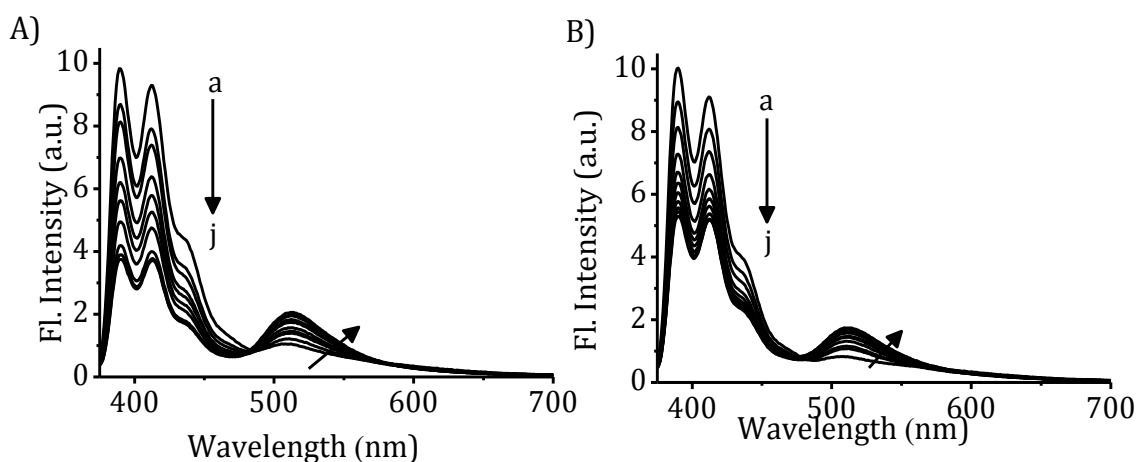


Figure 4.15. Changes in the emission spectra of **1** (10 μM) with addition of A) poly(dG.dC)-poly(dG.dC) and B) poly(dA.dT)-poly(dA.dT) in phosphate buffer (10 mM, pH 7.4). [polynucleotide], (a) 0 and (j) 50 μM . Excitation wavelength, 362 nm.

4.3.4. Nature of DNA Binding Interactions

To determine the nature of the interactions of the conjugates with DNA, we have studied the effect of ionic strength of the medium. With successive additions of DNA to a solution of **1** in buffer containing 50 mM of NaCl, we observed a significant decrease in the ratio of I_{510}/I_{390} as compared to that of 2 mM NaCl (Figure 4.16). When the DNA titration studies were carried out in buffer containing 500 mM NaCl,

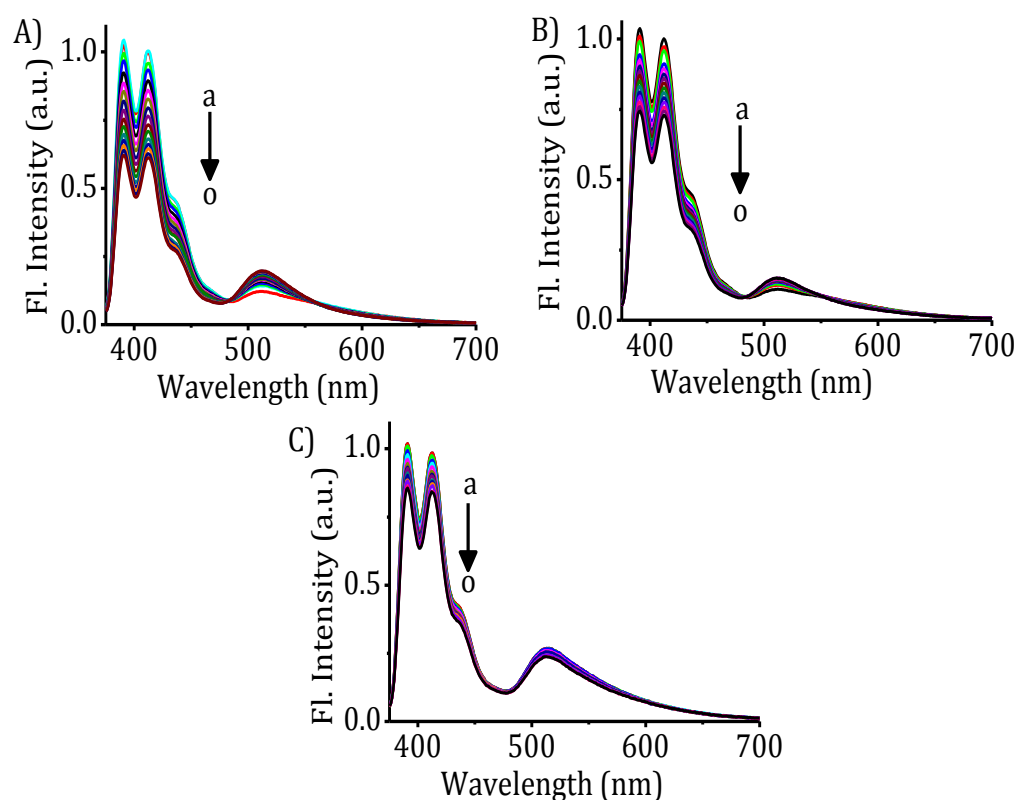


Figure 4.16. Changes in the emission spectra of the conjugate **1** (10 μM) in phosphate buffer (10 mM, pH 7.4) containing A) 50 mM, B) 100 mM, and C) 500 mM NaCl with increasing addition of DNA. [DNA], (a) 0 and (o) 50 μM. Excitation wavelength, 362 nm.

we observed negligible changes in the DNA mediated excimer emission of the conjugate **1** (Figure 4.16). The association constants for these interactions were calculated and are found to be $1.15, 0.85$ and $0.71 \times 10^4 \text{ M}^{-1}$ in buffer, containing 50, 100 and 500 mM NaCl. Similar observations were made with the conjugate **2**, which showed K_{DNA} values of $0.75, 0.58$ and $0.41 \times 10^4 \text{ M}^{-1}$, in buffer containing 50, 100 and 500 mM of NaCl, respectively.

The DNA binding affinity of the conjugates **1** and **2** were further studied by employing the competitive ethidium bromide (EB) binding assay.¹³ For example, with addition of ct-DNA to EB, we observed a significant enhancement in emission of *ca.* 2.4 fold at 630 nm, corresponding to the formation of EB/DNA complex. Subsequently, with the addition of the conjugate **1** to this EB/DNA complex, showed decrease in the emission intensity of *ca.* 1.7 fold ($\sim 70\%$) (Figure 4.17). Similar

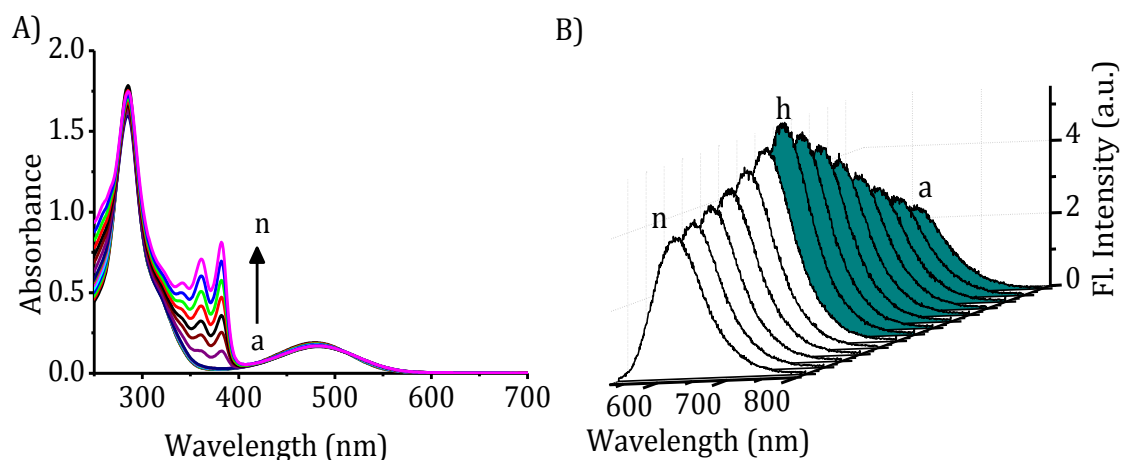


Figure 4.17. Changes in A) absorption and B) emission spectra of ethidium bromide ($20 \mu\text{M}$) with the successive additions of ct-DNA followed by the addition of the conjugate **1** in phosphate buffer (10 mM, pH 7.4). [ct-DNA] a) 0, and h) $60 \mu\text{M}$; conjugate [**1**], h) 0, and n) $20 \mu\text{M}$. Excitation wavelength 520, nm.

observations were made in the case of the conjugate **2**, wherein we observed *ca.* 1.5-fold ($\sim 62\%$) decrement in the emission intensity of EB/DNA complex. These results corroborate the fact that both the conjugates can efficiently displace EB, due to their intercalative mode of interactions with DNA.

The ligand–DNA interactions can be studied by virtue of the interpretation of induced CD (ICD) signals resulting from the coupling of electronic transition moments of the molecule and DNA bases within the asymmetric DNA environment.¹⁴ The CD spectrum of ct-DNA in general consists of distinctive peaks at 280 (+ve) and 245 (–ve) nm (Figure 4.18A). Upon addition of the conjugate **1** to the buffered solution of ct-DNA, a bisignated CD signal having maxima at 363 (+ve) and 411 (–ve) nm was observed. Both these bands were located on the either side of the absorption maximum of the free conjugate **1** having absorption at 382 nm. However,

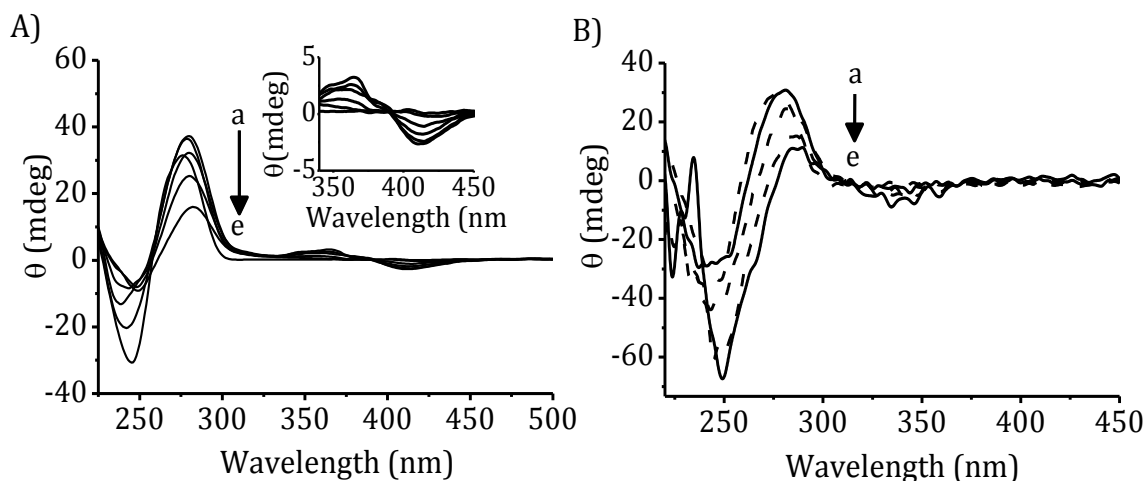


Figure 4.18. Changes in circular dichroism (CD) spectra of DNA (0.75 mM) with the increasing in addition of the conjugates, A) **1** and B) **2** in phosphate buffer (10 mM, pH 7.4) at 25 °C. Inset of A shows the zoomed portion of the CD changes. (a) 0, and (e) 0.14 mM.

the amphiphilic derivative **2** showed a negative ICD signal with maxima at 344 nm, which is similar those observed for the classical intercalators¹⁵ (Figure 4.18B).

Viscosity of DNA is known to be sensitive to the mode of the interaction of a ligand with DNA.¹⁶ For example, if a ligand binds through classical intercalative interactions, it exhibits significant increase in the length of the DNA, which results in the enhancement in the viscosity of DNA. The changes in the dynamic viscosity of DNA were monitored with the increase in concentration of the conjugates. We observed a value of 1.1 ± 0.02 mPas for ct-DNA (0.3 mM) in buffer at 25 °C, which gradually increased to 1.57 ± 0.01 and 1.43 ± 0.01 , in the presence of the conjugates **1** (0.1 mM) and **2** (0.1 mM), respectively, under identical conditions. The viscosity changes observed confirm the fact these systems undergo intercalative binding mode similar to that of the literature examples.¹⁶

To further evaluate the DNA binding affinity of the amphiphilic derivatives, thermal denaturation of synthetic duplex DNA was monitored in the presence and absence of the conjugates **1** and **2**. Intercalation of the ligands with duplex DNA (ds-DNA) and interstrand crosslink formation during irradiation are known to increase the DNA melting temperature (T_m), *i.e.* the temperature at which the double helix denatures to single strand DNA (ss-DNA). The molar extinction coefficient of DNA bases at 260 nm in the double helical form is much less than that of the single strand form; hence, thermal melting of the duplex DNA leads to an increase in the absorption at this particular wavelength. Therefore, the helix to coil transformation

can be conveniently determined by monitoring the absorbance of the ds-DNA at 260 nm as a function of temperature. For example, the synthetic polynucleotide poly(dA.dT)-poly(dA.dT) that we have chosen for the present study showed a melting temperature (T_m) of 44 °C (Figure 4.19). However, in the presence of the conjugates **1** and **2** (1 equivalent of each), we observed substantially increased T_m of 66 and 54 °C, respectively, under similar conditions.

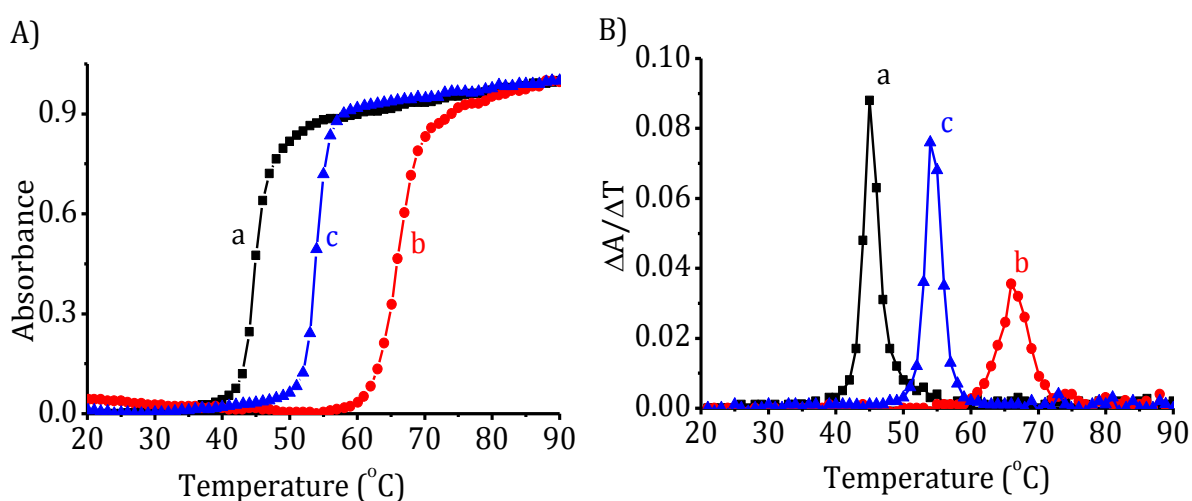


Figure 4.19. A) Thermal denaturation and B) differential thermal denaturation curves for poly(dA-dT).poly(dA-dT) (8.3 μ M), in the (a) absence ($T_m = 44$ °C) and presence of (b) **1** (8.3 μ M, $T_m = 66$ °C) and (c) **2** (8.3 μ M, $T_m = 54$ °C). Absorbance monitored at 260 nm.

4.3.5. DNA Mediated Disassembly

As these conjugates **1** and **2** exhibited good solubility in the aqueous medium, we have investigated the interactions of DNA with the vesicular structures of the conjugate **1** formed at CAC of 0.4 mM. Interestingly, upon addition of DNA (0.3 mM) to the vesicular solution of **1**, we observed a significant hypochromicity (*ca.*

36%) in the absorption spectrum. Similarly, in the emission spectrum, we observed a significant enhancement in the excimer intensity ($I_{510}/I_{390} = 1.6$) (Figure 4.20). To further understand the observations made, we have carried out the morphological analysis of the vesicular structures in the presence and absence of DNA through DLS and TEM techniques (without negative staining). As shown in Figure 4.21A, we observed prominent changes in the size distribution curves and the amplitude of the correlogram in the presence of DNA (0.4 mM) (Figure 4.21B). Under these conditions, we observed only the reticulate fibers of width *ca.* 300 nm confirming thereby the disassembly of the vesicles. Evidence was obtained for the disassembly of the vesicular structures of the conjugate **1** through the analysis of TEM images under similar conditions (Figure 4.22A).

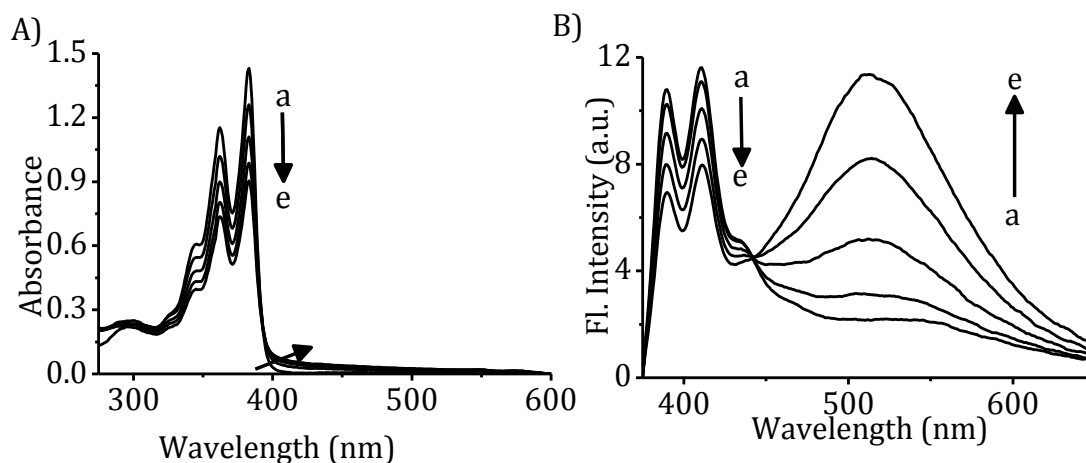


Figure 4.20. Changes in A) absorption and B) emission spectra of the conjugate **1** (0.4 mM) in the presence of ct-DNA, a) 0, and e) 0.3 mM. Path length of the cell, $l = 0.1$ cm, Excitation wavelength, 362 nm.

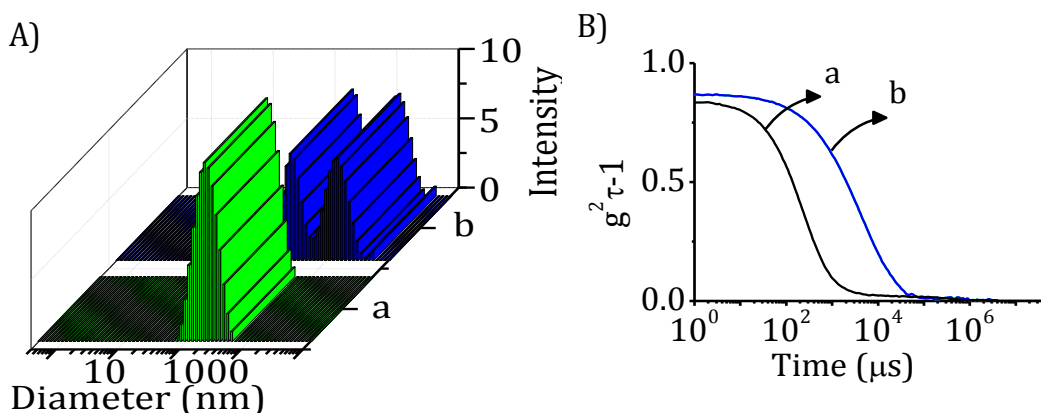


Figure 4.21. A) Size distribution and B) correlation data of the conjugate **1**, a) alone (0.4 mM) and b) in the presence of ct-DNA (0.4 mM).

To explore the potential of DNA as stimuli, we have investigated the encapsulation and release of the hydrophobic dyes through the disruption of the vesicular structures. Figure 4.22B shows the changes in the absorption and emission properties of the encapsulated Nile red in the vesicular solution of the conjugate **1** in

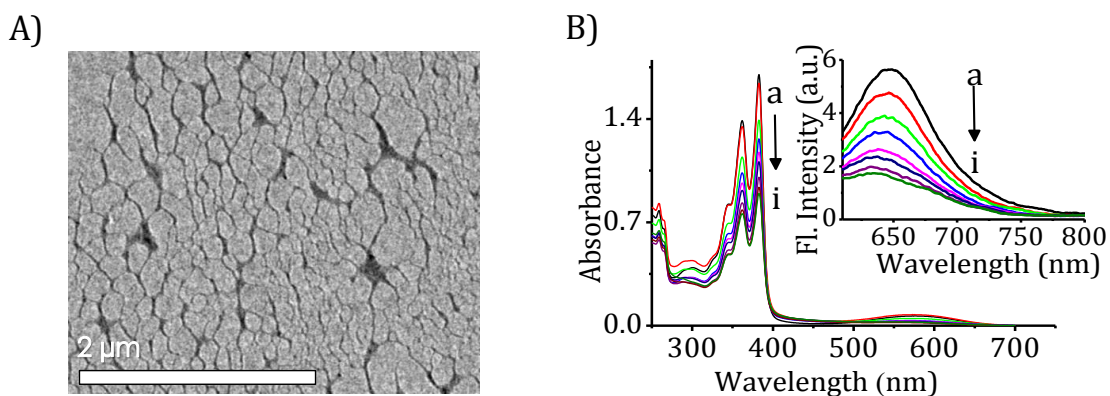


Figure 4.22. A) TEM image of the vesicular solution of the conjugate **1** (0.4 mM) in the presence of ct-DNA (0.4 mM). B) Changes in the absorption and emission (inset) spectra of Nile red encapsulated (100 μ M) in the vesicles of the conjugate **1** with the addition of ct-DNA; a) 0 and i) 0.3 mM.

the presence and absence of DNA. With the addition of DNA, the vesicular solution having Nile red encapsulated showed a significant hypochromicity at 530 nm, corresponding to the released dye molecules. Concomitantly, we observed the quenching in the fluorescence intensity at 630 nm due to the release of the Nile red dye. These results demonstrate the potential of the vesicular structures of the conjugate **1** as carriers of the hydrophobic dye molecules through encapsulation and release of the same through their disassembly employing DNA as stimuli.

4.4. DISCUSSION

The amphiphilic conjugates **1** and **2** used in the present investigation exhibited favourable photophysical and self-assembly properties in the aqueous medium. Of these two systems, the bolamphiphile **1** formed the spherical particles in the aqueous medium at and above critical aggregation concentration (CAC). These particles were further characterised as vesicles through microscopic techniques. Interestingly, the thickness of the wall of these nanostructures was found to be same as that of the extended length of the conjugate **1**. As shown in the Figure 4.23, The formation of the vesicular structures can be rationalized as a result of the cumulative effect of π -stacking interactions between the naphthalene diimide chromophores and the curvature provided by the minimum exposure of the central hydrophobic chain to the water.¹⁷ On the other hand, the amphiphilic derivative **2** showed the formation of the lamellar flakes at its CAC, probably due to the possibility of strong intermolecular interactions between the naphthalimide

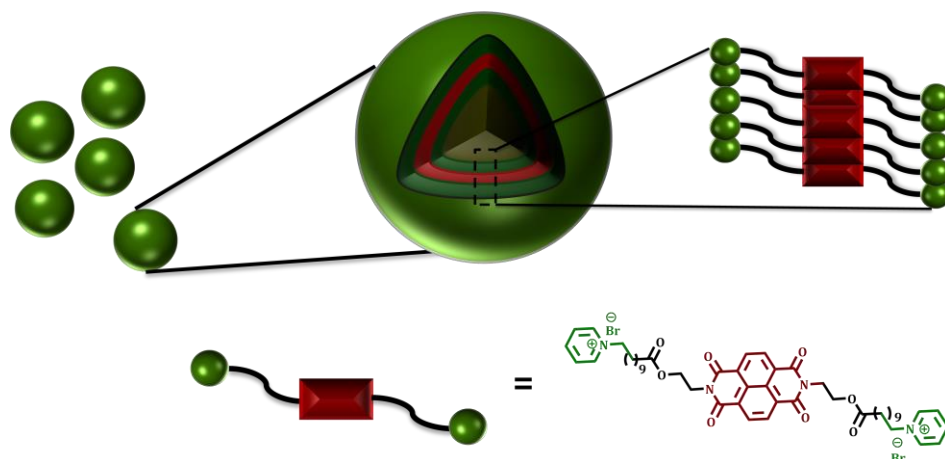


Figure 4.23. Schematic illustration of vesicular aggregates formation of the bolamphiphile **1** in water at and above critical aggregation concentration of 0.4 mM.

chromophores and thus restricting the formation of curvature required for the vesicular aggregates.

Interestingly, both these conjugates **1** and **2** showed strong interactions with DNA through intercalation as evidenced through various photophysical and biophysical techniques as well as ethidium bromide displacement assay. Moreover, the electrostatic interactions between the positively charged amphiphiles **1** and **2** with the phosphate backbone of DNA facilitate the formation of stable complex as evidenced through the effect of ionic strength of the medium. The observation of decrease in the K_{DNA} association constants of the both the derivatives upon increasing ionic strength of the medium clearly suggests that electrostatic interactions play an important role in binding interactions with DNA.¹⁸ Furthermore, the observation of the induced CD signals of the chromophores in the presence of DNA, the substantial increase in DNA viscosity and stabilization of the DNA duplex in

the presence of both the conjugates confirm that these systems predominantly undergo the intercalative mode interactions with DNA.^{19,20} Based on the negative results obtained with proteins, the driving force for the formation of the excimers of both **1** and **2** only in the presence of DNA could be attributed to the synergistic effects of both hydrophobic interactions at the intercalative sites and also the electrostatic interactions between the amphiphilic systems and the phosphate backbone of DNA. Moreover, the disassembly of the vesicular structures of the conjugate **1** induced by DNA could be attributed to the strong intercalative interactions of the naphthalene diimide chromophore of **1** with DNA, which eventually could be employed for the encapsulation and release of the hydrophobic molecules in the aqueous medium.

4.5. CONCLUSIONS

We synthesised two amphiphilic naphthalene imide conjugates **1** and **2** and have systematically investigated their photophysical, self-assembly and DNA binding aspects under different conditions. These conjugates showed good solubility in the aqueous medium and favourable photophysical properties. Of these two systems, the conjugate **1** based on naphthalene diimide chromophore exhibited vesicular structures in the aqueous medium at and above critical aggregate concentration of 0.4 mM, while the conjugate **2** aggregated to form the lamellar flakes (CAC \geq 0.25 mM). The self-assembled vesicular structures of the conjugate **1** were found to encapsulate the hydrophobic molecules such as Nile red dye efficiently.

Interestingly, these conjugates also exhibited strong affinity towards DNA with association constants in the range $5-8 \times 10^4 \text{ M}^{-1}$ as confirmed through various photophysical as well as biophysical techniques. Uniquely, in the presence of DNA, the vesicular structures of the conjugate **1** showed disassembly as analysed through various photophysical and microscopic techniques and such a transformation could be effectively employed for the release of the encapsulated hydrophobic molecules using DNA as stimuli. Of these two conjugates, the bolamphiphile **1**, which showed interesting photophysical, self-assembly and DNA binding properties and hence it can have potential use as a probe for DNA as well as carrier system for the delivery of the hydrophobic guest molecules in the aqueous medium.

4.6. EXPERIMENTAL SECTION

4.6.1. General Techniques

The melting points of the derivatives were determined on a Mel-Temp II melting point apparatus.²¹ The IR spectra were recorded on a Perkin Elmer Model 882 infrared spectrometer. The electronic absorption spectra were recorded on a Shimadzu UV-3101 or 2401 PC UV-Vis-NIR scanning spectrophotometers. The fluorescence spectra were recorded on a SPEX-Fluorolog F112X spectrofluorimeter. ¹H and ¹³C NMR were recorded on a 500 MHz Bruker advanced DPX spectrometer. The mass spectra were recorded on Thermo Scientific Exactive ESI-MS spectrophotometer. Quantum yields of fluorescence were measured by the relative method using the optically matched solutions. Fluorescence lifetimes were

measured using a IBH picosecond single photon counting system. The fluorescence decay profiles were deconvoluted using IBH data station software V2.1, and minimizing the χ^2 values of the fit to 1 ± 0.1 . Circular dichroism spectra were recorded on a Jasco J-810 spectropolarimeter.

A solution of calf thymus DNA was sonicated for 1 h to minimize complexities arising from DNA flexibility and filtered through a 0.45 μm Millipore filter ($M_w = 3 \times 10^5 \text{ g mol}^{-1}$). The concentrations of DNA solutions were determined by using the average value of $6600 \text{ M}^{-1} \text{ cm}^{-1}$ for the extinction coefficient of a single nucleotide at 260 nm.²² Polynucleotides were dissolved in phosphate buffer, and the concentrations were determined by using the average extinction coefficient value of $7400 \text{ M}^{-1} \text{ cm}^{-1}$ at 253 nm for poly(dG).poly(dC) and $6000 \text{ M}^{-1} \text{ cm}^{-1}$ at 260 nm for poly(dA).poly(dT).²³ Viscometric titrations were performed using LAUDA DLK10 automated viscometer, thermostatted at 25 °C in a constant temperature bath. The concentration of ct-DNA was 0.3 mM, and the flow times were measured with an automated timer. Each sample was measured three times and an average flow time was calculated. All experiments were carried out at room temperature 25 °C and solvents used were purified and distilled before use.

4.6.2. Materials and Methods

Starting materials. 1,4,5,8-Naphthalene tetracarboxylic dianhydride, 1,8-naphthalic anhydride, 11-bromoundecanoic acid, ethanolamine were purchased from Aldrich and S. D. Fine Chemicals, India.

4.6.3. Synthesis of the Conjugates 1 and 2

The model compounds, **NDI-OH**, (mp. >300 °C)^{24a,b} and **NMI-OH** (mp. 172-174 °C, lit. mp. 175–176 °C)^{24c} were synthesised from the corresponding anhydrides by the reaction with ethanolamine as per the reported procedures.

Synthesis of NDI-Br and NMI-Br: To a solution of 11-bromoundecanoic acid (1.12 mmol), EDC·HCl (1.4 mmol), and DMAP (0.28 mmol) in DMF (10 mL) was added **NDI-OH** (0.56 mmol) or **NMI-OH** (1.04 mmol) and the reaction was kept under stirring at 25 °C. After 12 h, DMF was evaporated under vacuum and the crude product obtained was dissolved in chloroform (20 mL). To this solid product, water (20 mL) was added and the aqueous layer was extracted with chloroform and the combined organic layers were washed with brine (50 mL), dried over MgSO₄, and concentrated under vacuum. The residue was purified by column chromatography over silica gel and on elution with a mixture (47:3) of CH₂Cl₂ and CH₃OH gave the corresponding ester.

2,2'-(1,3,6,8-tetraoxobenzo[lmn][3,8]phenanthroline-2,7-(1H,3H,6H,8H)-diyl)bis(ethane-2,1-diyl)bis(3-bromoundecanoate) (NDI-Br): 80%, mp 173-175 °C, ¹H NMR (CDCl₃, 500 MHz) δ 8.64 (4H, s), 4.55 (4H, t, J = 6 Hz), 3.50 (8H, m), 2.32 (4H, t, J = 7.5 Hz), 1.82 (4H, t, J = 7 Hz), 1.66 (4H, t, J = 7 Hz), 1.28 (22H, m); ¹³C NMR (CDCl₃, 125 MHz) δ 173.0, 159.4, 139.6, 135.2, 124.6, 61.2, 40.9, 34.2, 33.5, 29.6, 29.1, 28.5, 25.4; FAB-MS (+ve mode) m/z Calcd for C₄₀H₅₂Br₂N₂O₈: 848.65; Found: 848.24 (M⁺).

2-(1,3-dioxo-1H-benzo[de]isoquinolin-2(3H)-yl)ethyl-3-bromo-undecanoate (NMI-Br): 77%, mp. 78-80 °C; ¹H NMR (CDCl₃, 500 MHz) δ 8.60 (2H, d, J = 7 Hz), 8.22 (2H, t, J = 8.5 Hz), 7.76 (2H, t, J = 7.5 Hz), 4.58 (2H, t, J = 6.5 Hz), 4.56 (4H, t, J = 6.5 Hz), 2.72 (2H, t, J = 6 Hz), 1.80 (2H, t, J = 6 Hz), 1.54 (2H, t, J = 5.5 Hz), 1.22-1.12 (12 H, m) FAB-MS (+ve mode) m/z Calcd for C₂₅H₃₀BrNO₄: 487.13; Found: 487.20 (M⁺).

Synthesis of conjugates 1 and 2: NDI-Br (0.13 mmol) or NMI-Br (0.13 mmol) was dissolved in 5 mL of dry pyridine and heated at 85 °C for 8 h. Excess pyridine was removed under reduced pressure. The residue thus obtained was dissolved in methanol, precipitated with ether and recrystallized from ether-methanol mixture to afford brown coloured solid product **1** (66 %) and yellow viscous oil **2** (55%).

1,1'-(3,3'-(2,2'-(1,3,6,8-tetraoxobenzo[lmn][3,8]phenanthroline-2,7-(1H, 3H,6H,8H)-diyl)bis(ethane-2,1-diyl))bis(oxy)bis(3-oxoundecan-3,1-diyl)) dipyridinium bromide (1): 66%, mp. 54-57°C; ¹H NMR (DMSO-d₆, 500 MHz) δ 9.12 (4H, d, J = 6 Hz), 8.71 (4H, s), 8.61 (2H, t, J = 7.5 Hz), 8.17 (4H, t, J = 7 Hz), 4.60 (4H, t, J = 6 Hz), 4.35 (8H, s), 2.19 (4H, t, J = 7.5 Hz), 1.89 (4H, t, J = 7 Hz), 1.38 (4H, t, J = 7 Hz), 1.22 (8H, m), 1.12 (4H, m), 1.07 (12 H, m); ¹³C NMR (DMSO-d₆, 125 MHz) δ 172.9, 162.7, 145.5, 144.6 130.6, 128.1, 126.2, 99.5, 60.7, 33.3, 30.6, 28.6, 28.5, 28.3, 25.3, 24.16; ESI-MS m/z Calcd for C₅₀H₆₂N₄O₈²⁺: 847.07; Found: 848.40 (M+1).

1-(3-(2-(1,3-dioxo-1H-benzo[de]isoquinolin-2(3H)-yl)ethoxy)-3-oxoundecyl)pyridinium bromide (2): 55%, ¹H NMR (DMSO-d₆, 500 MHz) δ 9.08

(2H, d, J = 7.5 Hz), 8.60 (1H, t, J = 7 Hz), 8.58 – 8.49(4H, m), 8.15 (2H, t, J = 7 Hz), 7.88 (2H, t, J = 7.5 Hz), 4.58 (2H, t, J = 7 Hz), 4.34 (4H, s), 2.17 (2H, t, J=7 Hz), 1.89 (2H, t, J=7 Hz), 1.37 (2H, t, J=7 Hz), 1.28-1.21 (4H, m), 1.11-1.05 (8H, m); ¹³C NMR (DMSO-d₆, 125 MHz) δ 172.9, 163.6, 148.1, 138.07, 134.5, 131.2, 130.8, 128.0, 127.2, 124.6, 121.7, 60.9, 48.5, 45.4, 33.4, 31.9, 28.6, 28.5, 28.2, 28.1, 28.0, 26.1, 24.1; ESI-MS m/z Calcd for C₃₀H₃₅N₂O₄⁺: 487.61; Found: 488.70 (M+1).

4.6.4. DNA Binding Studies

The DNA binding studies were carried out in 10 mM phosphate buffer (pH 7.4) containing 2, 100 and 500 mM NaCl. The intrinsic binding constant of the amphiphilic conjugates **1** and **2** with ct-DNA was determined using absorbance at the respective maxima recorded after each addition of ct-DNA. The intrinsic binding constant K_{DNA} was determined from the half reciprocal plot of $D/\Delta\epsilon_{ap}$ vs D , where D is the concentration of DNA in base pairs, $\Delta\epsilon_{ap} = [\epsilon_a - \epsilon_F]$ and $\Delta\epsilon = [\epsilon_b - \epsilon_F]$.¹¹ The apparent extinction coefficient, ϵ_a , is obtained by calculating $A_{[obsd]} / [1 \text{ or } 2]$. ϵ_b and ϵ_F correspond to the extinction coefficient of the bound form of the conjugates and the extinction coefficient of the free conjugates, respectively. The data were fitted to equation 4.1, with a slope equal to $1/\Delta\epsilon$ and a y-intercept equal to $1/(\Delta\epsilon.K_{DNA})$. The

$$D/\Delta\epsilon_{ap} = D/\Delta\epsilon + 1/(\Delta\epsilon K_{DNA}) \quad (\text{Eq 4.1})$$

values of ϵ_b was determined from $\Delta\epsilon$ whereas K_{DNA} was obtained from the ratio of the slope to the y-intercept.

4.6.5 Determination of the Critical Aggregation Concentration (CAC)

The critical aggregation concentration (CAC) of the conjugates **1** and **2** were determined by using UV-Vis spectroscopic analysis. A stock solution of the conjugates **1** or **2** in water (5 mM) was prepared and from this a series of solutions of various concentrations were made (0.05 to 1 mM). These solutions were equilibrated for 2 h at 25 °C before the analysis. Then, the absorbance of the conjugates **1** and **2** at 382 and 344 nm, respectively, were plotted against concentration and the CAC value was estimated from the inflection point.

4.6.6. Encapsulation of Nile Red by the Vesicles of the Conjugate 1

A measured amount of a solution of Nile red in THF (3 mL, 0.1 mM) was placed in various glass vials and the solvent was evaporated. Solutions of various concentrations of the conjugate **1** were added to vials that contained Nile red and the mixture was sonicated for 15 min and allowed to stand for 2 h before fluorescence spectroscopic analysis (excitation wavelength, 530 nm). The final concentration of Nile red was 100 µM and the emission intensity of the encapsulated Nile red at 630 nm was plotted versus the concentration of the conjugate **1** and the inflection point of such a plot was taken as the CAC of the conjugate **1**.

4.6.7. Transmission Electron Microscopy (TEM) Analysis

The TEM analysis was performed on JEOL 100 kV high resolution transmission electron microscope. The derivatives **1** and **2** were dissolved in water

and drop casted on the top of carbon-coated Cu grid. The grids were mounted on reverse tweezers and the samples were dried in air at 25 ± 1 °C. The accelerating voltage of the transmission electron microscope was 100 kV and the beam current was 65 A. Samples were imaged using a Hamamatsu ORCA CCD camera.

4.6.8. Scanning Electron Microscopy (SEM) Analysis

The SEM studies were carried out using ZEISS EVO MA and LS series scanning electron microscope. The operating range was between 100-230 V at 50-60Hz single phase with a consumption of 2.5 kVA. The sample solution in water (CAC) was drop casted directly on the top of the mica substrate and placed on aluminum grid. The solvents were allowed to evaporate at ambient conditions. The obtained sample was coated with gold to attain the easy passage flow of electrons.

4.6.9. Dynamic Light Scattering (DLS) Analysis

The DLS experiments were carried out on a Nano Zeta Sizer, Malvern instruments. The samples were prepared in water with varying concentrations. The light scattering experiments were performed under low polydispersity index by using glass cuvettes. The hydrodynamic diameters and polydisperse indices of the vesicles were determined using a Malvern Zeta Nano-ZS system.

4.6.10. Fluorescence Microcopy Analysis

The fluorescence microcopy was performed using NikonHFX35A Optiphot-2 light optical microscope. For this analysis, the Nile red encapsulated vesicular solution samples were prepared in water at a concentration of 0.4 mM. The samples

were placed in between two fresh cover slips. The samples were excited with an excitation wavelength of 530 nm. The images were taken using a CCD camera attached to NikonHFX35A at 25 °C.

4.7. REFERENCES

1. a) J.-H. Fuhrhop and T. Wang, *Chem. Rev.*, **2004**, *104*, 2901; b) X. Zhang, S. Rehm, M. M. Safont-Sempere and F. Würthner, *Nature Chem.*, **2009**, *1*, 623; c) L. Jiang, Z. Gao, L. Ye, A. Zhang and Z. Feng, *Biomater. Sci.*, **2013**, *1*, 1282.
2. a) D. F. Evans and H. Wennerstrom, *The Colloidal Domain* 2nd ed.; Wiley-VCH: New York, **1999**; b) A. Sorrenti, O. Illa and R. M. Ortuño, *Chem. Soc. Rev.*, **2013**, *42*, 8200.
3. a) J.-M. Lehn, *Science*, **2002**, *295*, 2400; b) G. M. Whitesides, J. P. Mathias and C. T. Seto, *Science*, **1991**, *254*, 1312; c) L. Brunsveld, B. J. B. Folmer, E. W. Meijer and R. P. Sijbesma, *Chem. Rev.*, **2001**, *101*, 4071; d) Z. Chen, A. Lohr, C. R. Saha-Müller and F. Würthner, *Chem. Soc. Rev.*, **2009**, *38*, 564.
4. a) C. Wang, Z. Wang and X. Zhang, *Acc. Chem. Res.*, **2012**, *45*, 608; b) C. Wang, Z. Wang and X. Zhang, *Small*, **2011**, *7*, 1379; c) P. Xing, T. Sun and A. Hao, *RSC Adv.*, **2013**, *3*, 24776; d) Y. Kang, K. Liu and X. Zhang, *Langmuir*, **2014**, *30*, 5989.
5. a) A. Almutairi, S. J. Guillaudeu, M. Y. Berezin, S. Achilefu and J. M. J. Fréchet, *J. Am. Chem. Soc.*, **2008**, *130*, 444; b) Y. Bae, N. Nishiyama, K. Kataoka, *Bioconjugate Chem.*, **2007**, *18*, 1131; c) C. Wang, K. C. Tam, R. D. Jenkins and

- C. B. Tan, *J. Phys. Chem. B*, **2003**, *107*, 4667; d) S. Lecommandoux, O. Sandre, F. Checot, J. Rodriguez-Hernandez and R. Perzynski, *Adv. Mater.*, **2005**, *17*, 712; e) D. Schmaljohann, *Adv. Drug Delivery Rev.*, **2006**, *58*, 1655; f) A. P. de Silva, C. M. Dobbin, T. P. Vance and B. Wannalarse, *Chem. Commun.*, **2009**, 1386.
6. a) M. D. Burke, J. O. Park, M. Srinivasarao and S. A. Khan, *J. Controlled Release*, **2005**, *104*, 141; b) P. D. Thornton, G. McConnell and R. V. Ulijn, *Chem. Commun.*, **2005**, 5913; c) M. A. Azagarsamy, V. Yesilyurt and S. Thayumanavan, *J. Am. Chem. Soc.*, **2010**, *132*, 4550.
7. a) I. Saito, M. Takayama and S. Kawanishi, *J. Am. Chem. Soc.*, **1995**, *117*, 5590; b) I. Saito, M. Takayama, H. Sugiyama, K. Nakatani, A. Tsuchida and M. Yamamoto, *J. Am. Chem. Soc.*, **1995**, *117*, 6406; c) J. E. Rogers, S. J. Weiss and L. A. Kelly, *J. Am. Chem. Soc.*, **2000**, *122*, 427; d) S. Banerjee, S. A. Bright, J. A. Smith, J. Burgeat, M. Martínez-Calvo, D. C. Williams, J. M. Kelly and T. Gunnlaugsson, *J. Org. Chem.*, **2014**, *79*, 9272; e) S. Banerjee, E. B. Veale, C.M. Phelan, S. A. Murphy, G. M. Tocci, L. J. Gillespie, D. O. Frimannsson, J. M. Kelly and T. Gunnlaugsson, *Chem. Soc. Rev.*, **2013**, *42*, 1601.
8. S. V. Bhosale, C. H. Janiab and S. J. Langford, *Chem. Soc. Rev.*, **2008**, *37*, 331.
9. a) M. R. Molla, D. Gehrig, L. Roy, V. Kamm, A. Paul, F. Laquai and S. Ghosh, *Chem. Eur. J.*, **2014**, *20*, 760; b) C. Kulkarni and S. J. George, *Chem. Eur. J.*, **2014**, *20*, 4537.

10. a) S. Banerjee, J. A. Kitchen, S. A. Bright, J. E. O'Brien, D. C. Williams, J. M. Kelly and T. Gunnlaugsson, *Chem. Commun.*, **2013**, 49, 8522; b) S. Roy, S. Saha, R. Majumdar, R. R. Dighe and A. R. Chakravarty, *Inorg. Chem.*, **2009**, 48, 9501; c) K. J. Kilpin, C. M. Clavel, F. Edafe and P. J. Dyson, *Organomet.*, **2012**, 31, 7031.
11. a) E. Kuruvilla and D. Ramaiah, *J. Phys. Chem. B*, **2007**, 111, 6549; b) J. Joseph, E. Kuruvilla, A. T. Achuthan, D. Ramaiah and G. B. Schuster, *Bioconjugate Chem.*, **2004**, 15, 1230; c) E. Kuruvilla, P. C. Nandajan, G. B. Schuster and D. Ramaiah, *Org. Lett.*, **2008**, 10, 4295; d) M. Hariharan, J. Joseph and D. Ramaiah, *J. Phys. Chem. B*, **2006**, 110, 24678; e) S. C. Karunakaran, D. Ramaiah, I. Schulz and B. Epe, *Photochem. Photobiol.*, **2013**, 89, 1100.
12. a) C. V. Kumar and E. H. Asuncion, *J. Am. Chem. Soc.*, **1993**, 115, 8541; b) P. P. Neelakandan, K. S. Sanju and D. Ramaiah, *Photochem. Photobiol.*, **2010**, 86, 282.
13. D. L. Boger, B. E. Fink, S. R. Brunette, W. C. Tse and M. P. Hedrick, *J. Am. Chem. Soc.*, **2001**, 123, 5878.
14. a) D. G. Dalglish and A. R. Peacocke, *Biopolymers*, **1971**, 10, 1853; (b) R. J. Fiel and B. R. Munson, *Nucleic Acids Res.*, **1980**, 8, 2835; (c) B. Nordén and F. Tjerneld, *Biopolymers*, **1982**, 21, 1713; (d) M. Kubista, B. Aakerman and B. Nordén, *J. Phys. Chem.*, **1988**, 92, 2352.
15. a) A. Rodger, S. Taylor, G. Adlam, I. S. Blagbrough and I. S. Haworth, *Bioorgan. Med. Chem.*, **1995**, 3, 3861; b) A. Rodger, I. S. Blagbrough, G. Adlam and M. L. Carpenter, *Biopolymers*, **1994**, 34, 1583; c) *Circular Dichroism. Principles and*

- Applications*, N. Berova, K. Nakanishi and R. W. Woody, (Eds.) Wiley-VCH, New York, **2000**.
16. a) J.-Z. Wu, L. Yuan and J.-F. Wu, *J. Inorg. Biochem.*, **2005**, *99*, 2211; b) J. Talib, D. G. Harman, C. T. Dillon, J. A. Wright, J. L. Becka and S. F. Ralph, *Dalton Trans.*, **2009**, 504; c) H. Ihmels, J. Mattay, F. May and L. Thomasa, *Org. Biomol. Chem.*, **2013**, *11*, 5184.
17. M. R. Molla and S. Ghosh, *Chem. Eur. J.*, **2012**, *18*, 9860.
18. a) C. Cantor and P. R. Schimmel, In *Biophysical Chemistry*, W. H. Freeman (Ed.), San Francisco, **1980**, *Vol 2*; b) E. C. Long and J. K. Barton, *Acc. Chem. Res.*, **1990**, *23*, 271; c) H. M. Berman and P. R. Young, *Annu. Rev. Biophys. Bioeng.*, **1981**, *10*, 87; d) G. Dougherty and W. J. Prigam, *Crit. Rev. Biochem.*, **1982**, *12*, 103.
19. M. Nakamura, T. Okaue, T. Takada and K. Yamana, *Chem. Eur. J.*, **2011**, *18*, 196.
20. a) F. P. Gasparro, *Psoralen DNA Photobiology*, CRC Press Inc. Boca Raton, Florida, 1988; b) D. J. Patel and L. Cannel, *Proc. Natl. Acad. Sci. USA*, **1976**, *73*, 674.
21. a) R. R. Avirah, K. Jyothish and D. Ramaiah, *Org. Lett.*, **2007**, *9*, 121; b) K. T. Arun and D. Ramaiah, *J. Phys. Chem. A*, **2005**, *109*, 5571; c) D. D. Gayathri, T. R. Cibir, D. Ramaiah and A. Abraham, *J. Photochem. Photobiol. B*, **2008**, *92*, 153; d) K. T. Arun, D. T. Jayaram, R. R. Avirah and D. Ramaiah, *J. Phys. Chem. B*, **2011**, *115*, 7122.

22. a) B. C. Baguley and E.-M. Falkenhaus, *Nucleic Acids Res.*, **1978**, *5*, 161; b) H. Deng, J. Cai, H. Xu, H. Zhang and L. Ji, *J. Chem. Soc. Dalton Trans.*, **2003**, 325.
23. S. Takenaka, T. Ihara and M. Takagi, *J. Chem. Soc. Chem. Commun.*, **1990**, 1485.
24. a) J. E. Rogers, S. J. Weiss, and L. A. Kelly, *J. Am. Chem. Soc.*, **2000**, *122*, 427; b) C. Kulkarni and S. J. George *Chem. Eur. J.*, **2014**, *20*, 4537; c) Fierz David and H. E. C. Rossi, *Helv. Chim. Acta*, **1938**, *21*, 1466.

LIST OF PUBLICATIONS

1. Dansyl–Naphthalimide Dyads As Molecular Probes: Effect of Spacer Group on Metal Ion Binding Properties, **B. H. Shankar** and D. Ramaiah *J. Phys. Chem. B*, **2011**, *15*, 13292–13299.
2. Photomorphogenesis of γ -Globulin: Effect on Sequential Ordering and Knock Out of Gold Nanoparticles Array, D. T. Jayaram, **B. H. Shankar** and D. Ramaiah, *RSC Advances*, **2013**, *3*, 13463–13469.
3. A Reversible Dual Mode Chemodosimeter for the Detection of Cyanide Ions in Natural Sources, **B. H. Shankar**, D. T. Jayaram and D. Ramaiah, *Chem. Asian J.*, **2014**, *9*, 1636–1642.
4. Selective and Dual Naked Eye Detection of Cu^{2+} and Hg^{2+} Ions using a Simple Quinoline-Carbaldehyde Chemosensor, C. L. Devi, S. Thurakkal, **B. H. Shankar** and D. Ramaiah, *Sensors and Actuators B*, **2014**, *204*, 480–488.
5. *In Vitro* and *In Vivo* Demonstration of Photodynamic Activity and Cytoplasm Imaging through Self-Assembled Nanoparticles of Tetraphenylethene Conjugates, D. T. Jayaram, S. Ramos, **B. H. Shankar**, C. Garrido, J. Blanco and D. Ramaiah, *ACS Chem. Biol.*, **2015** (Under Revision).
6. Naphthalene Imide Conjugates: Formation of Supramolecular Assemblies, Encapsulation and Release of Dyes through DNA Mediated Disassembly, **B. H. Shankar**, D. T. Jayaram and D. Ramaiah, *Chem. Eur. J.*, **2015** (Communicated).
7. Effective Amyloid Defibrillation by Polyhydroxyl Substituted Squaraine Dyes, D. T. Jayaram, **B. H. Shankar** and D. Ramaiah, *Chem. Asian J.*, **2015** (Communicated).
8. Supramolecular Construction of Aggregation Induced NIR Emitting Nanostructures with Charge Transfer and Conductivity Properties, D. T. Jayaram, **B. H. Shankar**, D. Mahendran and D. Ramaiah, *Adv. Mater.*, **2015** (Under Preparation).

PAPERS PRESENTED IN CONFERENCES

9. **B. H. Shankar** and D. Ramaiah, (2012) Dansyl–Naphthalimide Dyads as Molecular Probes: Effect of Spacer Group on Metal Ion Binding Properties, A Poster Presented at the 8th JNC Research Conference on Chemistry of Materials, Trivandrum, Kerala, India, October 01–03.
10. **B. H. Shankar**, D. T. Jayaram and D. Ramaiah, (2014) A Reversible Dual Mode Chemodosimeter for the Detection of Cyanide Ions in Natural Sources, A Poster Presented at 8th Mid-Year CRSI National Symposium in Chemistry, CSIR-NEIST, Jorhat, Assam, India, July 10-12 (Awarded Best Poster).